Low-Dimensional Control Representations for Muscle-Based Characters : Application to Overhead Throwing

Ana Lucia Cruz Ruiz

UNIVERSITE
BRETAGNE
LOIRE

THÈSE / ENS RENNES
sous le sceau de l'Université Bretagne Loire

pour obtenir le titre de
DOCTEUR DE L'ÉCOLE NORMALE SUPÉRIEURE DE RENNES
Mention : Informatique
École doctorale MATISSE

présentée par
Ana Lucia Cruz Ruiz
Préparée à l'unité mixte de recherche 6074
Institut de recherche en informatique
et systèmes aléatoires

Low-dimensional Control Representations for Muscle-based Characters: Application to Overhead Throwing

Thèse soutenue le 2 décembre 2016
devant le jury composé de :

Michiel van de Panne / *Rapporteur*
Professeur, University of British Columbia, Vancouver
Philippe Souères / *Rapporteur*
Directeur de Recherché, LAAS-CNRS, Toulouse

Laurence Chèze / *Examinatrice*
Professeur, Université Claude Bernard, Lyon
Sophie Sakka / *Examinatrice*
Maître de Conférences, Ecole centrale de Nantes, Nantes

Nicolas Mansard / *Invité*
Chargé de Recherché, LAAS-CNRS, Toulouse

Georges Dumont / *Directeur de thèse*
Professeur, Ecole Normale Supérieure de Rennes, France
Charles Pontonnier / *Encadrant*
Maître de Conférences, Ecoles de Saint-Cyr Coëtquidan/
Ecole Normale Supérieure de Rennes, Rennes

Think and wonder, wonder and think.

Dr. Seuss

Résumé

Contrôler les personnages virtuels, c'est l'art de leur donner vie. La capacité à les doter de la possibilité de se mouvoir et de réaliser différentes actions de motricité, similaires aux humains. L'un des éléments essentiels à cette performance est le contrôleur de mouvement, capable de transformer les actions souhaitées en mouvements synthétisés chez le personnage. La conceptualisation de ces contrôleurs a profondément évolué grâce à l'apport des connaissances en biomécanique et qui a conduit à l'utilisation de modèles de personnages encore plus détaillés, en s'inspirant de l'appareil squelettique et surtout musculaire de l'être humain.

Ce fut un cap pour les applications de contrôle basées sur les lois de la physique, marquant la transition entre les personnages actionnés par des servomoteurs et les personnages à modèle musculaire et ce, dans différents champs d'activité, allant de la rééducation fonctionnelle à l'animation. En rééducation par exemple, les personnages à modèle musculaire sont utilisés pour exercer les patients sur des prothèses virtuelles avant de pouvoir passer à leurs prothèses réelles [SALC03]. En biomécanique, ils permettent de simuler et d'analyser des scénarios de marche pathologiques [HZN+06]. Et pour ce qui est du domaine de l'animation, ils permettent la synthèse de mouvements correspondant au plus près aux mouvements humains sur un plan cinématique et également dynamique [CRPPD16].

Le modèle musculaire dynamique a de nombreux avantages dus aux propriétés non linéaires des muscles et son utilisation permet : une meilleure stabilité, des dynamiques passives réalistes [GvdBHZ98, GvdPvdS13], des mouvements physiologiquement réalisables, une meilleure estimation de l'énergie requise et de la fatigue encourue [WHDK12], un système mécanique capable de réaliser des fonctionnalités de contrôle par lui-même [GH10] ainsi qu'une plus grande facilité de simulation des anomalies musculo-squelettiques, des pathologies possibles ou fatigue physique [LPKL14]. Néanmoins, des modèles de personnage plus perfectionnés impliquent

forcément de nouveaux défis en termes de contrôle, comme la redondance d'actionnement, véritable défi qui sera traité dans cette thèse.

La redondance est un phénomène qui se produit lorsqu'un personnage possède plus d'actionneurs que nécessaire à l'exécution d'une tâche spécifique. Cela signifie donc, qu'il existe plusieurs façons d'actionner et de commander le personnage pour l'accomplissement d'un même mouvement, ce qui évidemment complique considérablement la tâche au contrôleur qui se voit contraint de choisir entre plusieurs solutions et coordonner tous les actionneurs afin d'achever la tâche avec succès. Dans le cas des personnages à modèle musculaire, la problématique est décuplée par le fait qu'en plus d'être non linéaires, les muscles contrairement aux servos sont également des actionneurs unidirectionnels et donc, par conséquent, il en faut au moins deux pour permettre la rotation de chaque degré de liberté (DOF).

Le challenge que représente la redondance d'actionnement soulève alors d'importantes questions : Comment contrôler efficacement les personnages de type musculaire ? Est-ce possible d'éviter un contrôle redondant malgré la redondance d'actionnement ? Ou en d'autres termes, est-ce possible d'utiliser un nombre réduit de variables de commande malgré un grand nombre d'actionneurs ? Les humains sont de loin le meilleur exemple de complexité de systèmes musculo-squelettiques et de leur capacité à être rapidement maîtrisés, intuitivement et efficacement que ce soit pour des mouvements simples ou complexes. Ainsi, la réponse aux questions citées ci-dessus pourrait résider dans la compréhension et la réplication des stratégies de contrôle moteur humain.

L'une de ses stratégies, bien répandue maintenant et largement utilisée en neurosciences, est celle de la théorie des synergies musculaires. Cette théorie fait l'hypothèse que pour réaliser une tâche, le système nerveux central (SNC) transforme dans un premier temps les objectifs à atteindre en une multitude de modules, appelés aussi synergies, encodant l'information d'activation transmise aux muscles. En combinant ces modules en fonction de la tâche à réaliser, le SNC est capable d'envoyer un nombre conséquent de signaux d'activation pour l'exécution de différentes tâches motrices [ADN+13]. En d'autres termes et si l'on tient compte de cette théorie, les synergies sont les variables en quantité moindre que le SNC utilise pour contrôler les nombreux muscles du système musculo-squelettique humain. L'existence de ces variables de contrôle élémentaire et de leur modulation en fonction des différents objectifs à réaliser ainsi que de leurs spécificités cinématiques (ou variables définissant le mouvement) a déjà été mise en évidence par de nombreuses études. Certains de ces auteurs ont démontré que pour un mouvement, des synergies sont modulées selon la direction de celui-ci [dPFL06, dFPL08, MBdF10]. D'autres ont découvert que les réponses posturales pouvaient être encodées en synergies modulées en fonction des directions prises par la perturbation [TOT07] et les cinématiques du centre

de masse du sujet [ST11]. D'autres encore ont trouvé que la locomotion pouvait être définie à travers les synergies reliées aux cinématiques des pieds [IGZ+03, IPL04].

Nous verrons ici, que les synergies sont utilisées comme un nombre réduit de variables de contrôle nécessaires à la commande d'un nombre important de muscles chez un personnage virtuel et que deux étapes sont nécessaires : une analyse de mouvement et la génération de ce mouvement. La phase d'analyse consiste à identifier les caractéristiques cinématiques et les synergies chez les humains, alors que la phase de génération consiste en un système de dynamique directe visant l'adaptation de ces synergies à un ensemble d'objectifs et à un personnage virtuel (modèle musculaire). Afin de tester à la fois ce système et la théorie de la synergie musculaire, cette approche a été appliquée et testée sur des mouvements de jet (lancers avant). C'est une tâche qui n'a pas encore été étudiée selon la théorie de la synergie musculaire et connu pour son haut caractère redondant, non linéaire et ultra dynamique (vélocités élevées et avec élan) [KXY+10] nécessitant coordination, précision et maîtrise.

En présentant, ici, une solution basée sur les synergies s'appuyant sur une analyse de mouvement et en testant cette approche sur un mouvement aussi dynamique, cette thèse apporte deux contributions principales. Premièrement la validation de la théorie de la synergie musculaire en l'utilisant pour l'étude d'un nouveau mouvement et pour tenter de contrôler un personnage virtuel. Deuxièmement, une contribution à l'ensemble des domaines impliquant des simulations corporelles et ayant recours aux personnages à modèle musculaire (comme par exemple, la réhabilitation ou l'animation) en leur proposant une solution de contrôle permettant de réduire la redondance.

Tout d'abord, sont revus dans le Chapitre 2, les modèles de contrôle musculaire pour les personnages virtuels et l'un de leur grands défis : la redondance (Section 2.1), complétée par une vue d'ensemble des synergies musculaires, mécanisme de réduction de la redondance chez les humains, mettant en évidence leur potentiel concernant le contrôle de personnages virtuels (Section 2.2). La première contribution de cette thèse est ainsi présentée au Chapitre 3, avec l'analyse de mouvements de lancer et l'extraction des synergies d'après les séquences EMG, en utilisant un algorithme de factorisation en matrice non négative (NMF). Les résultats mettent en évidence le fait que pour les sujets et mouvements analysés, seules deux synergies sont nécessaires à l'encodage des modes d'activation, importante, d'un collectif de 6 à 14 muscles, et que ces synergies sont modulées en fonction de la distance de lancer. Plus spécifiquement, une synergie agoniste et une synergie antagoniste ont été extraites, chacune faite d'une composante spatiale (tâche indépendante) et temporelle (tâche dépendante), et dont l'intensité du déclenchement augmenterait en fonction de la distance de lancer, la vitesse et la hauteur de la main au moment

du tir.

La seconde contribution de cette thèse est présentée au Chapitre 4, dans lequel les synergies précédemment extraites ont été utilisées comme signaux de contrôle d'entrée à une simulation de dynamique directe d'un personnage virtuel. Celui-ci adapte les synergies à la dynamique du personnage à modèle musculaire et à l'ensemble des objectifs cinématiques. Cette adaptation a été réalisée grâce à une optimisation statique, modulant l'aspect temporel des synergies selon les objectifs en cinématique. Preuve par les résultats : 1) La faisabilité de cette solution dans le cadre de la réduction de la redondance, en démontrant que le mouvement peut être reproduit en utilisant moins de variables de contrôle que d'actionneurs (deux synergies ont été utilisées pour contrôler 6 muscles du bras du personnage), et 2) Les synergies initiales encodent l'essentiel de l'information d'activation musculaire puisqu'elles représentent d'importants changements d'orientation des liaisons cinématiques (articulations), partiellement préservées après la procédure d'adaptation.

Enfin, le Chapitre 5 conclut sur l'ensemble des contributions apportées par cette thèse et les futures perspectives (discussions) de ces travaux, comme : l'extrapolation de ce système à la synthèse de nouveaux mouvements de lancer, en exploitant les relations observées entre les synergies et les caractéristiques cinématiques de la tâche à exécuter, son exploitation pour une variété de morphologies de personnage en utilisant des modèles génériques de synergie et enfin en l'appliquant à d'autres mouvements grâce au catalogue de classification des données recueillies sur les synergies.

Le terme "synergie" signifie littéralement "travailler ensemble". On sait déjà que nos muscles travaillent ensemble pour réaliser toutes sortes de tâches motrices, en revanche la façon dont nos muscles sont contrôlés reste une énigme qui nécessite d'être minutieusement élucidée. Toutefois, la supposition que cette collaboration ait une origine neuronale, est intéressante car cela expliquerait pourquoi les humains sont capables de contrôler si rapidement et efficacement leur système musculo-squelettique à très haute redondance. Si l'objectif de réaliser des simulations basées sur les lois de la physique avec des personnages virtuels est de mimer la façon dont les humains bougent, alors il paraît naturellement logique de mimer et reproduire le contrôle des mécanismes qui créent le mouvement et qui commandent ce système complexe d'actionneurs. Cette thèse avait pour but d'accomplir cette démarche en identifiant les synergies comme mécanismes de contrôle chez les humains, et en les utilisant pour construire des solutions simples, modulables et à faible dimension, dans le but de commander un personnage "musculaire" virtuel.

Abstract

Using virtual characters in physics-based simulations is interesting for a variety of applications seeking to analyze or generate motion, which range from rehabilitation to animation. However, new challenges have emerged in this subject due to an increase in the level of detail of character modeling. Servo-based characters have evolved into muscle-based characters. Mainly, due to advantages in terms of final motion quality and control, that stem from the use of muscles as actuators instead of ideal servo motors (e.g., physiologically feasible motions, ease to simulate musculoskeletal defects, control via the mechanical system itself).

Nevertheless, in spite of these advantages a challenge which prevents a wider adoption of muscle-based characters for forward dynamics simulations is actuation redundancy. Actuation redundancy results when the character has more actuators than needed to perform a specific task. This poses an important control challenge due to the fact that the character's motion controller must be able to select an appropriate actuation solution among numerous possibilities to achieve the desired task. This thesis aims at addressing this challenge through a practical use of knowledge from neuroscience. Low-dimensional controllers will be designed for muscle-based characters inspired by the *theory of muscle synergies*. A theory which argues that the human central nervous system manages redundancy intuitively and efficiently by controlling muscles in groups through fewer control variables than actuators.

Thus, synergies are proposed and tested as control functions in forward dynamics simulations with a muscle-based character. This was achieved through two main stages : a motion analysis and a motion generation stage. The motion analysis stage consisted in the extraction of synergies and kinematic features from human motions, while the motion generation stage consisted in the design and testing of a synergy-driven forward dynamics pipeline which adapted the extracted synergies in order to reproduce motions with a muscle-based character. This approach was tested on overhead throwing motions. An unconstrained and redundant motion which would

challenge the control of any overactuated character and the muscle synergy theory.

The results evidence the existence of low-dimensional control representations across subjects and throwing distances, given the degrees of freedom and muscles analyzed. Such representations allow the reproduction of motion through less control variables than actuators, while also allowing a partial preservation of the original synergies or control signals. These findings contribute to the variety of domains involving physics-based simulations with muscle-based characters, by evidencing the potential of synergies for reducing redundancy. Moreover, their use within a motion generation context contributes to the validation of the synergy theory, by challenging it on a new motion and testing it on a virtual character.

Keywords : Control, redundancy, muscle synergies, physics-based simulation, virtual characters

Acknowledgements

And so this represents another stage in a journey that began ten years ago: my dream to become a scientist. In spite of the all kinds of expected and unexpected adversities, this has been possible, not only due to hard work and passion, but also thanks to a group of people that have contributed in one way or the other along each step of the way.

To start, I would like to thank my thesis supervisors, Georges Dumont and Charles Pontonnier, who contributed to this thesis with their advise and counsel. I also wish to acknowledge Prof. Michiel van de Panne and Dr. Philippe Souères who kindly accepted to review this manuscript. An acknowledgment also goes to the other members of the jury and invited members, Prof. Laurence Chèze, Dr. Sophie Sakka, and Dr. Nicolas Mansard, for their availability to attend my defense and their constructive comments that enriched this work.

I would also like to thank all my colleagues of the Mimetic Team and INRIA with whom I shared countless personal and professional experiences that I will never forget. I would like to especially thank Helen, who was not only my office mate, but a great friend, that inspired me with her dedication, patience, and love for her work.

Lastly, I would like to thank and dedicate this work to my inspiration, force, and motivation: my family. Giovanni, for his unconditional support, encouragement and love in any new adventure I undertake, for being the best friend that I could have never imagined, and my greatest motivation. My parents, Mauro and Elsa, who awoke in me a passion for science and learning, who motivated me to reach higher and break stereotypes, who with their example, their words, their work, selflessness and faith, taught me that everything we put our time into should have a higher purpose and leave lasting marks in ourselves and those around us, and without whom this thousand mile, 5 year journey in France would have not been possible. And finally, I would like to thanks my sisters and brother (Ana Jose, Gaby, Andres),

for their support, for believing in me, bringing me joy, and so many other reasons. Thank you!

Contents

List of Figures **xiii**

List of Tables **xvii**

Chapter 1 Introduction **1**

Chapter 2 Muscle-based control: virtual characters and humans **5**

2.1 Control of virtual characters actuated by muscles 6

2.1.1 Modeling and simulating muscle-based characters 9

2.1.1.1 Skeletal modeling 9

2.1.1.2 Muscle modeling 10

2.1.1.3 Simulating the dynamics of muscle-based characters 13

2.1.2 Muscle-based control in animation and the challenge of redundancy 15

2.1.2.1 Optimization 15

2.1.2.2 Motor control laws 16

2.1.2.3 Controller optimization methods 18

2.1.2.4 Trajectory optimization methods 20

2.1.3 Conclusion 26

2.2 Muscle synergies as low-dimensional representations of human motion control 27

2.2.1 Synergy models 27

2.2.2 Synergy extraction process 30

2.2.3 Evidence of muscle synergies 32

2.2.4 Conclusion 36

2.3 Conclusion 37

Chapter 3 Identification of kinematic features and synergies in overhead throwing **39**
3.1 Biomechanics of overhead throwing . . . 39
3.2 Experimental setup and data processing . . . 41
3.2.1 Subjects . . . 41
3.2.2 Task . . . 41
3.2.3 Data acquisition and processing . . . 42
3.2.4 Data selection . . . 43
3.3 Kinematic features identification . . . 44
3.3.1 Definition . . . 44
3.3.2 Extraction . . . 45
3.4 Synergy models identification . . . 46
3.4.1 Definition . . . 46
3.4.2 Extraction . . . 47
3.5 Identifying representative kinematic and control features . . . 48
3.5.1 Kinematic feature identification ($\mathbf{f}_{T,All}$) . . . 51
3.5.2 Control feature identification (W_{All}, $\overline{C}_{All}$) . . . 51
3.6 Results . . . 52
3.6.1 Methodology and muscle set validation . . . 52
3.6.2 Representative kinematic and control strategy for overhead throwing . . . 61
3.6.2.1 Representative kinematic strategy . . . 61
3.6.2.2 Representative control strategy . . . 63
3.7 Conclusion . . . 71

Chapter 4 Muscle synergies as control functions for virtual characters **73**
4.1 A synergy-driven forward dynamics pipeline for overhead throwing . 75
4.2 Character modeling . . . 76
4.3 Muscle parameter adaptation (Offline) . . . 78
4.4 $c_i(t)$ optimization and filtering (Online) . . . 80
4.5 Results . . . 81
4.5.1 5-synergy driven motion . . . 83
4.5.2 2-synergy driven motion . . . 86
4.5.3 5-synergy versus 2-synergy driven motion . . . 88
4.6 Limitations . . . 89
4.7 Conclusion . . . 90

Chapter 5 Conclusions and perspectives **93**
5.1 Summary and contributions . . . 93

5.2 Open issues and perspectives 94

Appendix A Synopsis of muscle-based control in animation 97
A.1 Muscle-based controllers 97
A.2 Cost functions 104

Appendix B Data acquisition details 107

Appendix C Character modeling details 111

References 113
Thesis related publications 113
Bibliography 113

List of Figures

2.1 A muscle-based control framework in a physics-based simulation 6
2.2 Examples of muscle-based characters in animation 9
2.3 A biomechanical upper limb model 10
2.4 Commonly used musculotendon model for musculoskeletal simulations . 11
2.5 Force generation capacity of muscles 12
2.6 Muscle reflex models for locomotion generation 17
2.7 Controller optimization methods 18
2.8 Trajectory-optimization methods 21
2.9 Concept of time-invariant synergies 28
2.10 Concept of time-varying muscle synergies 29
2.11 Evidence of muscle synergies in postural control tasks 34

3.1 An overhead throwing motion and its main stages 40
3.2 Experimental setup 41
3.3 EMG electrodes and reflective marker placement 42
3.4 Kinematic features in the task space 45
3.5 Example of a dendrogram 50
3.6 Activation reconstruction quality across synergy models per muscle set . 53
3.7 Synergy vectors $\mathbf{w}_i$ per muscle set 55
3.8 Average synergy combination coefficients $\bar{c}_i(t)$ per muscle set 57
3.9 Average energy of combination coefficients $c_i(t)$ per throwing distance . 58
3.10 Task space features per throwing distance 58
3.11 Activation reconstruction of the muscles in Set_6 and Set_8 (7m throw) . 60
3.12 Activation reconstruction of the muscles in Set_{11} and Set_{14} (7m throw) 60
3.13 Task space features per subject and throwing distance 61
3.14 Task space cluster separation quality using k-means 62
3.15 Task space cluster separation using hierarchical clustering 62

3.16 Representative task space strategy for all subjects ($\mathbf{f}_{T,All}$) 63
3.17 Activation reconstruction quality across synergy models per subject . . 64
3.18 Representative control strategy (synergies) W_{All} and W_{kmeans} for all subjects 65
3.19 Synergy cluster separation quality using k-means 66
3.20 Synergy clusters using hierarchical clustering 66
3.21 Average combination coefficient $c_1(t) \in C_{All}$ per subject at each throwing distance 67
3.22 Average combination coefficient $c_2(t) \in C_{All}$ per subject at each throwing distance 68
3.23 Representative control strategy (combination coefficients) $\overline{C}_{All}$ for all subjects 68
3.24 $c_i(t)$ triggering order and co-activation per subject and throwing distance 69
3.25 $c_i(t)$ energy per subject and throwing distance 70
3.26 Example 1: Activation reconstruction using W_{All} and C_{All} 71
3.27 Example 2: Activation reconstruction using W_{All} and C_{All} 71

4.1 A general synergy-driven forward dynamics pipeline using *synchronous time-invariant synergies* 74
4.2 A synergy-driven forward dynamics pipeline for overhead throwing . . . 76
4.3 Full body skeletal model and musculoskeletal arm model 77
4.4 Musculotendon geometric model 77
4.5 5-synergy model 82
4.6 2-synergy model 82
4.7 5-synergy model: Synergy-driven motion without muscle parameter adaptation 83
4.8 5-synergy model: Synergy-driven motion with adapted muscle parameters 84
4.9 5-synergy model: Synergy-driven motion after muscle parameter adaptation and $c_i(t)$ optimization and filtering 85
4.10 5-synergy model: Initial coefficients ($c_i(t)$) and coefficients after optimization and filtering ($c_{i_{new}}(t)$) 85
4.11 2-synergy model: Synergy-driven motion without muscle parameter adaptation 86
4.12 2-synergy model: Synergy-driven motion with adapted muscle parameters 87
4.13 2-synergy model: Synergy-driven motion after muscle parameter adaptation and $c_i(t)$ optimization and filtering 87
4.14 2-synergy model: Initial coefficients ($c_i(t)$) and coefficients after optimization and filtering ($c_{i_{new}}(t)$) 87

4.15 Cross-correlation between the initial coefficients $c_i(t)$, and the optimized and filtered coefficients $c_{i_{new}(t)}$ for both synergy models 89

B.1 Reflective marker placement 110

List of Tables

3.1 Recorded muscles 42
3.2 Muscle sets for synergy extraction 44
3.3 Assessment of k-means clustering quality 49
3.4 Similarity between the synergies extracted from different muscle sets . . 56
3.5 Similarity between the synergies in Set_6 and higher order sets 56
3.6 $\overline{c}_i(t)$ repeatibility across throwing distances 57
3.7 $c_i(t)$ inter-subject comparison at each throwing distance 68
3.8 $c_i(t)$ inter-subject and inter-distance comparison 69

4.1 Synergy models used as input control functions for the pipeline 82
4.2 Quality of motion reconstruction 88

A.1 Main muscle-based controllers for animation 99
A.2 Neuromuscular objectives used in animation 105

B.1 Recorded muscles and their function 107
B.2 Recorded markers and their placement 108

Chapter 1

Introduction

CONTROLLING virtual characters is the art of bringing them to life. The art of granting them with the ability to move and perform a variety of motor tasks, similarly to humans. An essential component behind this is the character's motion controller, which transforms desired tasks into synthesized motions. The way these controllers are designed is being profoundly transformed through the integration of knowledge from biomechanics, which motivates the idea of using more detailed character models, inspired by the human musculoskeletal system. This has triggered a transition from classical servo-based characters to muscle-based characters in physics-based control applications within domains that range from rehabilitation to animation. For instance, muscle-based characters are used in rehabilitation applications to teach patients how to use virtual prosthetics before using real ones [SALC03], in biomechanics to simulate and examine pathological gait patterns [HZN+06], and finally, in animation to synthesize motions that are closer to human motions at a kinematic and dynamic level [CRPPD16] .

The advantages of using these character models derive from the non-linear properties of muscles, which result in: better stability and realistic passive dynamics [GvdBHZ98, GvdPvdS13], physiologically feasible motions, better estimates of energy or fatigue [WHDK12], a mechanical system able to perform control functions by itself [GH10], and an ease to simulate musculoskeletal defects, pathologies and physical fatigue [LPKL14]. Nevertheless, more detailed character models also imply new control challenges, such as actuation redundancy. A challenge that is addressed in this thesis.

Redundancy occurs when a character possess more actuators than needed to perform a specific task. This means that there exist numerous ways to actuate and control the character which achieve the same motion. This complicates the task of the motion controller because it needs to choose one of these solutions to coordinate all actuators and achieve the task successfully. In the case of muscle-

based characters, this problem escalates due the fact that muscles unlike servos, are not only non-linear, but also unidirectional actuators, and thus, at least two of them are needed to rotate each degree of freedom (DoF).

Therefore, the challenge of actuation redundancy raises some important questions: How to control muscle-based characters efficiently? Is it possible to avoid control redundancy in spite of actuation redundancy? Or in other words, is it possible to use a reduced number of control variables, in spite of a large number of actuators? Humans are by far the best example of how complex musculoskeletal systems are managed fast, intuitively, and efficiently in simple and complex motions. Thus, the answer to the above questions could lie in understanding and replicating human motor control strategies.

A popular motor control strategy, which is widely investigated in the domain of neuroscience, is the theory of muscle synergies. This theory assumes that to perform a task, the central nervous system (CNS) first transforms task goals into a few modules or synergies, which encode the activation information of groups of muscles. By combining these modules in a task-dependent fashion, the CNS is able to generate a large number of activation signals for different motor tasks [ADN+13]. In other words, according to this theory, synergies are the reduced number of variables, that the CNS uses to control the numerous muscles of the human musculoskeletal system. The existence of this elementary control variables, and their modulation with respect to different task goals and kinematic features (or variables characterizing the motion) has been evidenced by a variety of studies. Some authors have shown that in reaching motions, synergies are modulated according to the movement direction [dPFL06, dFPL08, MBdF10]. Others have discovered that postural responses can be encoded in synergies that are modulated according to the perturbation direction [TOT07] and the kinematics of the subject's center of mass [ST11]. While others have found that locomotion can be characterized through synergies that are linked to foot kinematics [IGZ+03, IPL04].

In this work synergies are used as the reduced number of control variables needed to command the numerous muscles of a virtual character. This is achieved through two stages: a motion analysis and a motion generation stage. The motion analysis stage consists in identifying kinematic features and synergies from humans, while the motion generation stage consists of a synergy-driven forward dynamics pipeline to adapt these synergies to a set of kinematic goals and a muscle-based character. To challenge both the pipeline and the muscle synergy theory, this approach was be applied and tested on overhead throwing motions. A task that has not been studied through the synergy theory, and is known for being highly redundant, nonlinear, and hyper dynamic (high velocities and momentum) [KXY+10], requiring coordination, accuracy, and skill.

By presenting a synergy-based solution from a motion analysis and motion generation point of view, and testing it on a such a dynamic motion, this thesis has two main contributions : 1) a contribution to the validation of the muscle synergy theory by using it to study a new motion, and challenging it with the control of a virtual character, and 2) a contribution to the variety of domains involving physical simulations with muscle-based characters (e.g, rehabilitation, animation) by proposing a control solution that reduces redundancy.

First, Chapter 2 begins with a review of muscle-based control frameworks and one of their main challenges: redundancy (Section 2.1). This review is then complemented with an overview of muscle synergies as a redundancy reduction mechanism in humans, evidencing their potential for the control of virtual characters (Section 2.2). The first contribution of this thesis is then presented in Chapter 3, where overhead throwing motions are analyzed, and low-dimensional control strategies are extracted. These results evidence that only two synergies are necessary to encode the important activation trends of different muscle sets during the execution of this motion, and that these control variables are modulated according to the throwing distance. Next, the second contribution is presented in Chapter 4, where the previously extracted synergies are used as input control functions in a synergy-driven forward dynamics pipeline. This pipeline adapts the synergies to the distinct dynamics of a muscle-based character and a set of kinematic goals. The results evidence the feasibility of this solution for reducing redundancy, by showing that motion can be reproduced using only two synergies as control variables, while preserving important characteristics in the original synergies. Finally, in Chapter 5 the previous contributions are summarized and future perspectives are discussed, such as the extension of the pipeline to a variety of character morphologies by using generic synergy models, and to other motions through the construction of synergy databases.

Chapter 2

Muscle-based control: virtual characters and humans

MUSCLE-BASED control is related to the study of how muscles are controlled to generate motion. One of its uses is the reproduction or synthesis of motions using muscle-based virtual characters in physically-simulated environments. This encompasses a variety of applications, such as rehabilitation through virtual prosthetics, simulation and examination of pathological motions, and animation.

The interest in using muscle-based characters in these applications is due to the advantages, in terms of control and quality of the resulting motion, that stem from the non-linear properties of muscles, such as: better stability and realistic passive dynamics, physiologically feasible motions, better estimates of energy or fatigue, a mechanical system able to perform control functions by itself, and an ease to simulate musculoskeletal defects, pathologies and physical fatigue. However, despite these advantages, one of the major challenges of using these characters is handling actuation redundancy, or choosing how to coordinate a high number of non-linear actuators to generate the desired motion.

Humans are by far the best example of how this redundancy is managed fast and efficiently. Thanks to a powerful CNS, humans are capable of planning motions fast, intuitively, an efficiently, regardless of having to coordinate numerous muscles simultaneously. Thus, the answer to handling actuation redundancy efficiently in virtual characters, may lie in a study of human motor control. In this context, this chapter presents an overview of muscle-based control for virtual characters (Section 2.1), and a human motor control theory with a great potential to address one of its main challenges, actuation redundancy (Section 2.2).

2.1 Control of virtual characters actuated by muscles

The control of virtual characters actuated by muscles or muscle-based characters, can be essentially described as the control of a dynamical system. In general, such systems can be represented as:

$$\dot{\mathbf{x}} = f(\mathbf{x}(t), t) + g(\mathbf{x}(t), t)\mathbf{u}(t) \tag{2.1}$$

$$\mathbf{y}(t) = h(\mathbf{x}(t)) \tag{2.2}$$

Where t is the time variable, $\mathbf{x}(t)$ is the system's state variable, $\mathbf{u}(t)$ is the system's control input, and $\mathbf{y}(t)$ is the system's output or controlled variable at time t. The controlled variable is function of the system's state. It can consist of attaining a desired value at a specific instant ($\mathbf{y}(t_f) = \mathbf{y}^d$ where t_f is the desired reaching time) or tracking a desired trajectory ($\mathbf{y}(t) = \mathbf{y}^d(t)\ \forall\ t$, where $\mathbf{y}^d(t)$ is the trajectory to be tracked). In the case of a muscle-based control framework the system is a virtual character which is commanded by muscle-based controller, as shown in Figure 2.1.

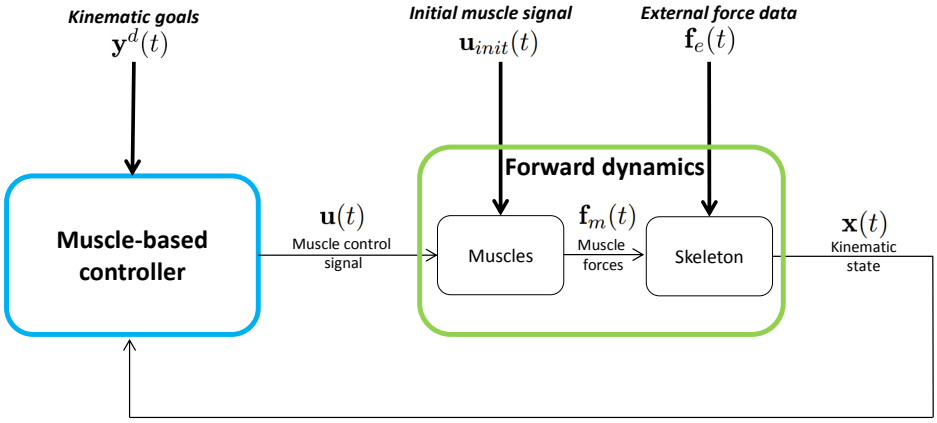

Figure 2.1 – **A muscle-based control framework in a physics-based simulation.**

The character's state ($\mathbf{x}(t)$) usually includes kinematic variables (e.g., joint positions $\mathbf{q}(t)$, velocities $\dot{\mathbf{q}}(t)$) but muscle variables (lengths and velocities of shortening or lengthening) may also be included. This state is updated according to the external forces ($\mathbf{f}_e(t)$) in the environment (e.g., gravity, force perturbations) and internal forces ($\mathbf{f}_m(t)$) in the character (muscle forces) in a *forward dynamics simulation*, as shown in Equation 2.6, Section 2.1.1.3. The internal forces or muscle forces are generated by a muscle-based controller, which produces muscle control signals ($\mathbf{u}(t)$) according to kinematic goals ($\mathbf{y}^d(t)$). The control signals can consist of excitations, activations, or forces, while the kinematic goals can consist of a single value (e.g., a

locomotion speed, joint configuration), or an entire trajectory (e.g., hand trajectory, joint trajectory).

Using these frameworks is interesting for motion generation due to the advantages (at the kinematic and control level) that come with the use of muscle-based characters. The non-linear properties present within the muscles, such as the force-length and force-velocity relationships (Section 2.1.1) imply:

- **Stability and realistic passive dynamics:** The musculoskeletal system is able of achieving passive adjustments and these adjustments are robust across certain changes in the environment and perturbations [vdKdGF+09]. This is due to the fact that the non-linear properties of muscles grant the body with a first defense to counteract mechanical perturbations [HR11]. Their presence gives place to adjustments such as *preflexes*, which are mechanical responses that precede stretch reflexes when a muscle is activated.

  The authors of [GvdBHZ98], investigated to what extent these properties contributed to the recovery from perturbations during locomotion by using different models with different actuators: servos, muscle models, and models without force-length and force-velocity relationships. They concluded that the character actuated by muscle models (with both properties) had substantially better resistance to both static and dynamic perturbations (gravity and impulsive forces). The role of these properties has also been investigated in the control of explosive movements, such as vertical jumping [vSB93]. The authors concluded that the force-length-velocity properties of muscles were responsible for a reasonable performance when small perturbations were applied to the initial position of the skeletal system (segment angle perturbations).

- **Physiological feasible motions and better energy estimates:** The inclusion of muscles motivates physiologically feasible motions. An example of this can be found in [KSK00], where the physiological infeasibility of interpolating user-input postures was shown, and it was later reduced based on muscle dynamics. Muscles also provide better estimates of energy expenditure, which is a popular quantity used to synthesize motions in physics-based animation in general. In [WHDK12], visual, kinematic, and dynamic comparisons evidenced that walking motions synthesized via energy estimates using muscles were closer to real human data than the estimates based on torques. Recently, comparisons have also been made between servo-based and muscle-based simulations of human swimming [Si13]. The former yielded plausible results but high control gains and a smaller numerical time step were necessary.

- **Control via motion mechanics:** Thanks to the presence of muscles, the mechanical system of the character is granted with the ability to accomplish control functions, not only for counteracting perturbations, but also for tasks such as human walking. For instance, instead of trying to create control models that mimic complex neural circuits (for either servo or muscle-based characters), biomechanisists have discovered that locomotion requires little control if certain principles of legged mechanics are used. In [GH10], these principles were encoded as muscle reflexes, which were used to reproduce human walking without any higher level controller. These reflexes were inspired in spinal reflexes, which link sensory information directly into muscle activations, bypassing the inputs from the central nervous system (such reflexes will be further described in Section 2.1.2). Other authors have demonstrated that specific mechanical behaviors observed during walking can be encoded in a single, simple muscle reflex [PGB97, GSB03]. Nevertheless, more evidence of the performance of such legged mechanics principles, in terms of walking on uneven terrain and in various directions, is still needed. This evidence is important to show the extent to which reflexes can deal with such tasks without a higher level controller.

- **Ease to simulate musculoskeletal defects, pathologies, and physical fatigue:** Another advantage of muscle-based control is the fact that muscles provide a natural solution to simulate musculoskeletal defects, pathologies, and physical fatigue. By taking into account an anatomical structure (musculoskeletal system), it is easier to simulate phenomena that derive from this structure. For instance, fatigue and recovery muscle models can be used to simulate a motion where a human gradually gets tired [KSK00] by limiting the maximal force that the muscle can produce with respect to the history of muscle force [GML93, GML96]. Cost functions that minimize the force of a specific muscle can be used to synthesize motions with pain avoidance behaviors [LPKL14]. Changing muscle parameters and properties such as maximal strength, can be used to weaken muscles, and generate well known pathologies and defects [WHDK12]. Finally, injuries can also be simulated by displacing muscles [KSK00].

These advantages highlight the potential of muscle-based control frameworks for motion generation. However, using these frameworks also implies solving an important challenge: actuation redundancy. Redundancy occurs when a character possess more actuators than needed to perform a specific task. As will be seen in Section 2.1.1, muscle-actuated virtual characters are actuated by numerous muscles per DoF, which results in over-actuation or the fact that there may exist several

muscles with the same actions per DoF. This means that there exist numerous actuation solutions or control signals $\mathbf{u}(t)$ which achieve the same motion. It is the task of the motion controller to choose one of these solutions to achieve the kinematic goals $\mathbf{y}^d(t)$ successfully.

To better understand these advantages and challenges, the following sections describe the different components in muscle-based control frameworks (Figure 2.1) in detail. Section 2.1.1 explains how to model and simulate muscle-based characters, and Section 2.1.2 presents a review of muscle-based control methods in the domain of animation, previously presented in [CRPPD16].

2.1.1 Modeling and simulating muscle-based characters

Muscle-based characters are composed of a skeletal system and an actuation system (muscular system), as shown in Figure 2.2. Describing the skeletal system involves specifying the joints and segments, along with their respective masses and inertias. Describing the actuation system involves specifying the muscles, their properties, and interactions with the different joints.

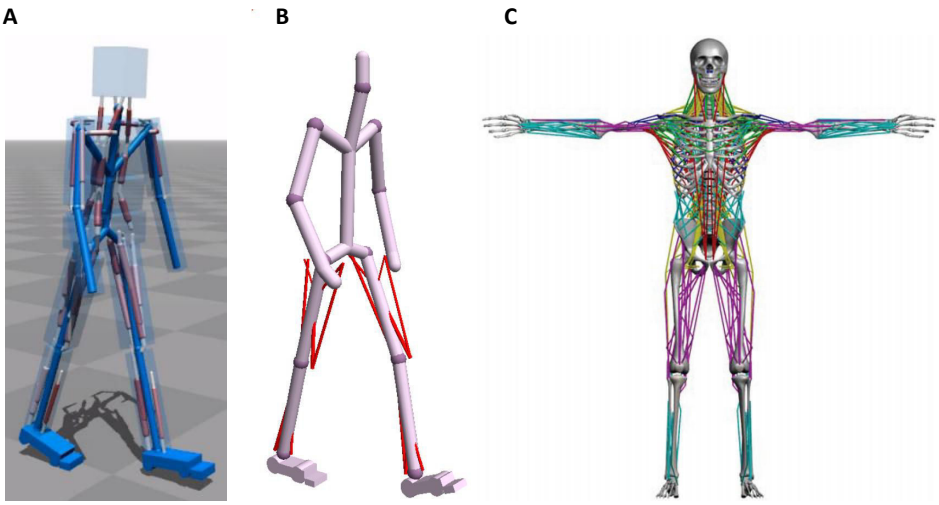

Figure 2.2 – **Examples of muscle-based characters in animation**. Muscle-based characters in (A) [GvdPvdS13], (B) [WHDK12], and in (C) [SLST14].

2.1.1.1 Skeletal modeling

Describing the skeletal system involves specifying the kinematical chains in the character's body. In biomechanics, skeletal models are often anatomically based [WSA+02, WvdHV+05] and exhibit a high level of detail as they have to be accurate enough to provide clinically relevant biomechanical quantities [CMD16]. Thus, in many cases, kinematical closed chains are used, which make both kinematics and

dynamics studies more complex [PSVV07, VDH94]. In other fields, such as animation, simple chains with functional degrees of freedom (e.g., the resulting motion of the anatomical ones) and segments that directly link their articular centers are implemented.

A complete description of these kinematical chains, also implies specifying the lengths, masses, and inertias of all of their segments. In biomechanics, as motion is generally recorded to be analyzed (using tracking or motion capture systems that allow the estimation of joint kinematics [DCD10, MS14]), the lengths of the segments are computed from marker positions [LAdZR11, MGPD15]. If this information is not available, regression laws based on cadaver measurements [Dem55] are used. Cadavers measurements can also be used to scale the masses and inertias of the model [dL96, DCV07]. However, advances in medical imaging, (e.g., scanner or MRI scanners) opened the door to subject-specific scaling of musculoskeletal models and showed interesting perspectives for clinical applications [BAGD07]. Moreover, other approaches have emerged which rely only on exterior measurements of the body, such as 3D point clouds, to determine subject-specific bone geometry and motion [ZHK15]. However, in spite of these advances, in animation applications these parameters are determined manually or through optimizations [GvdPvdS13, HMOA03].

2.1.1.2 Muscle modeling

Specifying the actuation system of muscle-based characters implies choosing a muscle model, its properties, and describing its interactions with the skeletal system. Historically, virtual characters have been actuated by servos Figure 2.3 (left).

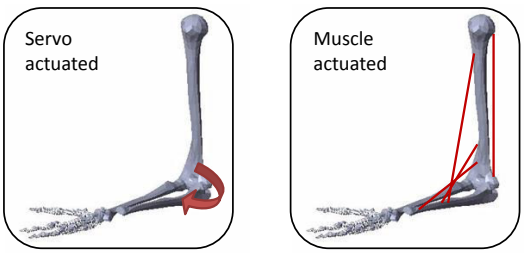

Figure 2.3 – **A biomechanical upper limb model [CRPPD16]**. On the left, the elbow is actuated by a virtual servo. On the right, the elbow is actuated by muscles.

However, progressively, muscles have been incorporated as non-direct actuators of the joints. Early implementations consisted of mass-spring systems. Contrary to the usual angular-spring dampers and PD-controllers, these systems (like muscles) are non-direct actuators of the joints. Meaning, they produce first forces, not torques, which interact with the skeletal system to produce motion. Like muscles, these systems use force action lines, determined by their insertion or attachment

site to the skeletal structure. Nevertheless, nowadays, more faithful muscle representations, such as biomechanical muscle models, are actively incorporated into virtual characters.

A popular choice is the Hill muscle model [Hil38]. Although this model was developed decades ago, its current usefulness is evidenced by its various adaptations and implementations within the biomechanics and animation community. These adaptations have come to be known as Hill-type models, such as the Hill-Stroeve model [Str96], and the widely used adaptation made by [Zaj89] for numerical simulations. As shown in Figure 2.4, the model consists of a contractile element CE (non-linear visco-elastic relationship) in parallel with a passive element PE (non-linear spring). The contractile element represents the active tension, or forces, created by the contractile proteins in the muscle, while the passive element represents the passive tension or the force that results from the elongation of the connective tissue components in the musculotendon unit. The tendon is represented by a serial non-linear spring SE of length l_t, α represents the pennation angle or the orientation of the fibers with regard to the tendon, l_m represents the muscle length, and l_{mt} the length of musculotendon unit. The length l_{mt} is computed by adding the muscle l_m and tendon l_t lengths. This model has been widely used even if the numerous parameters necessary to completely define its behavior are difficult to obtain in vivo [HKVdH+07].

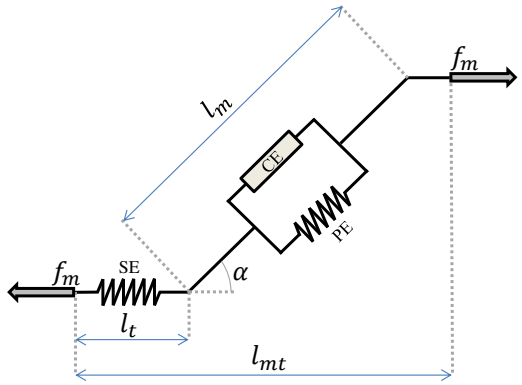

Figure 2.4 – **Commonly used musculotendon model for musculoskeletal simulations [CRPPD16]**. Inspired from [Zaj89, EMHvdB07].

The muscle force f_m generated by a musculotendon unit j can be summarized as the sum of the contractile and passive forces:

$$f_{mj} = [f_p(\bar{l}_m) + a_j \cdot f_l(\bar{l}_{mj}) \cdot f_v(\dot{\bar{l}}_{mj})] \cdot f_{0j} \tag{2.3}$$

where f_p is the passive force relationship, a_j is the muscle activation, f_l is the force-length relationship, f_v the force-velocity relationship, f_{0j} the maximum

isometric force, and $\bar{l}_{mj}$ the normalized length of the muscle unit (normalization is usually made using the resting length of the muscle). Several models have been proposed to approximate the f_l and f_v relationships with regard to experimental data [RAPC10]. Example models are presented in Figure 2.5. The force-length relationship documents how muscle force varies at different muscle lengths, and it is related to the "Sliding Filament Theory": at a microscopic level, muscle fibers are composed of smaller structures called actin and myosin filaments that make bindings to form muscle contractions. Peak muscle force can be generated when most of these bindings or cross-bridges are created. This event corresponds to the resting length of the muscle (usually near the middle of the range of motion) [Knu07]. The force-velocity relationship explains how the force of fully activated muscle varies with velocity. It states that the force the muscle can create decreases with increasing velocity of shortening (concentric actions), while the force the muscle can resist increases with increasing velocity of lengthening (eccentric actions) [Knu07].

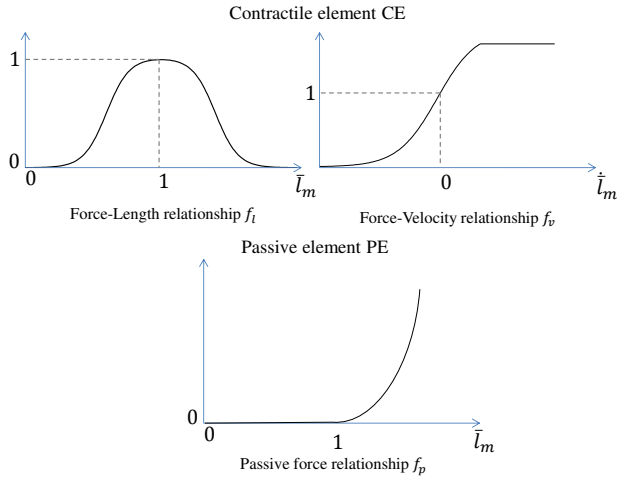

Figure 2.5 – **Force generation capacity of muscles [CRPPD16]**. Inspired by [RAPC10, EMHvdB07].

The tendon force f_{tj}, or output of the musculotendon unit, is obtained by taking into account the pennation angle:

$$f_{tj} = f_{mj} \cdot \cos \alpha_j \tag{2.4}$$

However, in many studies the pennation angle is neglected. Complete dynamics of the musculotendon unit also includes the activation dynamics, which describes the non-linear temporal relationship between the neural excitation e_j and the effective activation a_j of the muscle [BLMB04]. In many works [VYN05, VYN06, PD09], this non-linear relationship is approximated by a differential equation, exhibiting different time constants for activation and deactivation:

$$\dot{\gamma}_j = (e_j - \gamma_j)/\tau_{ne}$$

$$\dot{a}_j = \begin{cases} (\gamma_j - a_j)/\tau_{act} & , \quad e \geq a \\ (\gamma_j - a_j)/\tau_{deact} & , \quad e < a \end{cases} \tag{2.5}$$

Where e_j is the neural excitation, a_j the muscle activation, γ_j an intermediate variable, τ_{ne} the neural excitation constant time (often neglected), and τ_{act} and τ_{deact} the activation and deactivation time constants respectively. In animation, activation dynamics is sometimes modeled using equal activation and deactivation time constants [GvdPvdS13, WHDK12].

Once the functional model is chosen, its interactions with the skeletal system are given by the chosen muscle geometry. This geometry involves specifying the attachment sites of the muscles to the skeleton (origin and insertion points), and their shapes (or routing). The muscle routing can consist of straight lines between attachment points, or more complex paths specified using via points [HMD05]. This routing allows to compute the direction of the muscle forces, their moment arms in different kinematic positions, and finally the torques they exert on a given DoF.

Finally, other muscle models exist which describe specific functional characteristics (such as fatigue [SCSB16, SCMB15]), visual characteristics (such as muscle deformation) or both functional and visual characteristics [LGK+10]. The latter models offer a next level of fidelity. However to this date they are not usually used for the control of virtual characters due to the fact that they would render the control computationally expensive.

2.1.1.3 Simulating the dynamics of muscle-based characters

To simulate a muscle-based virtual character as in the framework in Figure 2.1, a dynamic simulation needs to constructed describing the relationship between the different variables in Equation 2.1. That is, the relationship between the character's state ($\mathbf{x}$), the control variables ($\mathbf{u}$), and the external forces in the environment ($\mathbf{f}_e$). The character's state consist of joint positions and velocities ($\mathbf{x} = (\mathbf{q}, \dot{\mathbf{q}})$), while the control variables include muscle forces or activations ($\mathbf{u} = \mathbf{f}_m$ or $\mathbf{u} = \mathbf{a}$).

For a character with $nDoF$ degrees of freedom and D muscles, this relationship is given by Newton's second law of motion, that can be expressed as [Pan01]:

$$M(\mathbf{q})\ddot{\mathbf{q}} + C(\mathbf{q}, \dot{\mathbf{q}})\dot{\mathbf{q}} + \mathbf{g}(\mathbf{q}) + R(\mathbf{q})\mathbf{f}_m(\mathbf{a}, \mathbf{f}_o, \mathbf{l}_m, \dot{\mathbf{l}}_m) + \mathbf{f}_e = 0 \tag{2.6}$$

The variables in the above equation are time dependent, however for simplicity this time dependency was omitted. Furthermore, in Equation 2.6, $M(\mathbf{q})$ is the

mass matrix of the system that gathers masses and inertias of all the segments ($nDoF \times nDoF$), $\ddot{\mathbf{q}}$ is the vector containing the joint accelerations ($nDoF \times 1$), $C(\mathbf{q}, \dot{\mathbf{q}})\dot{\mathbf{q}}$ represents the coriolis and centrifugal effects ($nDoF \times 1$), $\mathbf{g}(\mathbf{q})$ represents the vector of gravity torques ($nDoF \times 1$), and $\mathbf{f}_e$ represents the external forces. Finally, $R(\mathbf{q})\mathbf{f}_m$ represents the action of the muscles on the joints (muscular joint torques, $nDoF \times 1$) , where $R(\mathbf{q})$ is the matrix containing the muscular moment arms ($nDoF \times D$) and $\mathbf{f}_m$ are the muscle forces ($D \times 1$), which are function of the muscle activations ($\mathbf{a}$), maximal forces ($\mathbf{f}_o$), lengths ($\mathbf{l}_m$), and velocities of shortening or lengthening ($\dot{\mathbf{l}}_m$). In a dynamics simulation, such quantities can be automatically constructed by using algorithms such as the ones developed in [Fea14].

From equation 2.6, two different problems can be derived: the *forward dynamics* problem and the *inverse dynamics* problem. The muscle-based control framework in Figure 2.1 is based on a forward dynamics simulation. This kind of dynamic simulation involves generating control variables, muscle forces ($\mathbf{f}_m$) or activations ($\mathbf{a}$), to synthesize (or reproduce) a desired motion. The equation to solve in this case, issued from equation 2.6, can be written as follows:

$$\ddot{\mathbf{q}} = M^{-1}(\mathbf{q})(-C(\mathbf{q}, \dot{\mathbf{q}})\dot{\mathbf{q}} - \mathbf{g}(\mathbf{q}) - R(\mathbf{q})\mathbf{f}_m(\mathbf{a}, \mathbf{f}_o, \mathbf{l}_m, \dot{\mathbf{l}}_m) - \mathbf{f}_e) \tag{2.7}$$

The forward dynamics problem is usually incorporated in a physics simulation involving collision detection algorithms (that provide external forces to apply to the system) and a numerical integration (e.g., Runge-Kutta methods) to obtain the current system state ($\mathbf{q}, \dot{\mathbf{q}}$) from the computed accelerations ($\ddot{\mathbf{q}}$).

On the other hand, inverse dynamics simulations involve computing control variables, muscle forces or activations, from a recorded or specified motion, as follows:

$$R(\mathbf{q})\mathbf{f}_m(\mathbf{a}, \mathbf{f}_o, \mathbf{l}_m, \dot{\mathbf{l}}_m) = -(M(\mathbf{q})\ddot{\mathbf{q}} + C(\mathbf{q}, \dot{\mathbf{q}})\dot{\mathbf{q}} + \mathbf{g}(\mathbf{q}) + \mathbf{f}_e) \tag{2.8}$$

In this approach a specified motion and external forces are applied to a musculoskeletal model and then the forces or activations that generate the recorded motion are computed. This equation is usually solved thanks to the Newton-Euler algorithm [Win05, Fea14, RHWZ08], which considers each segment separately from distal to proximal, or more robust methods considering closed loops [Kuo98, vdBS08]. Such simulations are used mainly for motion analysis, however they can also be used to generate new motions (e.g., fatigued or injured motions) by replaying the computed muscle forces while altering muscle parameters [KSK00, WHDK12, LPKL14].

2.1.2 Muscle-based control in animation and the challenge of redundancy

An important component of muscle-based control frameworks (Figure 2.1) is the muscle-based controller. The main task of this controller is choosing an optimal actuation solution that allows the character to achieve a desired task. Determining this is especially difficult due to the fact that musculoskeletal models exhibit actuation redundancy that leads to numerous actuation solutions, as there are less equations (dynamics equations) than unknowns (muscle signals). These models may also exhibit underactuation, which stems from the fact that a single muscle can actuate several joints simultaneously, such as bi-articular muscles.

The next sections detail how these challenges are solved in a domain known for its interest and contributions in the control of virtual characters: animation. First, important tools to construct muscle-based controllers will be presented in Sections 2.1.2.1 and 2.1.2.2, and finally a classification and description of state of the art controllers will be given in Sections 2.1.2.3 and 2.1.2.4.

2.1.2.1 Optimization

The optimization can either directly compute the muscle actuation signals or optimize a motor control law that produces such signals. In any case, the optimization consists in minimizing a cost function ($f(X)$) encoding motion goals, and/or bio-inspired objectives that motivate natural motion. It is usually formulated through a non-linear constrained optimization problem:

$$\text{Find } X \text{ which minimizes } f(X) \tag{2.9}$$

$$\begin{gathered}\text{subject to,} \\ \alpha_i(X) \leq 0, i = 1, 2, ..., m \\ \beta_k(X) = 0, k = 1, 2, ..., p\end{gathered}$$

Where the constraints enforce that:

- the actuation signals (i.e muscle forces, activations, or excitations) achieve the kinematic goals;
- the muscles are only pulling and they have physiological-based force limits (positive muscle forces);
- the actuation signals may respect any additional set of unilateral (α) or bilateral constraints (β), such as nonnegative muscle activations.

The constraints $\alpha_j(X)$ and $\beta_k(X)$ may be specified as hard constraints (as in the formulation above), or as soft constraints (as additional cost functions). The optimization can be a static or dynamic one (often an optimal control problem [ZDG+96]). A static optimization refers to the process of minimizing or maximizing an objective function at a time instant, while a dynamic optimization refers to the process of minimizing or maximizing an objective function over an interval of time of non-zero duration.

This optimization may contain different cost functions $f(X)$, which can be categorized according to the criterion proposed by [ZW90]. In this categorization a generalized performance criterion was proposed which could contain 3 types of cost functions: task specific objectives (tracking a given trajectory, minimizing jerk), neuromuscular objectives (minimizing muscle stress, neural effort), and bone joint objectives (minimizing contact forces, avoiding certain ranges of motion). Appendix A.2 contains a detailed description and listing of neuromuscular cost functions, which represent one of the novelties of muscle-based control frameworks with regard to servo-based control frameworks.

The neuromuscular and bone joint objectives are usually the same for different tasks. However, the task specific objective is the means by which the user can describe the motion that the character is supposed to perform. This objective can consist in a desired walking speed and direction, or task space and joint trajectories.

The optimization problem is usually solved via popular algorithms such as sequential quadratic programming (SQP) [Rao09, KSK00, ZCCD06, Si13] and simplex methods [GT95, DZS08]. However, recently evolutionary algorithms, such as the covariance matrix adaptation (CMA) [Han06] have also been implemented [HMOA03, WHDK12, GvdPvdS13].

2.1.2.2 Motor control laws

The previously described optimization can either directly compute the muscle actuation signals or be used to optimize a motor control law. These laws are based on motor control findings and theories such as: hierarchical systems, central pattern generators, equilibrium point theory, muscle reflexes, and muscle synergies. The following paragraphs briefly present these theories and their applications in controlling virtual characters for animation.

Hierarchical control systems have been used in animation thanks to studies that outline how the motor system's components or neural organs work together to generate muscle excitations for voluntary and reflexive actions. This hierarchy has inspired multiple level controllers in animation to synthesize breathing motions [ZCCD06].

Another well known motor control model are *central pattern generators (CPGs)*. CPGs are biological neural networks that produce rhythmic patterns without relying on sensory feedback or higher control centers [Hoo01]. The CPG models created by [Tag98, TYS91] for bipedal locomotion are popular in the robotics domain [Ijs08, AT05, AT06, ENMC05] and are also beginning to be present in the world of animation, specifically for the synthesis of swimming [Si13] and walking motions [HMOA03].

Control laws based on the *equilibrium point theory* [Fel66] have also been used for controlling virtual characters [NF02]. This theory argues that the nervous system controls movement through the specification of final equilibrium positions of the limb. The equilibrium trajectory is specified by virtual positions corresponding to variations in muscular activations. These muscle activations move the limb from each real position to the virtual ones in order to generate motion.

Finally, lower level control laws, such as *muscle reflex models* [GH10] have recently been incorporated for muscle-based control [GvdPvdS13, WHDK12]. These models suggest that reflex inputs (which serve as mediators between the CNS and mechanical environment) dominate in contributions to muscle activations during locomotion. Such reflexes are modeled as positive or negative feedbacks of muscle fiber length and force [GSB03] that modulate muscle activation. Figure 2.6 features an example of how these reflex models can be used for generating locomotion patterns.

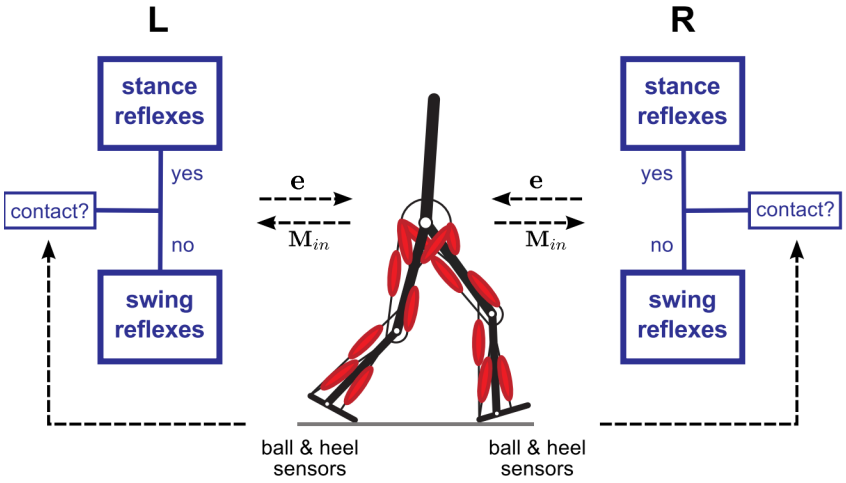

Figure 2.6 – **Muscle reflex models for locomotion generation [GH10]**. An example of muscle reflexes for generating walking motions. A series of reflexes are modeled as positive or negative feedbacks of muscle length and force. These reflexes produce excitations (**e**) the activate the muscles in the left (L) and right legs (R), and move the skeletal system according to the foot contact state. The resulting mechanical inputs M_{in} (e.g., muscle forces, lengths, joint angles) are then re-used by the reflexes to produce new excitations.

2.1.2.3 Controller optimization methods

As seen in the previous section, the main role of a muscle-based controller is to compute a set of muscle signals (excitations, activations, or muscle forces) that allows the character to achieve a desired task. These controllers are usually optimization-based, and when this procedure is used to optimize a bio-inspired control law to produce muscle signals, they can be referred to as *controller optimization methods* [CRPPD16].

Controller optimization methods seek to determine a set of control parameters ($\mathbf{p}$) that will achieve the desired motion goals ($\mathbf{y}^d(t)$) throughout an entire period of time. These parameters depend on the specific control law, but in general they can be summarized as: feedback control law gains (such as PD controller gains, force feedback gains and spring gains) and CPG unit weights.

An overview of such methods is featured in Figure 2.7. The user specifies the kinematic goals ($\mathbf{y}^d(t)$), external forces ($\mathbf{f}_e(t)$), initial control ($\mathbf{u}_{init}(t)$), and also an initial guess of the control parameters ($\mathbf{p}$) and joint trajectories ($\mathbf{x}^d(t)$) that fulfill the task. An optimization procedure continually updates $\mathbf{p}$ and $\mathbf{x}^d(t)$ until the cost function is minimized.

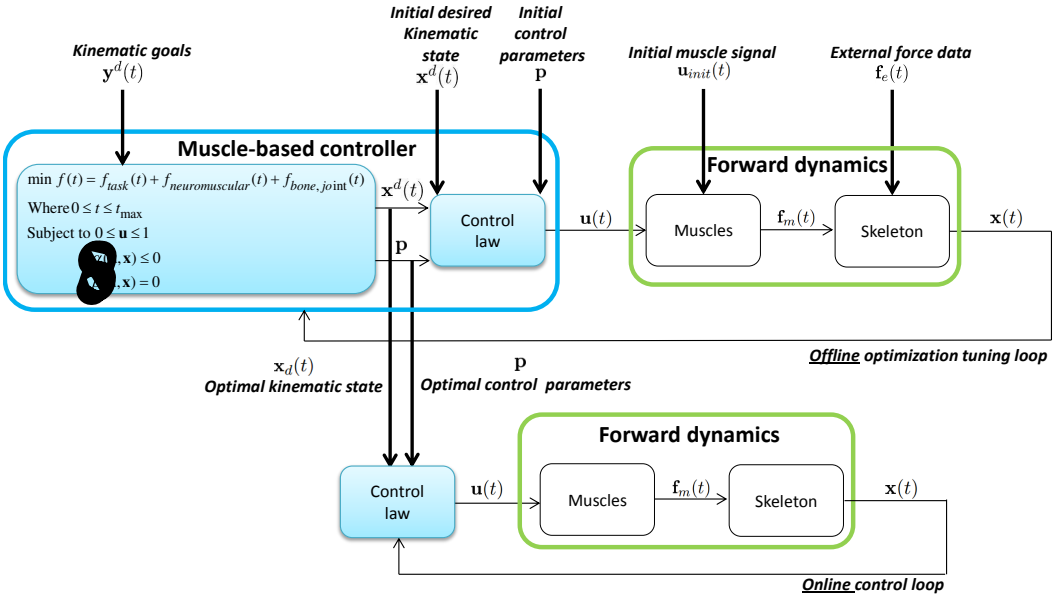

Figure 2.7 – **Controller optimization methods [CRPPD16].** The tuning process, which is usually made over a group of time steps [GvdPvdS13], is iterated until the cost function is minimized or the desired motion is obtained (the tunning process may also consist of a locally weighted regression [Si13] or manual parameter and target specification [NF02]). The optimal parameters and joint trajectories are then used in an online closed control loop. (Note: instead of joint trajectories [WHDK12] desired muscle lengths [Si13] might also be used.)

Once the control parameters and joint trajectories have been determined, the

control law executes online and directly generates the actuation signals that accomplish natural looking motions while satisfying task related objectives. Examples of control laws include, antagonistic control, PD-controllers, muscle reflexes, and neural networks. These laws have been used for generating a variety of motions, that range from locomotion (walking, running, hopping) [GvdPvdS13, WHDK12] to postural adjustments [NF02].

PD controllers and muscle reflexes have been recently used for synthesizing locomotion with humanoids and/or imaginary bipeds [WHDK12, GvdPvdS13] . In these approaches, PD controller gains, and force and length feedback gains were optimized to achieve kinematic goals, such as desired walking speeds. The optimization was based on a muscle effort term, called the rate of metabolic energy expenditure [And99], and soft constraints to track kinematic objectives, and ensure stable gaits. The reflexes [GH10] encoded principles of legged mechanics, such as natural joint compliance in stance phase and dorsiflexion during the swing phase. The PD controllers could either be employed in the task space for different body segments [GvdPvdS13] (inspired in the jacobian transpose control) [SADM94], or for each muscle in the character [WHDK12].

PD controllers have also been used with neural networks for synthesizing periodic swimming motions [SLST14, Si13]. This approach consisted of a high level controller, CPGs, and PD controllers. In this case, the control gains were fixed, and the parameters in the optimization were the weights in the CPG model. The CPGs were assigned to specific muscle groups, and encoded desirable properties such as trajectory reproduction and external perturbation compensation. They produced desired time-varying muscle lengths for specific swimming modes, which were later converted into muscle activations by PD controllers. An interesting contribution of this approach was that it reduced actuation redundancy by allowing muscles to be controlled in groups. For instance, turns were induced by decreasing the activation amplitudes of the muscles on one side of the body relative to muscles on the opposite side.

Another interesting controller optimization method, was the antagonistic controller of [NF02], which is based on the *equilibrium point hypothesis* proposed in [Fel66] (Section 2.1.2). In this approach, each degree of freedom of a human skeleton was actuated by two angular springs representing the antagonistic grouping of muscles around joints. Movement was achieved by varying the equilibrium point of each joint (the point where the sum of the forces acting on the joint equaled to zero). The variation of the equilibrium point was made by adjusting the spring parameters according to desired angles specified by the user, and a method that took samples of external forces and recalculated the spring parameters.

Controller optimization methods have allowed the implementation of well known biomechanical mechanisms and motor control theories through simple control laws. Some of which rely on the character's mechanical structure itself, without the need of a higher level controller [GH10]. One of the main drawbacks of these methods is computational efficiency. Computation times still need to be improved, since to synthesize 10 seconds of animation, the controllers yielding the most impressive results require approximately 10 hours of tuning [WHDK12].

A challenge common to most of the controllers discussed in this section is the task of balancing. Ensuring balance is a complicated task with muscle-driven simulations, as it is with torque-driven simulations. Most of the controllers used a SIMBICON-style balance correction [YLvdP07] to determine leg orientation [GvdPvdS13] or to adjust hip target angles [WHDK12]. While, others used automatic balance controllers [NF02] based on the balancing simulations of [Woo98]. Finally, actuation redundancy is another important challenge for these controllers, however except for [SLST14], none of the controllers address this explicitly. The usual solution is to compute an activation per muscle individually, which does not simplify control complexity or redundancy.

2.1.2.4 Trajectory optimization methods

Another type of muscle-based control method are *trajectory optimization methods* [CRPPD16]. In this methods the optimization itself is used to compute the muscle signals. Control variable trajectories ($\mathbf{u}(t)$) are generated which minimize or maximize a measure of performance while also respecting a set of constraints. Such methods are for now mostly used in robotics. In the domain of character animation, these methods remain mostly a static optimization, solving a given set of equations at each discrete step. Alternatively, they can also be referred to as "model-predictive control methods" when they are used online and with a finite time horizon.

A schematic overview of these methods is featured in Figure 2.8. Generally, the user specifies a set of kinematic goals ($\mathbf{y}^d(t)$), external forces ($\mathbf{f}_e(t)$), and initial muscle signals ($\mathbf{u}_{init}(t)$). The optimization iterates until the cost function is minimized, producing the optimal muscle signals that fulfill the task. Among the variety of motions that have been synthesized through this approach are locomotion patterns [Mil88, GT95, GTH98, KSK97, MWTK13, TTL12], and human upper body movements such as breathing [ZCCD06, DZS08], arm flexion [LST09], and hand movements [SKP08, AHS03].

Two types of trajectory optimization methods have been distinguished: those that rely on the assumption of a specific function (periodic or polynomial functions) as a control trajectory and use it to control muscles in groups, and those that don't.

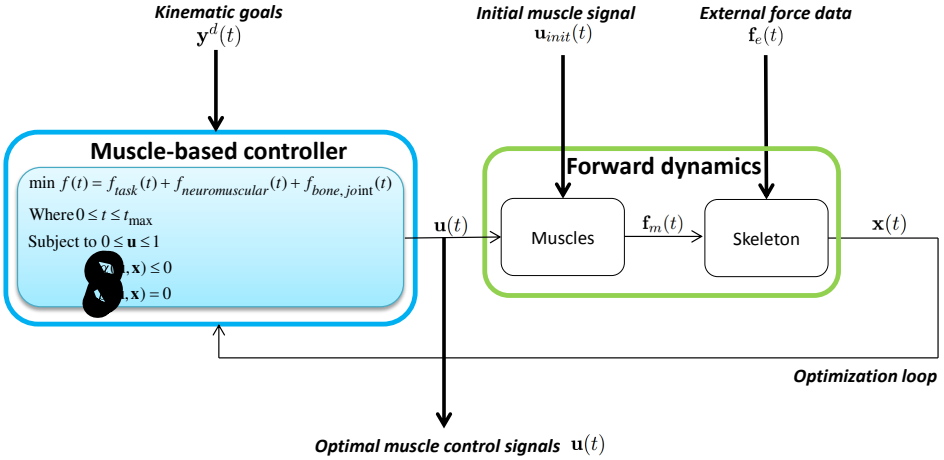

Figure 2.8 – **Trajectory-optimization methods [CRPPD16].** The optimization process directly computes the muscle control signals according to the motion goals, and the minimization of a cost function. These signals can be computed at each time step (static optimization) or in a defined simulation period (dynamic optimization or optimal control). Some approaches include additional components, such as neural networks to generate the desired joint stimuli [HMOA03, LT06].

The following paragraphs explain each type and provide further insight into how these controllers are used in animation.

Methods based on function primitives and muscle groups

One of the simplest motion control strategies consists in synthesizing motions through the generation and tuning of periodic signals. These controllers are mainly used for the generation of oscillatory motions, such as those seen in the locomotion of fishes, worms, snakes, and in human chest motions. The signals generally drive spring-like muscles, which are gathered into muscle groups to reduce the number of controlled variables.

Early implementations manually tuned periodic functions to generate the desired motions [TT94, Mil88, ZCCD06]. [TT94] controlled artificial fishes by converting a desired swim speed into a spring contraction amplitude and frequency. This mechanism was based on the observation that the speed of most fishes can be proportional to the amplitude and frequency of the tail's lateral oscillation.

The authors of [Mil88] used controllers that produced sine waves to generate waves of compression, which replicated the elastic deformation present in the locomotion of snakes and worms. Sine waves have also been used jointly with step functions to generate human motions. [ZCCD06] used these functions as varying parameters to synthesize human breathing. The first parameter was a contraction ratio, which was determined according to modeled and measured human muscle contraction ratios during breathing. The second parameter was a binary timing,

which was defined by the desired breathing frequency. Finally, polynomial function primitives, such as spline curves, have also served as a means for human motion synthesis. [AHS03] synthesized hand motions in real-time by specifying muscle contraction values at keyframes and interpolating them via spline functions.

Recent implementations have automated the generation of periodic functions by using optimization procedures. An example is the torso controller of [DZS08] for synthesizing human breathing and laughing. In this approach, an optimization attempted to minimize the tracking error between a desired lung pressure, computed from an audio soundtrack, and the current pressure of the model. This process generated the parameters of a set of sine waves that were used directly as muscle activation signals.

More complex motions have also been synthesized via function primitives. An example is the approach of [MWTK13], where control trajectories were encoded as splines, and trajectory optimization and spacetime constraints [WK88] were used for humanoid motion synthesis. One of the novelties of this approach was the use of a *Contact Invariant Optimization (CIO)* [MTP12]. This framework smoothed out the discontinuities in the objective function by allowing foot contact points to gradually invoke ground reaction forces at a distance until a real contact was made.

Methods without function primitives and muscle groups

The majority of trajectory optimization methods discussed in this review do not make assumptions on the trajectory of the control signal and rely more heavily on biomechanical and motor control concepts, such as the minimization of effort or fatigue. Moreover, most of them control muscles individually and not in groups. First, the controllers whose sole purpose is synthesizing rigid body motions are introduced; next, the controllers that also model the effect of this motion on soft tissues are discussed; and finally, the controllers designed for purely soft bodies (no skeleton) are presented.

Trajectory optimization methods have been used to synthesize a variety of rigid body motions. For instance, [KSK97] developed an open-loop feedforward controller to synthesize leg motion. This controller interpolated input postures and computed muscle forces via the inverse dynamics and prediction algorithm introduced by [CB81]. The same authors extended this approach in [KSK00], by converting input physiologically infeasible postures into feasible ones, and simulating fatigued and injured characters. To do this, an evaluation took place to determine if the muscle forces corresponding to the input motion respected force limits. Infeasible motions were then converted into feasible ones through an optimization based on: the minimization of the total supplementary torques needed if the motion is

infeasible, stability control [Vuk90], and additional muscle-related objectives which are explained in appendix A.2. Additionally, these motions could also be easily re-targeted by changing muscle parameters, such as maximum force limits, or even removing muscles.

Feedback controllers have also been developed with an adaptability to different physiological and environmental conditions. For instance, the authors of [LPKL14] synthesized biped gaits, which were adaptable to conditions such as, external forces, maximization of efficiency, and pain reduction. The approach consisted of a muscle optimization and a trajectory optimization. The purpose of the trajectory optimization was to modulate the reference motion and its step locations [KH10] to guarantee motion robustness and adaptability. Using this reference motion, the muscle optimization (which minimized muscle effort) computed the optimal activations to control the character in a per frame basis.

Other approaches couple trajectory optimization methods (as muscle-based controllers) and neuronal networks (as joint controllers). An example is the locomotion controller developed by [HMOA03], which employed a neuronal model and an optimization procedure. The neuronal model contained a central pattern generator (Section 2.1.2) that computed the required joint stimuli. This joint stimuli was later distributed as individual muscle forces through an online static optimization procedure that minimized muscle fatigue [CB81]. The neural parameters were determined through a genetic algorithm and criteria that enforced motion smoothness and muscle energy efficiency.

Similarly, [LT06] synthesized neck motions by using neural networks to generate musculoskeletal stimuli and adjusting this stimuli through a static optimization. The networks generated neck poses and stiffness signals according to desired head orientations. While the optimization generated desired muscle strain (deformation) and strain rates that ensured that the head converged to the desired orientations via minimal joint displacements. The outputs of the networks were combined into one feedforward signal, which was converted into muscle activations by a PD controller that was constantly monitoring the error in muscle strain and strain rate.

In addition to rigid body motion, some control methods also focus on synthesizing the movement of soft bodies (such as tendons and skin) and the interactions of these with rigid bodies. For instance, [TSF05] synthesized hand motions and muscle bulging through a controller which generated muscle activations for a set of desired joint orientations. The authors employed an optimization which minimized joint tracking error and muscle effort. Furthermore, a variety of hand motions were generated by using clinically motivated heuristics for *Repetitive Strain Injuries* diagnosis.

[SKP08] also synthesized hand motions and the movement of tendons and muscles under the skin thanks to a novel biomechanical simulator that used target rigid body velocities. The simulator involved an optimization procedure to compute muscle activations and a skin deformation algorithm. The optimization computed muscle activations, and was led by a muscle effort term and task related objectives which ensured a good tracking of the desired rigid body velocities. The transformation from activations to rigid body motion was enhanced by complex muscle routings or strands. These strands were modeled as cubic B-splines that were allowed to slide along predefined surfaces. Allowing this motion is important, because more realistic changes in muscle length and velocity are achieved, and these changes are known to affect the force generation properties of muscles.

The work of [SSB+15] is closely related to that of [SKP08]. It consisted in a hierarchical control framework for hands and tendinous systems, which performed tasks such as writing, and could simulate clinical deformities of the hand by altering tendon parameters. At the highest level, kinematic controls were computed to track a fingertip reference trajectory, and at the lowest level, an activation controller transformed these controls into muscle activations, using the formulation of [SKP08]. However, a difference with the latter approach is the fact that the optimization parameters could be determined through a general-purpose learning-based approach requiring no previous system knowledge.

Another interesting example is the work of [Lee08, LST09], who presented one of the most detailed biomechanical models of the human upper body and a controller to track a set of poses while achieving a desired level of muscle co-activation. The activations that satisfied these requirements were computed thanks to a static optimization procedure that minimized muscle effort, and was constrained by joint torques computed from input poses [Fea14]. The optimization was solved twice (once for each muscle in an antagonistic pair), with the difference that the antagonist activation was constrained by a torque of opposite sign. Once the agonist and antagonist activations were defined, they were modified proportionally to the target co-activation. Secondary skin motion was also synthesized through the simulation technique in [Sif07].

Muscle-based control frameworks have also been used to synthesize motions with purely soft bodied characters. One of the first examples is the controller created by [GT95, GTH98] for the locomotion of highly flexible animals. The control granted the characters with the ability to synthesize basic locomotion skills, remember them, and combine them efficiently to perform more complex tasks. The basic locomotion skills were learned through an optimization procedure containing task achievement objectives, such as the shortest distance to a goal, and a muscle effort objective. Next, the learned signals were converted into more compact rep-

resentations and used within a second optimization procedure with the objective of finding a proper combination of skills to achieve more complex behaviors. Once the compact representations were created, the method could be made to work in real-time.

More recently, the authors of [TTL12] also developed a trajectory-optimization based controller for soft bodied characters. This approach aimed at controlling the shape of soft bodied characters (and therefore the shape of their muscles) to achieve specific locomotion tasks. The procedure used an optimization at each time step to determine muscle lengths, and a contact planner, which predicted how the desired changes in muscle contraction affected contact points, allowing the characters to slide and break contacts with the ground.

Trajectory optimization methods are until now the most common solution for muscle-based control. One of their advantages is that they are more easily adaptable to different character morphologies. The reason for this is their centralized nature. Local controllers, which can be subject dependent (due to the fact that they are usually assigned to specific muscles or body sections), are not used. Examples of this flexibility are the works of [GT95], who implemented a controller for a variety of virtual fishes, and [TTL12], who used a variety of alphabet letters with diverse muscle arrangements.

One of the main drawbacks of these methods is their implementation. A considerable amount of knowledge is needed in optimization techniques and constrained dynamics. Another drawback is the fact that modeling biomechanical mechanisms (such as muscle reflexes), which would certainly aid in synthesizing motions, is not straightforward. The effect of such mechanisms could be encoded within a cost function, but implementing a model of the mechanisms (as is done by controller optimization approaches) is a more natural and efficient alternative.

The computational requirements and efficiency of these methods depend on many factors, such as the number of objectives and complexity of the character. However, as with controller optimization methods, computational efficiency still needs to be improved since the controllers have not reached real-time performance.

Several of the frameworks presented in this section needed to solve the difficult task of maintaining balance. Different strategies for balance were used, such as regulating linear and angular momentum [TTL12, MZS09], using the ZMP (zero moment point) [KSK00, Vuk90], or balance recovery techniques based on an estimated pendulum state [LPKL14, KH10].

Finally, as in the previous section, the problem of actuation redundancy was not explicitly addressed by most trajectory optimization controllers. Aside from the simulation of periodic motions (such as breathing) where spring-like muscles

are controlled as a group [TT94, Mil88, ZCCD06], usually, numerous muscles are controlled individually. The redundancy of actuation is kept, which also induces a redundancy of control.

2.1.3 Conclusion

Controlling virtual characters with muscles is interesting for reproducing and synthesizing motions. The non-linear properties within muscles (such as the force-length and force-velocity relationships) provide characters with control and motion quality advantages with regard to servo-actuated characters, such as: better stability and realistic passive dynamics, physiologically feasible motions, better estimates of energy cost or fatigue, a mechanical system with the ability to perform control functions by itself, and an ease to simulate musculoskeletal defects, pathologies, and physical fatigue.

Great advances have been made to control them in simple and complex motions, as shown by the variety of controller optimization methods presented in Section 2.1.2.3 and the trajectory optimization methods presented in Section 2.1.2.4 (also summarized in Appendix A.1 and A.2). However, a weakness of state of the art approaches is the fact that control complexity and computation times are high partly due to actuation redundancy. For now, most methods do not seek to reduce this redundancy. The usual solution is to compute a high number of control signals (one per muscle) independently, without questioning or exploiting the relationships between them. Determining such relationships could simplify the control of these characters and motivate a wider adoption of muscle-based control frameworks in a variety of domains, by reducing the number of control variables.

Some authors have already exploited this idea at a kinematic or torque level, either to identify low-dimensional control representations for virtual characters [SHP04] and robots [TST+10, TTSG13], to identify the DoF that have higher contributions to the motion and that need be controlled via a primary control strategy [JL11, YL08], or to learn low-dimensional feedback strategies [DLvdPY15]. Similarly, early implementations of trajectory optimization methods (Section 2.1.2.4) also address this redundancy explicitly by using function primitives to control groups of spring-like muscles. However, this is no longer the case, and although more sophisticated controllers are used, muscle activation signals tend to be computed individually.

In this work, a trajectory optimization method will be proposed to generate motions with a virtual character by controlling hill-type (Section 2.1.1.2) muscle models in groups. The next section presents the theory that will allow such a method to control muscles in groups and reduce actuation redundancy efficiently.

For now, this theory is popular in neuroscience as a means of decoding how the human CNS is able to perform muscle-based control fast and efficiently, in spite of a complex musculoskeletal system. However, it is an attractive solution that could simplify the control of muscle-based characters and promote their adoption in a variety of domains.

2.2 Muscle synergies as low-dimensional representations of human motion control

In humans, muscles are controlled by the central nervous system (CNS). This control system is able to plan complex motions fast and efficiently, in spite of having to coordinate numerous muscles at the same time [Ber67], and handling a high actuation redundancy. Several theories have been proposed which aim at unveiling how the CNS is able to choose from numerous solutions to a given motor task. One of this theories is the theory of muscle synergies. This theory suggests that the mechanisms that control motion are organized in a modular fashion. It states that the CNS translates task level commands into a reduced number of modules or synergies, which are later mapped into a larger set of individual muscle activations [Tin07]. A modular organization based on synergies is interesting because it would imply that the CNS uses and adapts a low-dimensional control representation, consisting of less control variables than muscles, to generate and learn new motions efficiently.

The following sections detail: the concept of synergies (Section 2.2.1), the methods to extract them (Section 2.2.2), and examples of studies evidencing their existence in a variety of motions (Section 2.2.3).

2.2.1 Synergy models

Muscle synergies are modules generated by the CNS, which encode the temporal and spatial activation of groups of muscles and are linearly combined to produce individual muscle activations. There are two popular models used by neuroscientists to represent synergies: the time-invariant synergy model and the time-varying synergy model.

In the time-invariant synergy model [MBdF10, IPL04, TOT07], a synergy $\mathbf{w}_i$ is defined as a $D \times 1$ vector of coefficients, specifying the relative activation level of D-muscles. Each synergy is paired with a time-varying combination coefficient $c_i(t)$, which determines its temporal evolution, as shown in Figure 2.9. A set of N-synergies can be linearly combined to generate distinct muscle activation patterns as follows:

$$\mathbf{a}(t) = \sum_{i=1}^{N} \mathbf{w}_i c_i(t) \tag{2.10}$$

Where, $\mathbf{a}(t)$ is the $D \times 1$ time-varying vector containing the activations of all muscles at time t.

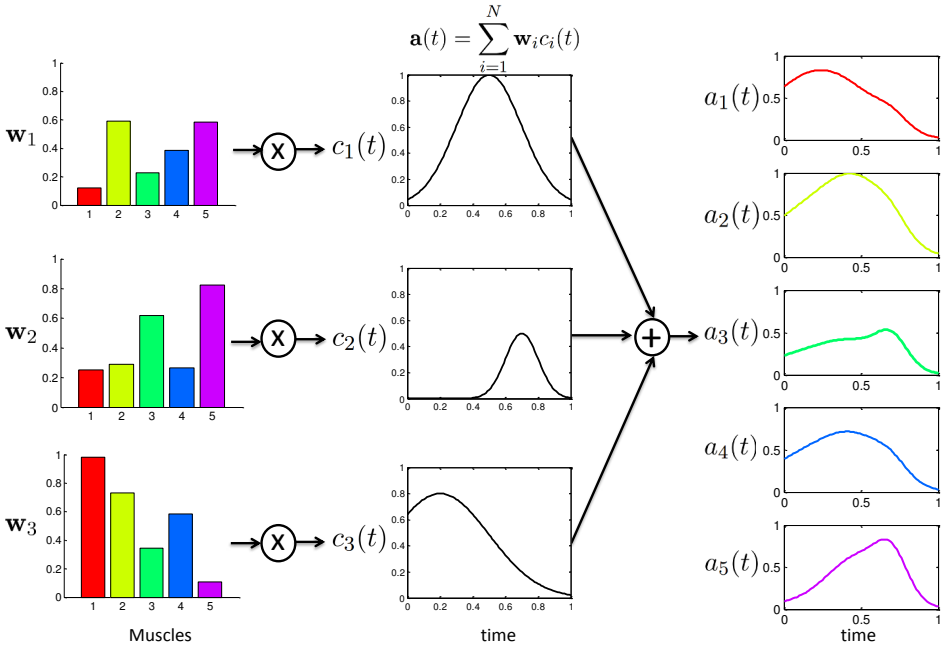

Figure 2.9 – **Concept of time-invariant synergies.** Three different synergies ($\mathbf{w}_i$) are presented. The vertical bars in each synergy represent the mean activation level of each muscle throughout the motion. By linearly combining the synergies ($\mathbf{w}_i$) and their combination coefficients ($c_i(t)$) a larger set of muscle activations ($\mathbf{a}(t)$) are generated. Each component in ($\mathbf{a}(t)$ represents the activation of an individual muscle j, and is denoted as $a_j(t)$.

In the time-varying synergy model [dT02], a muscle synergy $\mathbf{w}_i(t)$ is defined as a $D \times 1$ time-varying vector describing a collection of muscle waveforms, as shown in Figure 2.10. The synergies $\mathbf{w}_i(t)$ capture the time dependence of the muscle activations, and each synergy is paired with a single coefficient c_i and a single onset time t_i that scale them in amplitude and time. With this model a set of N-synergies can also be linearly combined to generate distinct muscle patterns:

$$\mathbf{a}(t) = \sum_{i=1}^{N} c_i \mathbf{w}_i(t - t_i) \tag{2.11}$$

The components in these models can be denoted as task-independent or task-dependent [ADN+13]. The task-independent part, are the components of the synergy model that are predefined by the CNS, while the task-dependent are the components that are modulated by the CNS to achieve a specific task or to adapt to new

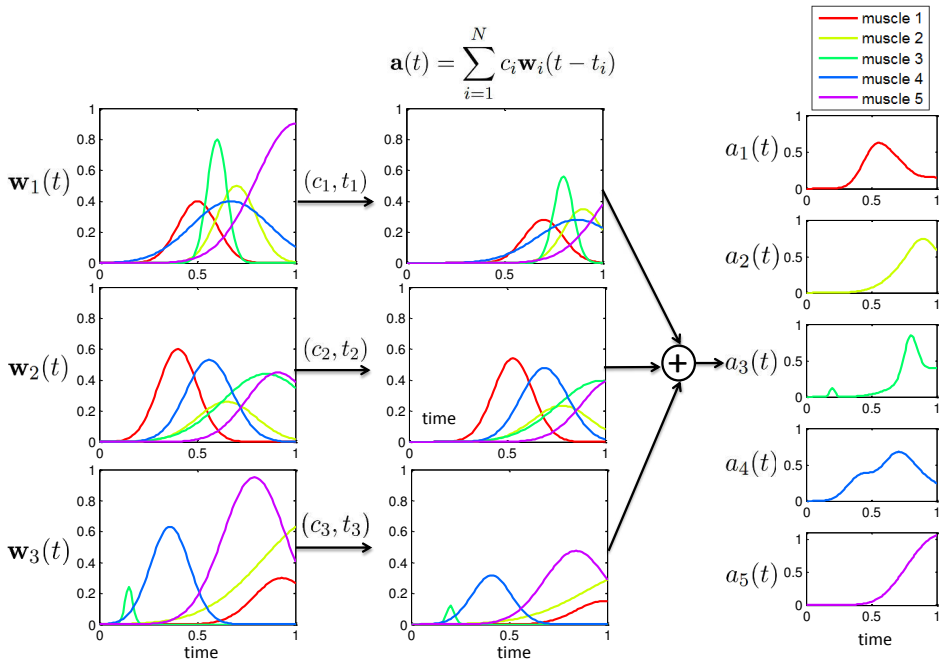

Figure 2.10 – **Concept of time-varying muscle synergies**. Three time-varying muscle synergies ($\mathbf{w}_i(t)$) composed by a collection of muscle activation waveforms are presented. By multiplying all waveforms of each synergy by a single scaling coefficient (c_i), shifting them in time by a single delay (t_i), and summing them together, a larger set of muscle activations ($\mathbf{a}(t)$) can be generated. Each component in ($\mathbf{a}(t)$ represents the activation of an individual muscle j, and is denoted as $a_j(t)$.

task conditions. In the time-invariant synergy model, when the synergies $\mathbf{w}_i$ are task-independent and the coefficients $c_i(t)$ are task-dependent, the model is called synchronous synergy model. Otherwise, when the synergies $\mathbf{w}_i$ are task-dependent and the coefficients $c_i(t)$ are task-independent, the model is called temporal synergy model. Regarding the time-variant synergy model, the task-independent part are always the time varying synergy vectors $\mathbf{w}_i(t)$, while the single coefficients c_i and onset times t_i are task-dependent.

The way the dimensionality reduction is done depends on which of the above models is used to represent the control done by the CNS. Specifically, it depends on which components are task-dependent or modulated in the model. For instance, given a muscle activation space of $D \times T$ dimensions (where T is the total number of time samples), the synchronous synergy model provides a dimensionality reduction to a $N \times T$ space containing the combination coefficients $c_i(t)$, only when $N < D$. On the other hand, the temporal synergy model always provides a reduction from the muscle space to a $D \times N$ space containing the synergy vectors $\mathbf{w}_i$. Lastly, the time-varying synergy model always provides a dimension reduction to a $2 \times N$ space containing the amplitude and time scaling coefficients of each synergy.

2.2.2 Synergy extraction process

Several algorithms have been used to identify or extract muscle synergies. Synergies are usually extracted from electromyographic (EMG) signals recorded during the execution of a task. EMG signals are formed by changes in potential of muscle fiber membranes when innervated by motor units. In other words, they are signals encoding the electrical activity produced by skeletal muscles when excited by the CNS. These signals can be collected using an electromyograph which is an instrument that detects the electrical potential that is generated within the muscles, when they are neurologically activated . Pairs of surface or intramuscular electrodes are used to detect this activity. Surface electrodes [HFM+99] detect this activity on the skin above the muscle, while intramuscular electrodes detect it within the muscle.

Once the EMG signals are recorded, a pre-processing stage [Kon05] is needed to remove signal contaminations, due to the movement of electrodes on the skin, ground noise from the power net, muscle cross talk, and heartbeats (ECG contamination). Furthermore, the shape of raw EMG bursts cannot be precisely reproduced due to the fact that the set of recruited motor units constantly changes. Therefore, to overcome this problem, smoothing techniques (such as low-pass filters) are applied to extract the reproducible part of the signal. These smooth envelopes are then fed to the synergy extraction algorithms to identify muscle synergies.

Standard matrix factorization algorithms can be used to identify time-invariant and time varying synergies (without delays). Two primary techniques for the decomposition of EMG signals into synergies are principal component analysis (PCA) [MKB80], and nonnegative matrix factorization (NMF) [LS99]. Other examples include, independent component analysis (ICA) [BS95], ICA applied to a subspace defined by PCA (ICAPCA), probablisic ICA with nonnegativity constraints (pICA) [HSWH02] and factor analysis (FA) [Dar68]. For the case of time-varying synergies (with delays), iterative optimization algorithms such as [dT02, dSB03, dB05] have been developed to identify them.

Although a variety of matrix factorization algorithms are available, studies have shown that different algorithms can yield similar synergies [TCd06]. This consistency suggests that the muscle synergies found by a particular algorithm are not an artifact of that algorithm, but reflect the organization of muscle activation patterns behind the studied motions. Therefore, these algorithms can be profitably used to study the production of movements.

The choice of the algorithm depends on the assumption made on the nature of the synergies, such as non-negativity, orthogonality or statistical independence [TC10]. Non-negativity, that is positive synergy vectors, is assumed when physiologically meaningful synergies are sought (as explained later in this section). Orthog-

onality, that is perpendicular or linearly independent synergy vectors, is assumed when searching for a unique set of synergies which account for as much of variability in the data as possible. Finally, statistical independence, that is uncorrelated synergy vectors, is assumed when searching for synergies representing independent information sources. If orthogonality is assumed, PCA [MKB80] can be used to determine a set of orthogonal synergies that account for the largest amount of variablity in the data. FA [Dar68] can be used when searching for the smallest set of synergies that can account for the common variance or correlation of a set of muscles. If statistical independence is assumed, ICA [BS95] can be implemented to extract a set of synergies that represent independent sources of information. Finally, if non-negativity is assumed, NMF [LS99] can be used to extract a set of synergies and activation coefficients that are nonnegative but not necessarily independent.

The non-negativity constraints imposed by NMF are interesting, because they yield physiologically meaningful results: nonnegative synergies, which yield nonnegative muscle activations and forces. This is consistent with the nature of neural and muscle output: neurons are either firing (positive signal) or at rest (zero signal) [TC10], and muscles can only actively pull and not push. Furthermore, this algorithm does not assume that the synergies are independent, which is consistent with the observation that activations of multiple synergies are correlated [SWDd+01].

The quality of the extracted synergies is assessed by quantifying the similarity between the recorded activations and the activations reconstructed using the synergies. This assessment can be made through different indicators. The most popular being the Variance Accounted For (VAF) metric and the coefficient of determination (r^2) [TC10, ADN+13]. A high VAF or r^2 value indicate a good reconstruction of the muscle activations, which evidences the quality of the extracted synergies. Both indicators quantify the percentage of variability in the muscle activation dataset that is accounted for by the extracted synergies, and they are computed as follows:

$$1 - \frac{SS_{err}}{SS_{tot}} \tag{2.12}$$

Where, SS_{err} is the sum of squared errors (between the recorded and reconstructed activations), and SS_{tot} is the total sum of squares (of the recorded activations).

The difference between both indicators is that when computing r^2 the sum of squares is taken with respect to the mean, whereas for VAF it is taken with respect to zero. In other words, r^2 is based on a linear regression with an offset, and therefore it only compares shapes, while VAF is based on a linear regression that must pass through the origin, and therefore it compares actual values [TC10]. Thus, the r^2 indicator can be used to assess how well the shapes of the muscle signals are

reconstructed, while VAF can be used to assess how the actual muscle activation values are reconstructed.

These indicators can also be used to determine the dimension of the synergy space or number of synergies to extract. They are used within criteria that assume the most of the EMG variability is due to task-dependent muscle activations, whereas a small portion is due to sources of noise. Thus, in the case of VAF, the number of synergies is defined either by the point where the VAF-graph (a curve describing the trend of the VAF as function of the number of synergies) reaches a threshold (for example 90%) [TOMT06], or by its flattening point (the point corresponding to a significant decrease of slope). In the case of r^2, the number of synergies is chosen as the point corresponding to the sharpest change in slope of the r^2 curve (a curve describing the trend of r^2 as a function of the number of synergies) [dSB03, MBdF10]. This change in slope is interpreted as the point separating "structured" from noise-dependent variability. After this point, additional synergies start to capture only the small residual noise-dependent variability, therefore, this can be used to define the minimum number of synergies that capture the task-related features [dPFL06, TCd06, ADN+13].

2.2.3 Evidence of muscle synergies

The existence of muscle synergies can be shown through two different mediums: either by examining EMG recorded signals (indirect EMG-based evidence) or examining the CNS (direct neural evidence). This section focuses on indirect EMG-based evidence, which is the more popular for studying the control of human motions.

Many studies have been conducted to evidence the existence of muscle synergies from recorded EMG signals, in both animals and humans. These studies have evolved from the analysis of reflexive frog motions, to grasping in primates, postural responses in cats, and finally to human motions. In humans, muscle synergies have been found as early as in the neonatal phase. [DIC+11] identified two time-invariant synergies in stepping neonates. These synergies were kept through development and augmented by two new synergies in toddlers. Such patterns were similar to synergies in other animal species, suggesting that locomotion stems from common time-invariant synergies despite morphological differences.

Studies have also shown the existence of synergies in more complex behaviors, their robustness across task conditions, and their modulation according to task goals and/or features. In the context of human motion analysis task goals are variables encoding the objective of the motion, while the features characterize the motion. For instance, the authors of [IPL04] studied walking at different speeds and gravitational loads, and identified 5 synergies that accounted for a considerable fraction of

the EMG variance in a large number of muscles with important contributions to locomotion. These synergies were almost invariant across speeds and loads, and were timed according to the lift-off event in locomotion. In a later study, the authors of [IGZ+03], studied the locomotion of patients with spinal cord injury and healthy subjects, and found that 5 basic temporal components could be flexibly combined to reconstruct the muscle patterns in both control and patients. Furthermore, two of these components were linked to foot kinematics across different stepping speeds and loading conditions.

Another complex behavior that has been analyzed through synergies is human postural control. [TOT07] studied the postural responses of a variety of subjects to multidirectional support surface translations in 16 muscles of the lower back and leg. Their results revealed that 6 or less time-invariant synergies were required to reproduce the responses of each subject. These synergies were similar across subjects, and corresponded to well known balance strategies, such as the "hip" strategy, in which proximal muscles have larger activations than those of the ankle, causing a fast movement of the center of mass (CoM)[HFH98]. Another interesting finding was that the synergies were directionally tuned, in other words, they were activated for a specific range of perturbation directions, as shown in Figure 2.11.

The link between synergies and task features during postural responses has also been evidenced in [ST11]. In their experiments, subjects stood on a platform that was displaced on a horizontal place. They analyzed the ability of time-invariant versus time-varying synergies to reconstruct muscle activity, and concluded that time-invariant synergies produced more consistent and physiologically meaningful results. Their results also showed that the combination coefficients of these synergies could be well reconstructed using delayed feedback of CoM kinematics. These findings suggest that the CNS may used the CoM kinematics to recruit time-invariant synergies for controlling balance. Similarly, [KGZL03, KLSZ03] analyzed several postural response tasks to identify control mechanisms. In one of their experiments the action of releasing a load from extended arms was analyzed. This resulted in the identification of 3 modes, a push-back mode, a push-forward mode, and mixed-mode. Forward and backward shifts of the CoP (center of pressure) were associated to different combinations these 3 modes.

Synergies and their relationships with task goals have also been evidenced in upper-body tasks. An example is the work of [dPFL06]. In this study fast-reaching motions were analyzed for a variety of subjects. The motion consisted in point-to-point movements between a central location and 8 peripheral targets in 2 vertical planes. For each subject, $4-5$ synergies were identified whose combinations explained more than 70% of the EMG data variation. The general nature of these synergies, was also evidenced by the fact that they could accurately reconstruct

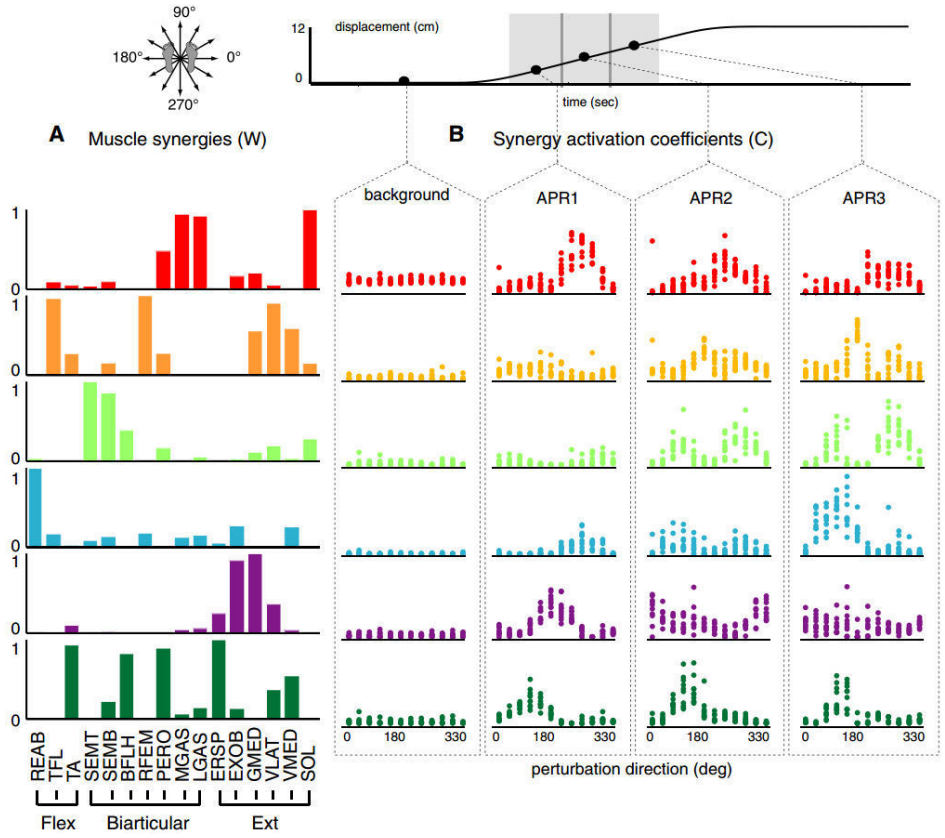

Figure 2.11 – **Evidence of muscle synergies in postural control tasks [TOT07].** Subjects stood on a support surface that was displaced in 12 different directions. Four time periods were analyzed: a background period (BK), and three consecutive automatic postural response periods (APR) after the perturbation. Synergies were then extracted from a matrix containing the muscle activity during these time periods, for all trials and directions. A) The muscle synergy vectors. B) The synergy coefficients during each time period against multiple perturbation directions. Each dot represents the activity of the muscle synergy in a single trial. Directional tuning of muscle synergies over the 3 APR periods can be observed. For example $\mathbf{w}_1$ is mainly active during APR1 in backward perturbation directions ($180° - 270°$), while $\mathbf{w}_4$ is active in APR3 in forward perturbation directions ($0° - 90°$).

the EMG activity during point-to-point movements with different loads, reversal movements, and movements with via-points. As in the postural responses, it is interesting to see that for these kinds of motions, the computed synergies were also directionally tuned. Each synergy had a "preferred direction", which was robust across changes of load, posture and endpoint.

The same authors [dFPL08], also investigated if synergies existed in more natural reaching motions, involving different speeds and requiring the control of both movement and posture. Their results evidenced that 3 time-invariant synergies encoded the variations of postural muscle patterns at the end of the motions, and that during the motion 3 phasic and 3 tonic time-varying synergies encoded the

activity of all patterns. The phasic synergies were modulated in amplitude and time by movement direction and speed, while tonic synergies were modulated in amplitude by motion direction only. Furthermore the directional tuning of both synergies could be described through cosine functions.

Another study showed that it is possible to identify a set of synergies to represent reaching motions in different directions [MBdF10]. In this study subjects performed multidirectional reaching motions in the horizontal plane, and synergies were extracted from concatenated EMG signals of reaching in different directions. The analysis showed that multijoint reaching could be accurately reconstructed in all directions by linearly combining either 4 synergies extracted from individual DoF or 3 synergies extracted from multijoint movements in at least 3 reaching directions. This suggests that common synergies can be used to represent a same motion type and different task conditions, provided that the synergies are extracted from a representative number of task conditions.

Reaching motions with perturbations have also been analyzed to show the robustness of muscle synergies across changes in target locations. In [dPL11] point-to-point movements in the frontal place with a change in target location were analyzed. The results revealed that a common mechanism existed for the perturbed and unperturbed motions, since the muscle patterns for perturbed reaching could be reconstructed by using 3 time-varying synergies extracted from unperturbed movements. Interestingly, these 3 modules could reconstruct perturbed motions better than the combination of the muscle patterns of the corresponding point-to-point movements.

The robustness of synergies across unperturbed and perturbed motions has also been studied in [GEPD13]. This study investigated the changes in muscle activity during a virtual reaching task, requiring isometric force generation. The task consisted in applying horizontal forces on a handle instrument to move a virtual sphere to different target positions. The task was done with no perturbations, and with a perturbation of 45 degrees clockwise rotation applied to the planar force. The analysis showed that the synergies extracted from unperturbed trials could be used to reconstruct the patterns in the perturbed trials, evidencing the robustness of the extracted synergies.

In addition to the previous examples, other motion tasks were evidence of muscle synergies has been found include hand postures [WF04], hand shape transitions (fingerspelling) [BSF07], running [CIPL06], and pedaling [HTCD11]. Finally, aside motion tasks, another scenario that provides evidence of muscle synergies are force generation tasks. These tasks have been less explored, however a recent study [RRB12] has shown the existence of synergies in the generation of three-dimensional

(3-D) isometric forces at the hand. In this study the activity of key elbow and shoulder muscles was analyzed during a variety of task conditions, such as load level and hand position. This resulted in 4 synergies that explained 95% of the variance in the recorded EMG signals. These synergies were preserved across task conditions and subjects, contradicting emerging evidence stating that the CNS employs different strategies for motion and force generation tasks.

2.2.4 Conclusion

Muscle synergies provide a low-dimensional control representation of motion. This representation reduces actuation redundancy significantly through the use of less control variables than muscles. Two popular muscle synergy models were presented: the time-invariant and the time-varying synergy model (Section 2.2.1). Both models provide a low-dimensional control representation through a few spatial and temporal components which describe how muscles should be activated to achieve a specific task. However, in the time-invariant model synergies are denoted as fixed activation levels which are modulated in time, while in the time-varying model synergies are denoted as time-varying activation curves that are scaled and shifted in time to generate motion. To identify these control strategies, analysis are conducted on human subjects where muscle activity is recorded from key muscles simultaneously. This data is then decomposed into synergies through either matrix factorization or iterative optimization algorithms (Section 2.2.2).

A variety of studies (Section 2.2.3) have provided evidence of the existence of both types of synergies, their robustness across task conditions, and their adaptability to certain task goals and features. For instance, synergies have been associated with balance strategies [KGZL03, ST11] and foot kinematics [IGZ+03] during walking motions and postural responses. They have also been linked to reaching directions [dPFL06] during point-to-point motions, and with perturbation directions [TOT07] during postural responses. However, most of these tasks involved constrained motions that do not require high skill or accuracy, and include a limited motion variability. It would be interesting to challenge this theory through unconstrained and more dynamic motor tasks, requiring accuracy and skill, such as overhead throwing to different distances. Overhead throwing is a motor task with well defined task goals, but it is also unconstrained (highly redundant) and hyper dynamic [KXY+10]. It is highly redundant because there exist numerous solutions or movements that achieve the same target hit, and it is also hyper dynamic because of the high velocities and momentum needed at certain motion phases.

The ability of synergies to encode rich actuation information in a few control variables, makes them a good candidate solution for controlling muscle-based vir-

tual characters in physics-based simulations. Thus, inspired by the muscle synergy theory and the previous challenges, this thesis will include the extraction of time-invariant synergies from humans to simplify the control of a muscle-based character during overhead throwing motions. An approach that will contribute in the validation of muscle synergies as low-dimensional representation of human motion control, and show their usability in a motion generation context.

2.3 Conclusion

The study of how muscles are controlled to generate motion is relevant for virtual character motion synthesis and human motion analysis. This chapter presented muscle-based control from the point of view of both of these domains in order to identify tools, challenges, and solutions that could be used to simplify the control of muscle-based virtual characters in physics-based simulations.

First, an overview of muscle-based control for virtual characters was presented in Section 2.1. The advantages, challenges, and tools for constructing muscle-based simulations were detailed, along with a state of the art of muscle-based control frameworks in animation. This overview demonstrated that using muscles as actuators brings several advantages in terms of control and quality of the resulting motion, and that by merging knowledge from biomechanics, robotics, and neuroscience a variety of control solutions have been developed allowing characters to accomplish simple and complex motions, which range from periodic motions, such as breathing, to explosive motions, such as jumping and kicking. However, in spite of these great advances, one drawback that prevents a wider adoption of muscle-based control frameworks is actuation redundancy, or the fact that the characters possess more actuators than needed to achieve motion tasks. This poses a great control challenge, due to the fact that the actuators in the character can be coordinated in numerous ways to achieve the same task. In more specific terms, numerous actuators translates to numerous control variables that can be combined in a variety of ways to achieve the same motion. However, can control redundancy be avoided in spite of actuation redundancy?

To answer to this question, Section 2.2 presented a popular motor control theory that aims at explaining how humans are able to deal with redundancy fast and efficiently, although possessing complex musculoskeletal systems. This theory is called the theory of muscle synergies, and it states that the CNS adapts in a task-dependent fashion, a low-dimensional control representation consisting of less control variables than muscles to generate motion. Such low-dimensional control representations have been evidenced in a variety of motions which range from walking to reaching motions. Thus, a low-dimensional control representation through

synergies could help solve the control redundancy of muscle-based characters in physics-based simulations.

In this thesis, a synergy-based solution will be proposed for simplifying the control of muscle-based characters. The following chapters detail how this solution was constructed through two main stages: An analysis stage, with the purpose of identifying synergies and kinematic features from human overhead throwing motions (Chapter 3), and a motion generation stage, to re-use and adapt the results of this analysis in a synergy-driven forward dynamics pipeline (Chapter 4). The results will evidence that a synergy-based solution can significantly reduce redundancy while generating motion with a muscle-based virtual character.

Chapter 3

Identification of kinematic features and synergies in overhead throwing

THIS chapter presents an analysis of overhead throwing motions (Section 3.1) with the purpose of identifying low-dimensional control representations that simplify the control of muscle-based virtual characters in physics-based simulations. This analysis began by a series of experiments where subjects performed overhead throws to different ranges (Section 3.2). Kinematic and muscle data were recorded and processed, and then a series of algorithms were used to extract synergies and kinematic features (Sections 3.3, 3.4, and 3.5). In the context of human motion analysis, features are variable that characterize the motion (such as release speed), while task goals are variables encoding the objective of the motion (such as hitting a target at a certain distance). The results show the existence of a low-dimensional control representation that is modulated in amplitude according to kinematic features and changes in the throwing distance, and that is robust across subjects with different morphologies and physical conditions.

3.1 Biomechanics of overhead throwing

An overhead throwing motion consists in launching an object forward and above the shoulder by using one arm. It is the motion with which humans can throw the fastest and with the best accuracy, and it requires a high coordination and skill [Sak02]. The main use of this motion is in competitive sports, such as: american football, baseball, water polo, and dodgeball, where it is used with certain variation and different levels of difficulty. This work focuses on overhead throws such as those performed during football passing. This motion was chosen due the fact that

unlike the majority of motions that have been studied through muscle synergies, this task is unconstrained and hyper-dynamic [KXY+10], requiring high coordination and accuracy. Moreover, it is generic enough and more easily reproduced by non-professionals, as it is a throw characterized by lower speeds and rotational arm velocities than for instance, baseball throws [FEA+96].

In general, this motion consists of a sequence of coordinated movements [Knu07], in which potential energy is transferred through the linked system of the body. This energy is then transformed into kinetic energy as the projectile is released. The quality of the throw depends on the efficiency of this kinetic chain, and control variables such as, speed, height, and angle of release. The entire motion can be described through four main stages, as shown in Figure 3.1: starting position, cocking, acceleration, and finally, release and follow-through [KBWW02]. In the starting position the thrower positions his body sideways with respect to the intended target. The cocking phase consists of the motion between the starting position until maximum external rotation is reached, before the ball starts to move forward. The acceleration begins as the ball is moved forward and finishes when the ball is released. This phase is known as the most explosive phase during the motion since the velocity of the ball changes from zero to its maximum in a short time period. Finally, the release and follow-through phase consists in a deceleration of the throwing arm once the ball is released.

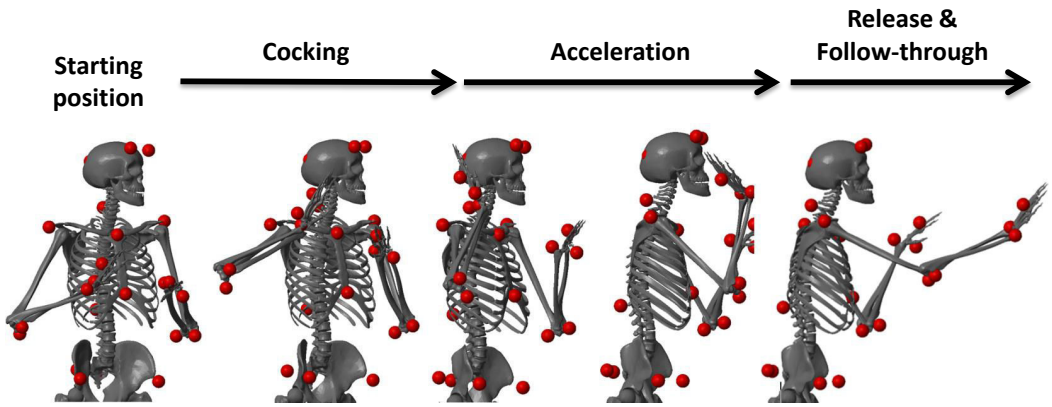

Figure 3.1 – **An overhead throwing motion and its main stages [CRPLD15, CRPD16]**. Example of an overhead football throw to a 4m target (bone graphics issued from [Any] and motion stages are based on [KBWW02]).

3.2 Experimental setup and data processing

3.2.1 Subjects

A series of experiments were conducted in order to extract kinematic features and muscle synergies from overhead throwing motions. Ten healthy men (age 29.8 ± 5.6 yr ; weight 72.4 ± 9.9 kg; height 1.7690 ± 0.0656 m) volunteered for these experiments. The subjects were all right handed, and all except one (subject 3) had never suffered injuries in the right arm. Furthermore, none of the participants were professional athletes, and they all had different physical conditions (with a mean number of hours of sport activity per week of 3.8500 ± 3.0736). Each subject provided written informed consent before participation and written approval of public data availability.

3.2.2 Task

In these experiments the task goal consisted of a right-hand overhead throw to a movable target placed at different distances from a fixed throwing site. The target was placed at $2m$, $4m$, and $7m$ along a straight line from the throwing site. Before beginning the experiments subjects underwent a short training where they practiced long distance throws for 5 to 10 minutes. Once the training was finished the experiments began. During these experiments, the throwing order was randomized (to reduce learning effects), and for each distance 10 throws were performed resulting in a total of 30 throws. A description of the motion and the experimental setup are featured in Figure 3.1 and Figure 3.2.

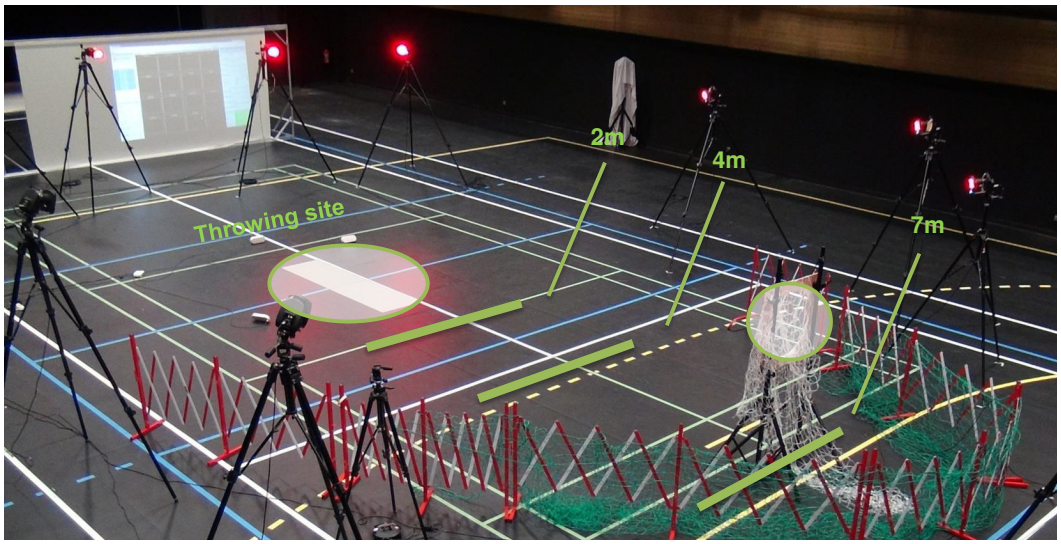

Figure 3.2 – **Experimental setup.** Throwing site and the different target positions.

3.2.3 Data acquisition and processing

During the throwing task the activity of several muscles of the right arm and body kinematics were recorded. A set of 16 muscles was recorded during the experiments. These muscles were chosen due to their important contributions during throwing [DJPP92, HKS+02] and their accessibility through surface EMG electrodes [HFM+99]. The recorded set included muscles located in the back, arm, and chest as shown in Figure 3.3 A and B and in Table 3.1. Detailed descriptions on their functions can be found in the Appendix B (Table B.1).

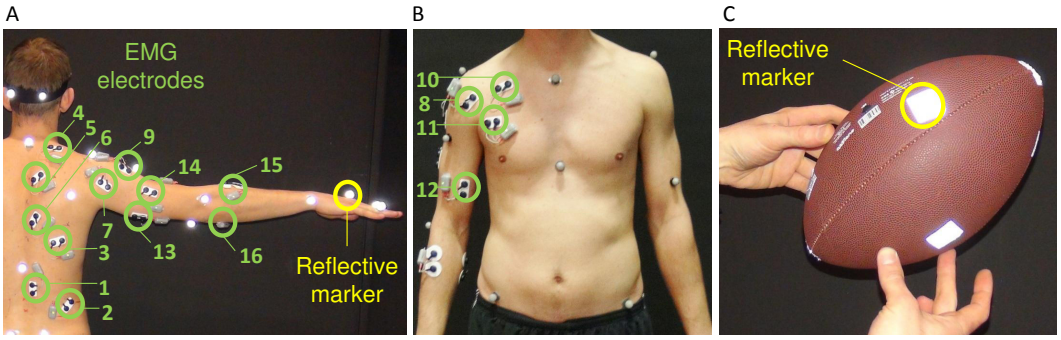

Figure 3.3 – **EMG electrodes and reflective marker placement.** (A) Back view: EMG electrodes and markers on the subject's body. (B) Frontal view. (C) The football used during the experiments and its reflective markers.

Table 3.1 – **Recorded muscles.** List of muscles recorded during the experiments and featured in Figure 3.3 A and B.

Recorded muscles		
Number	**Name**	**Short name**
1	Erector spinae longissimus	EreL
2	Erector spinae iliocostalis	Erllio
3	Lastissimus dorsi	Lasti
4	Upper trapezius	TrapU
5	Middle trapezius	TrapM
6	Lower trapezius	TrapL
7	Posterior deltoid	DeltP
8	Anterior deltoid	DeltA
9	Middle deltoid	DeltM
10	Pectoralis major (Clavicular head)	PecC
11	Pectoralis major (Sternocostal head)	PecS
12	Biceps	Bic
13	Triceps (long head)	TrpLg
14	Triceps (lateral head)	Trplt
15	Forearm extensor bundle	WrstE
16	Forearm flexor bundle	WrstF

The muscle activity was collected using wireless surface EMG electrodes (Cometa Waveplus EMG system) and well known electrode placement protocols [HFM+99, Cri10]. This activity was then processed using a standard protocol [Kon05]: The signals were amplified (gain 1000), digitized (1kHz), band-pass filtered (10-450Hz), rectified, and low-pass filtered (6Hz). Additionally, ECG artifacts were removed using an ICA-based filtering procedure [WDKvD12].

Furthermore, the subject's motion was captured using a Vicon system (15 cameras, 100Hz sampling rate) and reflective markers. The markers were placed on bony landmarks (49 markers, as shown in Appendix B, Table B.2), around the target (6 markers), and on the ball (9 markers) (Figure 3.3 A and C). Each of the marker trajectories was low pass filtered.

3.2.4 Data selection

After the data acquisition and processing procedures, only a subset of trials and muscles were selected for the analysis part of this work. Only 6 throws were selected per throwing distance, yielding a total of 18 throws per subject. Trials affected by signal loss due to our EMG wireless system were dismissed, and a maximal but equal number of trials for all subjects was chosen. Furthermore, only 14 muscles were selected, the pectoralis major (clavicular and sternocostal head) were not included. Their activation signals could not always be cleaned from the ECG artifacts due to the need of additional ECG information for the algorithm in [WDKvD12].

The 14 muscles were then used to construct different muscle sets for the synergy analysis (Table 3.2). These sets were constructed through a reduction process to gradually isolate the muscles of the arm, the body section with the most significant contribution (or rotation) during overhead football throws [FEA+96]. The first set (Set_{14}) contained all 14 muscles, the next set was constructed by excluding back muscles (Set_{11}), the following set by excluding muscles with actions on the scapula (Set_8), and the final set (Set_6) was constructed with antagonistic muscle pairs that actuate the DoF of the arm with highest contribution to throwing per segment (starting at the glenohumeral joint).

These DoF were: shoulder internal(+)/external(−) rotation ($q_1(t)$), and shoulder, elbow and wrist flexion(+)/extension(−) ($q_2(t), q_3(t)$ and $q_4(t)$). The shoulder internal/external rotation and elbow flexion/extension were especially selected due to the fact that they are the major upper limb actions during throwing [KXY+10] (mainly during the acceleration phase [Hui98]). The construction of Set_6 was also motivated by the idea of selecting muscles with matching actions to the virtual character (Section 4.2) that will be controlled via synergies in the next chapter.

Table 3.2 – **Muscle sets for synergy extraction.**

Muscle sets	
Set name	**Muscles** (Blue - muscles excluded to construct the next set)
Set_{14}	Erector spinae longissimus, erector spinae iliocostalis, lastissimus dorsi, upper trapezius, middle trapezius, lower trapezius, posterior deltoid, anterior deltoid, middle deltoid, biceps, triceps (long head), triceps (lateral head), forearm extensor bundle, forearm flexor bundle.
Set_{11}	Upper trapezius, middle trapezius, lower trapezius, posterior deltoid, anterior deltoid, middle deltoid, biceps, triceps (long head), triceps (lateral head), forearm extensor bundle, forearm flexor bundle.
Set_{8}	Posterior deltoid, anterior deltoid, middle deltoid, biceps, triceps (long head), triceps (lateral head), forearm extensor bundle, forearm flexor bundle.
Set_{6}	Posterior deltoid, anterior deltoid, biceps, triceps (long head), forearm extensor bundle, forearm flexor bundle.

3.3 Kinematic features identification

3.3.1 Definition

A set of kinematic features were selected to parametrize the kinematics strategy during overhead throwing. These variables not only characterize the motion, but also have an important impact on the outcome of the throw. Thus, they are the controlled variables during the motion, which allow to achieve the final motion goal (a target hit to a certain distance).

The selected features were defined in the task or operational space. The task space is the space where the kinematics of the subject's hand is defined. In this space, overhead throwing motions are determined by three factors: velocity of release, height of release, and angle of release [DBN06]. Based on this observation, the hand velocity (v) and height (h) of release were selected as task space kinematic features (Figure 3.4). The angle of release was not considered due to its difficult estimation caused by marker occlusion. Nevertheless, studies have shown that the most important parameter influencing throwing range is the release speed [Bar08, Lin01]. Furthermore as shown in [KXY+10], the square of the release speed is proportional to the throwing range, thus, it is more efficient to adjust this parameter rather than an angle during throwing.

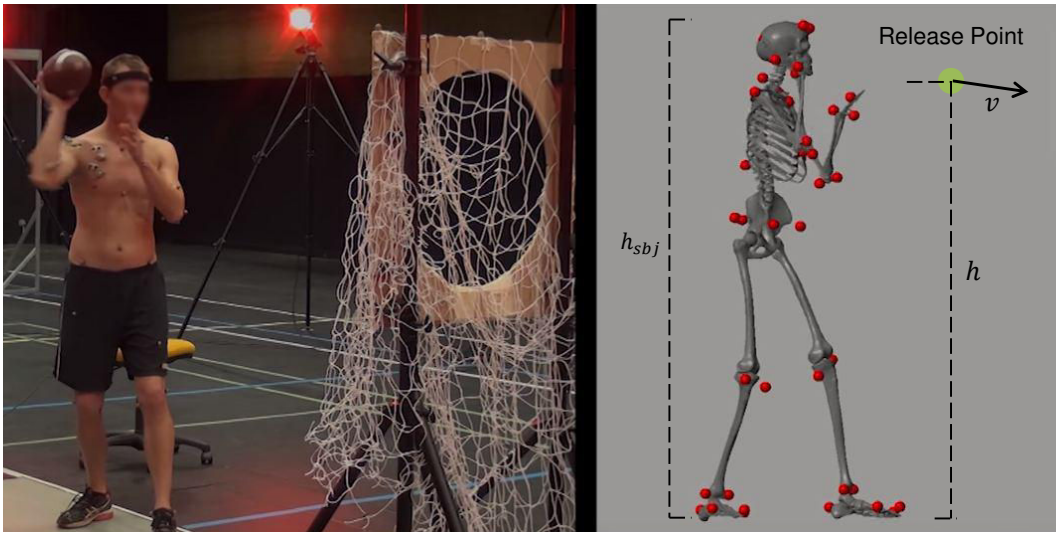

Figure 3.4 – **Kinematic features in the task space.** Two task space features were selected: velocity (v) and height (h) of release (which was normalized by the subject's height (h_s)).

These two task space features were used to construct a task feature vector per subject s, which describes the motion at different throwing distances d:

$$\mathbf{f}_{T,s} = \begin{bmatrix} \overline{v}_{2m,s} & \overline{v}_{4m,s} & \overline{v}_{7m,s} & \overline{h}_{2m,s} & \overline{h}_{4m,s} & \overline{h}_{7m,s} \end{bmatrix} \tag{3.1}$$

Where $s = 1...10$, and $\overline{v}_{d,s}$ and $\overline{h}_{d,s}$ are the mean release velocity and height at the distance d. Means were chosen in order to include representative values of all of the subject's throws at each distance. By generalizing Equation 3.1 to all subjects, a single task space feature vector can be obtained describing the representative kinematic strategy to multiple target distances:

$$\mathbf{f}_{T,All} = \begin{bmatrix} \overline{v}_{2m,All} & \overline{v}_{4m,All} & \overline{v}_{7m,All} & \overline{h}_{2m,All} & \overline{h}_{4m,All} & \overline{h}_{7m,All} \end{bmatrix} \tag{3.2}$$

3.3.2 Extraction

To extract these motion features from the experimental data, the time of release (t_{rel}) was first computed. This moment was determined as the instant at which the maximum hand velocity was reached, since it is known that this event occurs almost in parallel to ball release in the acceleration phase. For this purpose, a reflective marker was placed on the outer side of the hand (third metacarpal bone), as shown in Fig.3.3 A, and its position was recorded. After the derivation of this marker's trajectory, the maximum hand velocity or velocity at release (v) was determined as follows:

$$v = max\left(\sqrt{\mathbf{v}_x(t)^2 + \mathbf{v}_y(t)^2 + \mathbf{v}_z(t)^2}\right) \tag{3.3}$$

Where $\mathbf{v}_x(t)$, $\mathbf{v}_y(t)$, and $\mathbf{v}_z(t)$ are the velocity components of the hand marker. Next, the hand height at release (h) was determined as follows for each subject s:

$$h = \frac{\mathbf{h}_z(t_{rel})}{h_s} \tag{3.4}$$

Where $\mathbf{h}_z$ is the hand marker's position component along the z-axis (an axis perpendicular to the ground plane), and h_s is the height of the subject.

3.4 Synergy models identification

3.4.1 Definition

The synchronous time-invariant synergy model was selected to parametrize the control strategy during overhead throwing. These synergies describe how the subjects coordinated their muscles to achieve a set of kinematic features and task goals. Thus, they are the control variables during the motion.

To define these synergies, the time-invariant synergy model presented in Section 2.2.1 (Equation 2.10) was used. This model consists of a set of N-synergies that can be linearly combined to generate D-muscle activation signals. Such a model can be written in matrix form as:

$$A = WC \tag{3.5}$$

$$A = \begin{bmatrix} w_{11} & w_{12} & ... & w_{1N} \\ w_{21} & w_{22} & ... & w_{2N} \\ ... & ... & ... & ... \\ w_{D1} & w_{D2} & ... & w_{DN} \end{bmatrix} \begin{bmatrix} c_1(1) & c_1(2) & ... & c_1(T) \\ c_2(1) & c_2(2) & ... & c_2(T) \\ ... & ... & ... & ... \\ c_N(1) & c_N(2) & ... & c_N(T) \end{bmatrix} \tag{3.6}$$

Where, T is the total number of time samples, A is the $D \times T$ samples matrix containing the recorded muscle activations patterns or control signals, W is the $D \times N$ muscle synergy matrix, and C is the $N \times T$ samples combination coefficient matrix. The matrix A may contain the muscle signals of one or several trials. For instance, it can be constructed by concatenating the recorded signals of all throws of a particular subject s (matrix A_s), or all throws of all subjects (matrix A_{All}). In such cases the resulting combination coefficient matrix contains the temporal evolution of the synergies during all the concatenated throws.

Based on the previously described model, two control features were defined for each subject s: a time-invariant control feature (W_s) describing the relative activation level of muscles throughout a set of throws, and a time-variant control feature ($C_s = [\,C_{s,2m}\ C_{s,4m}\ C_{s,7m}\,]$) describing the temporal evolution of each synergy during each throw. Each sub-matrix $C_{s,d}$ is of dimensions $N \times T_d$, T_d being the total number of samples contained in the throws to distance d.

Finally, by generalizing these features (W_s and C_s) to all subjects, a single set of control features can be obtained describing the representative control strategy to multiple target distances: W_{All} and $\overline{C}_{All} = [\,\overline{C}_{All,2m}\ \overline{C}_{All,4m}\ \overline{C}_{All,7m}\,]$. Where W_{All} encodes the relative muscle activation levels for all subjects and throws, C_{All} are trial and subject specific coefficients, and $\overline{C}_{All}$ encodes the average way in which W_{All} was triggered for all subjects and throws. This averaging is needed due to the fact as per Equation 3.6 the time-invariant synergy model yields a single synergy matrix, but individual coefficients characterizing the time evolution of such synergies for each time sample.

In the results section (Section 3.6), the coefficients in this model will be described in terms of: 1) their shapes, 2) their triggering order, and 3) how their energy changes with throwing distance.

3.4.2 Extraction

Time-invariant synergies can be identified via matrix factorization algorithms, such as the NMF (Nonnegative Matrix Factorization) algorithm [KP08]. NMF was chosen due to the fact that it constraints the synergies to be nonnegative, but not necessarily independent. The non-negativity constraints yield physiologically meaningful results (as discussed in Section 2.2.2), and not imposing independence is consistent with the observed correlation among the activation of synergies [SWDd+01].

Essentially, the algorithm decomposes a non-negative matrix A into a non-negative linear combination of basis vectors contained in matrices W and C, by solving the following optimization problem:

$$\begin{aligned} \underset{W,C}{\text{minimize}} \quad & \frac{1}{2}||A - WC||_F^2 \\ \text{subject to} \quad & W \geq 0, C \geq 0 \end{aligned} \tag{3.7}$$

Where $||.||_F$ is the Frobenius norm. Before applying this algorithm the number of synergies to extract should be defined. To do this two criteria were used. The first, was choosing synergy models containing less synergies N than muscle signals in matrix A, and also less than the number of muscles in the virtual character in the next chapter (Section 4.2). This last constraint is important, since in a broader scope

the identified synergy models will be used to reduce the redundancy in the control of this character. The second criterion is based on the coefficient of determination (r^2) presented in Section 2.2.2. This coefficient was chosen due to the fact that it assess how well the shapes of the original muscle signals are reconstructed by the synergy model. The criterion states that the chosen number of synergies should correspond to the sharpest change in the slope of the r^2 curve. A curve that portrays the quality of activation signal reconstruction versus the number of synergies.

Once the synergy model was chosen, a metric was selected to describe the intensity with which the synergies were triggered per throwing distance. This metric was the synergy's energy. In signal processing terms, the energy in a signal is a measure of its size or strength, and it is quantified as the area under the square of the function. Thus, the average energy $\overline{E}_{c_i,d}$ of each combination coefficient $c_i(t)$ at each throwing distance d, was computed as follows:

$$\overline{E}_{c_i,d} = \frac{\sum_{n=1}^{T_d} |c_i(t_n)|^2}{Ntrials} \tag{3.8}$$

Where T_d is the total number of samples contained in the throws to distance d, $Ntrials$ is the number of trials per throwing distance, and t_n is the current time sample.

3.5 Identifying representative kinematic and control features

The previous extraction methods can be used to identify kinematic and control features (hand velocity and height at release, and synergies) for individual subjects. This section extends such methods to identify a common set of kinematic and control features (or synergies) representative of all subjects. Different algorithms were used to either identify common features after an individual subject analysis, or directly from the experimental data. For the first case, clustering algorithms were used. For the second case, a matrix-factorization based solution [dSB03] and cross-correlation were employed.

Clustering is a technique that consists in grouping features based on a similarity criteria. The number and separation between these groups can indicate the existence or not of a common feature, and therefore strategy (as will be later explained in Sections 3.5.1 and 3.5.2). To apply this technique, first, the features were standardized or normalized to the same scale, then two different types of clustering algorithms were implemented: a centroid-based clustering algorithm (*k-means clustering*) and a connectivity-based clustering algorithm (*hierarchical clustering*).

Different algorithms were used in order to verify if different techniques yielded similar strategies. Furthermore, the specific interest in using hierarchical clustering was to verify if the number of clusters of the k-means algorithm matched the natural divisions in the data.

K-means clustering is an iterative algorithm for data partitioning that assigns or classifies features into one of k clusters defined by centroids [Mac67]. The main steps of the algorithm are the following, given k: 1) select k initial cluster centroids, 2) compute the distances between each feature to each cluster centroid 3) assign the features to the cluster with the closest centroid all at once (phase 1), and individually reassign points if it reduces the sum of distances (phase 2), 4) obtain new centroids by averaging the features in each cluster, and 5) repeat steps 2-4 until the assignments do not change or the iterations reach their maximum. The k-means++ algorithm in MATLAB® was used with a squared euclidean norm to compute the distances. The advantage of this algorithm is that it uses the heuristic in [AV07] to find centroid seeds for k-means clustering. This results in a faster convergence to higher quality solutions, in other words, a lower sum-of-squares, point-to-cluster centroid distances (within each cluster). Finally, in order to assess the k-means clustering quality an indicator called cluster silhouette was computed [Rou87, KR08]. This indicator allows distinguishing clear-cut clusters from weak ones, or how well clusters are separated. It measures how similar the features are to features in their own cluster, when compared to features in other clusters, and is computed as follows:

$$Sil = \frac{(\eta_s - o_s)}{max(\eta_s, o_s)} \tag{3.9}$$

Where, o_s is the average distance from the feature s to the other features in the same cluster, and η_s is the minimum average distance from the feature s to features in a different cluster, minimized over clusters. The silhouette value can range from -1 to 1. By averaging the silhouette values of each feature and cluster, an average silhouette ($\overline{Sil}$) can be obtained for all clusters. Clustering quality is then assessed based on this value and by using the interpretation proposed by [KR08] in Table 3.3.

Table 3.3 – **Assessment of k-means clustering quality [KR08].** Subjective interpretation of the average silhouette value.

$\overline{\textbf{Sil}}$	**Proposed interpretation**
0.71-1.00	A strong structure has been found
0.51-0.70	A reasonable structure has been found
0.25-0.50	The structure is weak and could be artificial; try additional methods on data set
≤ 0.25	No substantial structure has been found

Therefore if $\overline{Sil} \geq 0.71$, the k clusters were said to be well separated, otherwise no clear separations could be made and only a single cluster existed.

Hierarchical clustering was then used to validate this assessment. Hierarchical clustering is an algorithm that aims at grouping features at different levels using a cluster tree or dendrogram. In agglomerative hierarchical clustering each feature starts in its own cluster [MR05], these clusters are then combined via a metric and a linkage criterion. The metric defines a distance between pairs of features, and the linkage criterion defines the distance between sets by computing the pairwise distances between features. An advantage of this algorithm over k-means is that it does not need an initial indication of the number of clusters, and therefore, it reveals the natural divisions in the data. For its implementation, the hierarchical algorithm tools in MATLAB® were used with the euclidean distance as metric, and an unweighted average distance (euclidean) for the linkage.

Finally, the clustering quality of this algorithm was assessed via dendrograms. Dendrograms are tree diagrams that illustrate the arrangement of clusters, the distance between them, and among their components (Figure 3.5). By making visual comparisons of these distances, the natural divisions in the data can be found. Such divisions exist when the distance between clusters is higher that the distance between their components. In other words, when the link joining a group of branches has a significantly different height from that of the links below it.

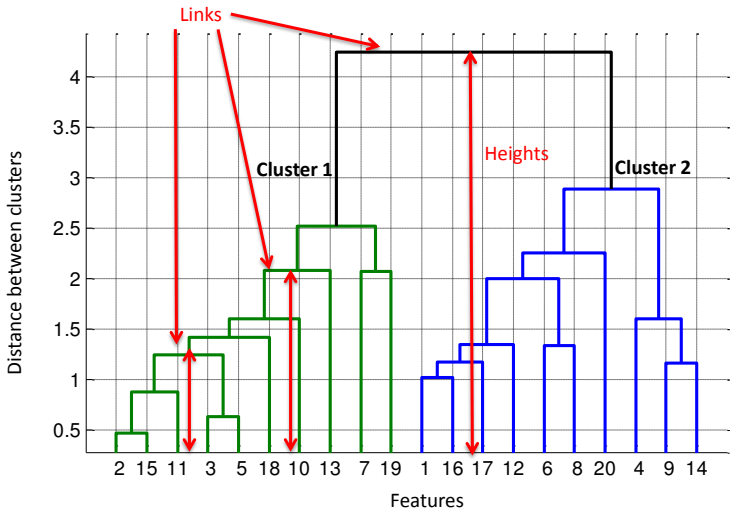

Figure 3.5 – **Example of a dendrogram.** A dendrogram composed of two well defined clusters. The height of each link indicates the distance between the connected components.

Section 3.5.1 describes how the above clustering techniques were used to identify common kinematic features. Then, Section 3.5.2 details how the synergy identification procedure in [dSB03] and clustering were used to extract common control features.

3.5.1 Kinematic feature identification ($\mathbf{f}_{T,All}$)

To determine if a common kinematic feature vector, and thus strategy, existed across subjects in task space, the feature vectors $\mathbf{f}_{T,s}$ in Equation 3.1 were given as inputs to the clustering algorithms. Since each subject is characterized by a 1×6 task vector, a unique strategy exists if $k = 1$. In other words if the features are so similar, that well separated clusters cannot be formed. When applying k-means this is evidenced by low silhouette values or a high number of clusters containing few or single features. On the other hand, when applying hierarchical clustering a unique strategy is evidenced when the heights of the top links in the dendrogram do not differ significantly from the links below them. In other words, when the distance between clusters is similar or shorter than the distance between their components. If this was the case, then the common task space feature vector $\mathbf{f}_{T,All}$ was computed by averaging the task feature vectors ($\mathbf{f}_{T,s}$) across subjects.

3.5.2 Control feature identification (W_{All}, $\overline{C}_{All}$)

The common control features (W_{All}, $\overline{C}_{All}$), and thus strategy, were extracted through the identification procedure in [dSB03] which allows a direct extraction from experimental data. In this method a matrix A_{All} was constructed by concatenating the activation signals for all trials of all subjects. NMF was then applied on this pool of signals, yielding: 1) one single synergy matrix (W_{All}) for all subjects, and 2) a set of subject and trial specific coefficients C_{All}. The next step was to identify a representative set of coefficients ($\overline{C}_{All}$). To do this, first, representative coefficients per subject and throwing distance were computed. Then, cross-correlation, which measures the similarity of two signals as a function of the lag of one relative to the other, was used to compare the coefficients. If the coefficients were similar among subjects (high cross-correlation at short lags), then a second averaging was performed across subjects at each throwing distance, yielding the final coefficients ($\overline{C}_{All}$).

Next, a second method was implemented in order to compare and validate the representative synergy matrix (W_{All}) with synergies extracted from individual subjects. This comparison was not made for the coefficients ($\overline{C}_{All}$) due to the fact that both methods are similar in the way they compute the coefficients: both first compute coefficients describing each subject and throw individually. However, the methods differ in the way the representative synergy matrix is computed, as will be evidenced shortly. This second method is based on grouping synergies via k-means (similarly to [SWDd+01]), and hierarchical clustering. It consists of 3 stages: 1) extraction of individual subject synergy models, 2) standardization of $\mathbf{w}_i$ vectors, and 3) application of k-means and hierarchical clustering algorithms. In the first

stage, a matrix A_s was constructed per subject, by concatenating the activation signals of each of his repetitions. Next, NMF was applied on each matrix A_s to obtain a single N-synergy model (W_s, C_s) per subject. Once a model was obtained for each subject, the synergy matrices W_s were standardized and each of its vectors $\mathbf{w}_i$ were used to create a feature pool for the clustering algorithms. Each of these vectors was treated individually, without specifying its correspondence to a specific subject.

The k-means algorithm was applied first while varying the number of clusters k. Since each subject is characterized N-synergies, a unique strategy exists if $k = N$, in other words if the number of clusters is equal to the number of synergies extracted for each subject. If this was the case, then the centroids of these clusters were taken as the representative control strategy (W_{kmeans}), and it was later compared with the synergy matrix of the first method (W_{All}).

Finally, hierarchical clustering was applied to determine if the natural divisions in the data matched the results provided by k-means. With this algorithm a unique strategy exists if N well separated branches are seen in the dendrogram. In other words, if the number of branches is equal to the number of synergies extracted for each subject.

3.6 Results

The previous methods were applied to identify a representative kinematic and control strategy for overhead throwing motions. First, a validation stage was made using a single subject (Section 3.6.1) with the purpose of: 1) selecting an appropriate muscle set for extraction, and 2) determining if the methods allowed the identification of a low-dimensional control strategy with links to task space features and goals. After this validation, the chosen muscle set was used in the procedures in Section 3.5. The results show the existence of a common low-dimensional control strategy across subjects, which is modulated according to the throwing distance (Section 3.6.2).

3.6.1 Methodology and muscle set validation

To identify a representative control strategy, it is first important to choose an appropriate set of muscles to analyze. The main reason for this, is that the choice and number of muscles may affect the structure of the identified synergies. The authors in [STP13] proposed that an appropriate muscle set should contain dominant muscles during the motion, as synergies extracted from such muscles reflect well the synergies extracted from significantly larger muscle sets, and thus encode repre-

sentative control strategies. In other words, the synergies extracted from dominant muscle sets are preserved in those extracted from larger sets. This preservation can be evidenced by high linear dependency among matching synergies in each set.

The purpose of this section is to identify and validate an appropriate muscle set from which to extract a representative control strategy for overhead throwing. To do this, a synergy analysis was made on a single subject using different muscle sets. As described in Section 3.2.4, these sets were constructed by gradually isolating muscles of the arm until arriving to a hypothetical dominant muscle set (Set_6), encoding important actions during throwing and with matching muscle actions to those of the virtual character in the next chapter. The results show that the synergy model extracted from this set is preserved in models extracted from higher order sets, evidencing that it encodes dominant muscle actions during throwing. The analysis also revealed the existence of a low-dimensional control strategy consisting of 2-synergies, an agonist and an antagonist synergy, whose triggering intensity increased with the kinematic features' magnitude as throwing distance increases.

Synergy models were extracted for the different muscle sets in Table 3.2, using the extraction procedure in Section 3.4.2. First, a muscle activation matrix (A) was constructed for each muscle set. Each matrix contained the concatenated muscle activations of all throws (18 throws in total), beginning with the 2m throws, then 4m throws, and finally 7m throws. Then, the NMF algorithm (Section 3.4.2) was applied while varying the number of synergies to extract to determine the synergy model order.

As explained in Section 3.4.2, the synergy model order should allow a reconstruction of the most important trends in the activation signals, and be less than the number of muscles in matrix A and in the virtual character (6 muscles) in Section 4.2. First, the muscle activation reconstruction quality was assessed through the coefficient of determination r^2, as shown in Figure 3.6.

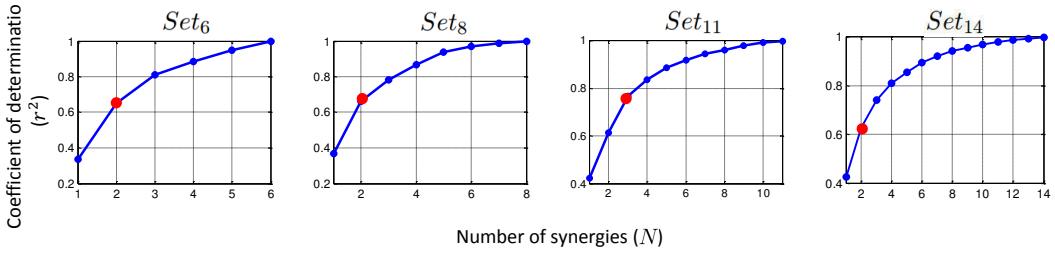

Figure 3.6 – **Activation reconstruction quality across synergy models per muscle set.** The NMF algorithm was applied on each muscle set while varying the number of synergies (N). The resulting curve depicts the r^2-values for each model. The sharpest changes in slope are denoted by the red dots.

For all muscle sets, the quality of reconstruction increases with the number of

synergies. For Set_6, Set_8, and Set_{14} the sharpest change in slope of the r^2-curve occurs at $N = 2$ synergies, while for the Set_{11} the sharpest change occurs at $N = 3$. The quality of reconstruction seems to depend on the muscle but in all cases a low-dimensional strategy exists which is less than the number of muscle in the A matrices, and in the virtual character. Therefore, since $N = 2$ for the majority of muscle sets, including the hypothetical dominant muscle set (Set_6), the following analysis will focus on 2-synergy models.

The 2-synergy models extracted for each set allow a reconstruction quality of $r^2 = 0.61$ to 0.66 (depending on the muscle set). To evaluate this reconstruction accuracy, several factors, besides the number of synergies, which are linked to the experiment itself should be considered, such as: the type of motion, how constrained or repeatable the task is, the number of repetitions used for extraction, number of muscles and subjects. Thus, a comparison was made to the closest motion to overhead throwing in the synergy analysis literature, the study of fast reaching motions in [dPFL06]. In this study an activation reconstruction accuracy between $0.7 - 0.8$ was achieved with $4 - 5$ synergies. However, the synergies were extracted from fairly constrained or repeatable motions (that used via points to guide the motion), and the EMG patterns used for extraction were averaged for several trials. In the present study the synergies are extracted from an unconstrained motion and a concatenation of trials, and thus, the r^2 criterion evaluates the reconstruction of each individual trial, and not of an average. Consequently, a quality of reconstruction ≥ 0.6 was taken as an acceptable reconstruction accuracy for the current experiments.

Next, each of the 2-synergy model was analyzed. Each model is composed by a synergy matrix W (Figure 3.7), containing the time-invariant synergy vectors, and a combination coefficient matrix containing the time evolution of each synergy (Figure 3.8). The resulting synergy matrices contain two synergies: an agonist ($\mathbf{w}_1$) and an antagonist synergy ($\mathbf{w}_2$) to the motion. The terms agonist and antagonist refer to muscles that provoke or inhibit movement. Agonist muscles cause movement by contracting, while antagonist muscles oppose this movement to control it or slow it down. These are not properties of muscles, but roles that depend on the specific motion. Such roles were used to refer to the synergies in this study since they grouped most muscles into agonists and antagonists to the motion. Thus, the agonist synergy contains a high activation of muscles that provoke the motion, or muscles corresponding to biomechanical actions such as: trunk extension (*erector muscles*), upward scapular rotation (*upper and lower trapezius*), shoulder internal rotation and flexion (*lastissimus dorsi and deltoid anterior*), and elbow extension (*triceps*). The antagonist synergy contains a high activation of muscles that oppose the motion, or muscles corresponding to scapular retraction and depression (*middle and lower trapezius*), elbow flexion (*biceps*), and a low activation of the deltoids.

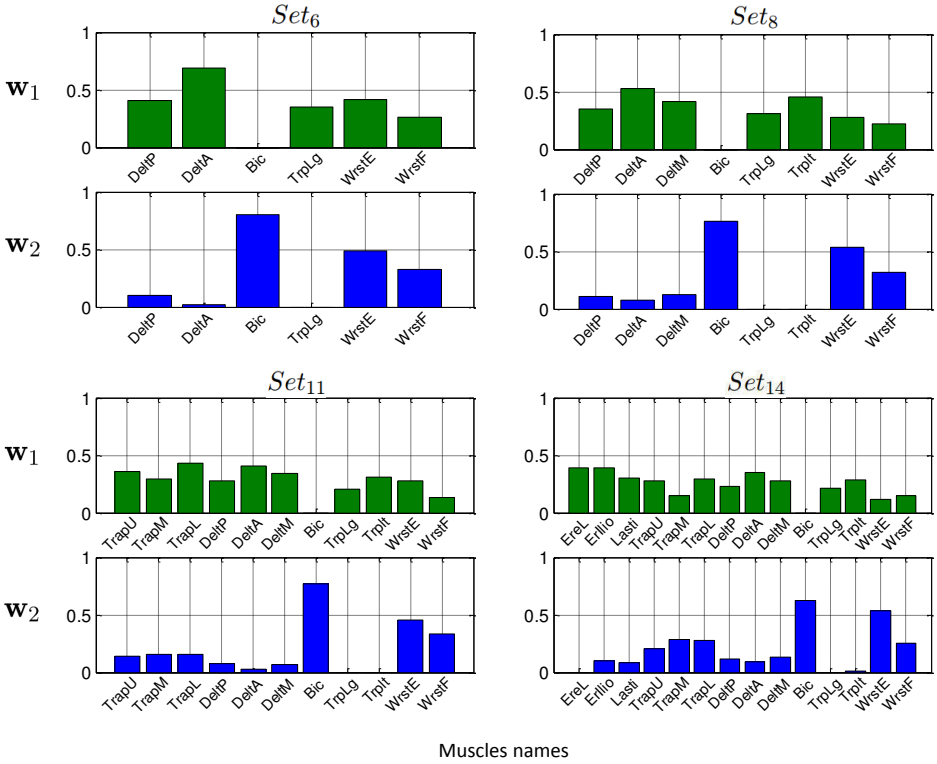

Figure 3.7 – **Synergy vectors $\mathbf{w}_i$ per muscle set.** A 2-synergy model was extracted for each muscle set. The resulting vectors ($\mathbf{w}_1$ and $\mathbf{w}_2$) contain the activation levels of each muscle throughout the concatenated motions. The synergies of Set_6 are preserved in those of higher order sets. This preservation is quantified in Table 3.5. Thus, Set_6 contains dominant muscle actions [STP13].

It is interesting to see how these agonist and antagonist organization is preserved across models, and that the synergies extracted from a lower number of muscles, are well preserved as the number of muscles increases. For instance, through visual inspection, it can be seen that the synergies of Set_6 are preserved in those of Set_8, the synergies of Set_8 are preserved in those of Set_{11}, and finally, the synergies of Set_{11} are preserved in those of Set_{14}. This preservation can also be shown by comparing the activation levels of muscles common to every two sets. To do this, the synergies from each set were compared to the same subset of muscles from the subsequent higher order sets. This comparison was made through the sample pearson linear correlation coefficient (ρ) between the best matching pairs of synergies for every two sets. The results of these comparisons are shown in Table 3.4.

In all comparisons the correlation coefficient ρ is high ($0.86 - 0.99$), indicating a high linear dependency among synergies, and thus their preservation across muscle sets. Furthermore, the synergies extracted from the smallest set of muscles (Set_6) are preserved in models extracted from higher order sets, as shown in Table 3.5. These preservation evidences the existence of a low-dimensional control strategy for

overhead throwing, and that Set_6 contains dominant and relevant muscles [STP13].

Table 3.4 – **Similarity between the synergies extracted from different muscle sets.** The pearson linear correlation coefficient (ρ) between the best matching pairs of synergies for every two sets was computed. A total positive correlation corresponds to $\rho = 1$. Correlations near this value indicate a high linear dependence, and thus a high similarity among synergies.

Correlation coefficient ρ between synergies		
Sets	$\rho_{\mathbf{w}_1}$	$\rho_{\mathbf{w}_2}$
Set_6 and Set_8	0.9835	0.9947
Set_8 and Set_{11}	0.9544	0.9922
Set_{11} and Set_{14}	0.8634	0.9418

Table 3.5 – **Similarity between the synergies in Set_6 and higher order sets.** The pearson linear correlation coefficient (ρ) between the best matching pairs of synergies of Set_6 with the rest of the sets. A total positive correlation corresponds to $\rho = 1$. Correlation near this value indicate a high linear dependence, and thus a high similarity among synergies.

Correlation coefficient ρ between synergies		
Sets	$\rho_{\mathbf{w}_1}$	$\rho_{\mathbf{w}_2}$
Set_6 and Set_8	0.9835	0.9947
Set_6 and Set_{11}	0.9849	0.9987
Set_6 and Set_{14}	0.9220	0.9685

The previous extractions not only revealed a low-dimensional control strategy, but also that this strategy was triggered similarly across throws, and modulated according to the kinematic features and throwing distance. Furthermore, this behavior was preserved across muscle sets. The resulting combination coefficients per trial were averaged at each distance d, resulting in the average coefficients ($\bar{c}_1(t)$ and $\bar{c}_2(t)$) in Figure 3.8. In this figure, the first coefficient ($\bar{c}_1(t)$) approaches a bell shaped profile (as the velocity profile in ballistic movements), while the second coefficient ($\bar{c}_2(t)$) is more irregular, it has a lower amplitude, and it tends to decrease as the throw is performed.

These average profiles and their standard deviation curves show visually repeatable trends among throws to the same distance and also across distances. This repeatability can be quantified by computing the cross-correlation scores among averages across throwing distances, as shown in Table 3.6. Such scores measure how similar the coefficients are as a function of the lag between them, allowing to compare their shapes. For all coefficients and muscle sets, high cross-correlation scores at lags (delay/signal length) near zero can be seen, evidencing that the synergies are triggered similarly across throwing distances.

Besides a repeatability in terms of shape, the coefficients also share temporal similarities. As seen in Figure 3.8, in general, in the beginning of the throw $\bar{c}_2(t)$

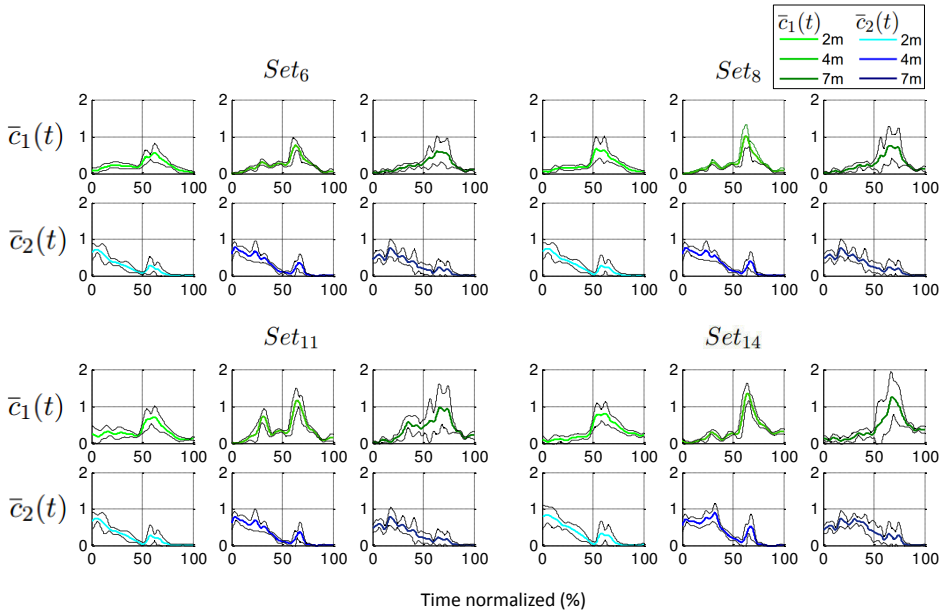

Figure 3.8 – **Average synergy combination coefficients $\bar{c}_i(t)$ per muscle set.** A 2-synergy model was extracted for each muscle set. The resulting coefficients were averaged per throwing distance d. Thus, $\bar{c}_1(t)$ and $\bar{c}_2(t)$, encode the general manner in which each synergy is triggered to perform a throw to distance d.

Table 3.6 – $\bar{c}_i(t)$ **repeatability across throwing distances.**

Cross-correlation and lags (delay/signal length)							
Set	$\bar{c}_i(t)$	$corr_{2m,4m}$	$corr_{2m,7m}$	$corr_{4m,7m}$	$lag_{2m,4m}$	$lag_{2m,7m}$	$lag_{4m,7m}$
Set_6	$\bar{c}_1(t)$	0.9657	0.9711	0.9689	0.0340	0.0437	0.0250
	$\bar{c}_2(t)$	0.9640	0.9197	0.9618	0	0.0017	0
Set_8	$\bar{c}_1(t)$	0.9648	0.9730	0.9670	0.0694	0.0833	0.0344
	$\bar{c}_2(t)$	0.9668	0.9261	0.9660	0	0.0007	0
Set_{11}	$\bar{c}_1(t)$	0.9345	0.9467	0.9613	0.0621	0.0805	0.0375
	$\bar{c}_2(t)$	0.9662	0.9200	0.9630	0	0.0014	0
Set_{14}	$\bar{c}_1(t)$	0.9552	0.9685	0.9675	0.0659	0.0725	0.0337
	$\bar{c}_2(t)$	0.9310	0.8961	0.9545	0.0056	0.0552	0.0028

(antagonist synergy) is activated, then its amplitude is diminished, until $\bar{c}_1(t)$ (agonist synergy) is activated. At this moment $\bar{c}_2(t)$ is activated again, and the most significant co-activation occurs among the synergies. This is consistent with the fact that ballistic movements exhibit concurrent agonist and antagonist muscle activation [LMO+99]. During these motions, a first activation is needed to accelerate the limb towards the target ($\bar{c}_1(t)$), followed by a second activation to decelerate and stop the movement ($\bar{c}_2(t)$). This sequence of bursts (from antagonist to agonist, and from agonist to antagonist) are characteristic of the antagonist activity in the upper extremity while throwing. Such "triad" burst sequences have been previously

identified in EMG analysis of throwing (at the wrist and elbow muscles) [HKS+02], and in badminton smash strokes [SO00].

Another characteristic of the coefficients that was analyzed was the changes in energy across throwing distances. Fig.3.9 shows the average energy of each coefficient at each throwing distance, as described in Equation 3.8. The results show that the energy changes in the coefficients are linked to changes in the task space features: Like the task space features, mean release velocity ($\overline{v}$) and height ($\overline{h}$) in Figure 3.10, the energy in the coefficients increases with the throwing distance.

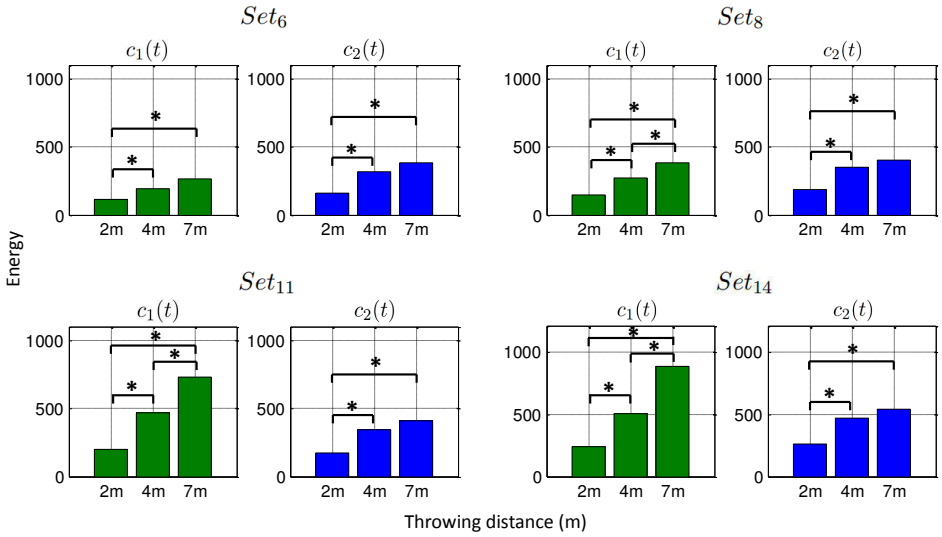

Figure 3.9 – **Average energy of combination coefficients $c_i(t)$ per throwing distance.** The average energy of each synergy increases with throwing distance. These increments are always statistically relevant from $2m$ to $4m$ and from $2m$ to $7m$.

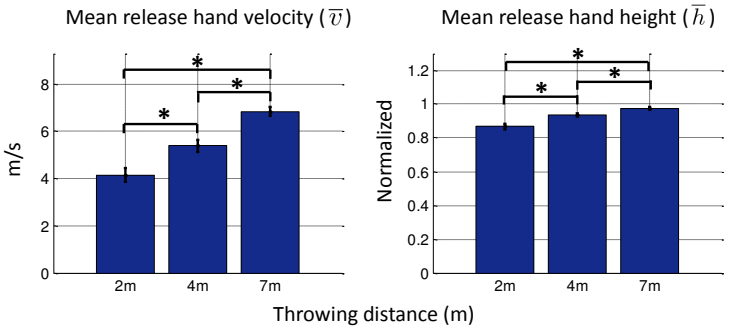

Figure 3.10 – **Task space features per throwing distance.** Mean hand velocity $\overline{v}$ and height $\overline{h}$ at each throwing distance. Statistically relevant increments are denoted by the symbol *.

The energy increments (from $2m$-$4m$ and $2m$-$7m$) are always statistically relevant for both synergies. This increment in the actuation signals (or synergies), is consistent with the increment in torque magnitudes observed during the synthesis of

throwing motions to different ranges [KXY+10]. Furthermore it is interesting to see that the average energy of the agonist synergy ($c_1(t)$) significantly increases as the number of muscle in the set increases. This can be due to the fact that this synergy recruits muscles with significant activations during the motion, such as back and shoulder muscles.

Finally, the synergies ($\mathbf{w}_i$) and coefficients ($c_i(t)$) in each model can be linearly combined (Equation 3.5) to reconstruct the recorded muscle activation patterns (A). These synergies are expected to encode important temporal and spatial information, that allow a reconstruction of the most important trends of the recorded muscle activations. The four synergy models that were analyzed allowed a reconstruction quality of $r^2 = 0.61$ to 0.66 for the 18 concatenated muscle activations, which as explained in the beginning of this section is an acceptable reconstruction quality considering the redundancy of the task, and the fact that each individual trial is being reconstructed and not an average of trials. Figures 3.11 and 3.12 show examples of the activation reconstruction of a single 7m throw using these synergy models.

Due to the fact that a minimal number of synergies were used, small oscillations, amplitudes, and delays are lost in some of the muscles. Part of this information loss will correspond to important trends in the activations, but as of the r^2 criterion, a majority of this information will be due to noise-dependent variability and most of the important activation trends will be preserved. An example of this can be seen in Figure 3.11 (Set_6), where the reconstructed muscle activation of the deltoid posterior is delayed and of lesser amplitude but its general activation profile and timing are similar to the recorded one. Another example can be seen in Figure 3.11 (Set_8), where the general activation profiles and timings are preserved for most muscles: the activation of the deltoids and triceps peak in the second half of the motion, while the biceps, wrist extensors and flexors are activated in the first and second halves. Finally, a similar behavior can be seen in Figure 3.12 for Set_{11} and Set_{14}. However, as more muscles are added, the quality of reconstruction decreases as seen by the loss of amplitude of the upper and medial trapezius. This decrease is expected, since the matrix factorization algorithm attempts to encode the activation information of a higher number of muscles in only 2 synergies.

The previous results evidence the existence of a low-dimensional control strategy during overhead throws in a single subject, consisting of an agonist and an antagonist synergy, which are linked to task space features and goals through their triggering intensity. Furthermore, an appropriate muscle set was identified containing dominant muscles during this motion. This set will serve as a basis for the analysis presented in the next section: the extraction of a representative control strategy for overhead throwing across subjects.

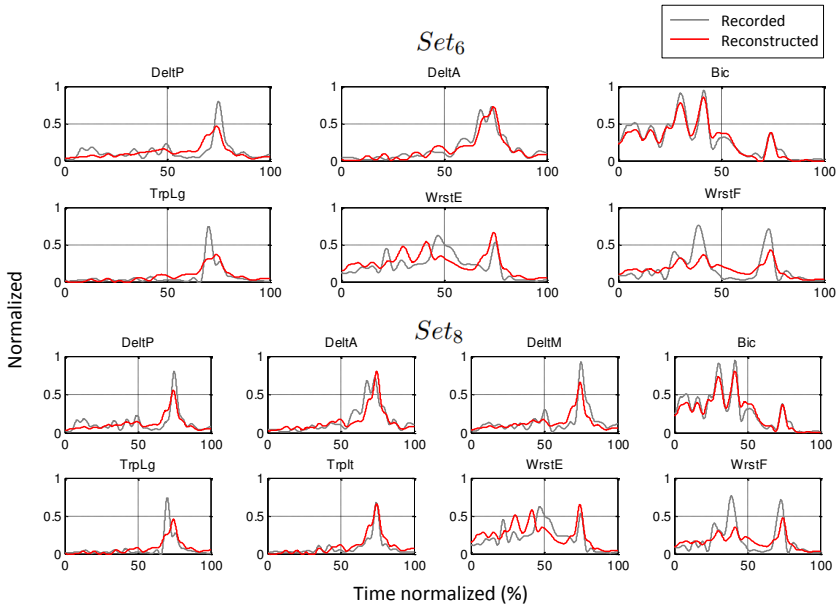

Figure 3.11 – **Activation reconstruction of the muscles in Set_6 and Set_8 (7m throw).** The 2-synergy models extracted from each set were used to reconstruct the recorded muscle activations.

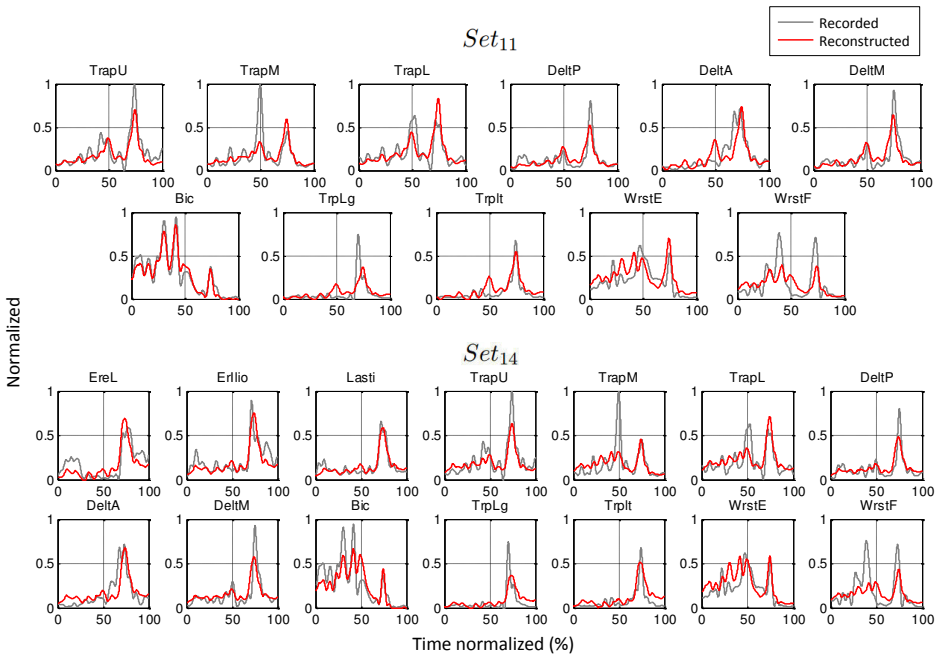

Figure 3.12 – **Activation reconstruction of the muscles in Set_{11} and Set_{14} (7m throw).** The 2-synergy models extracted from each set were used to reconstruct the recorded muscle activations.

3.6.2 Representative kinematic and control strategy for overhead throwing

After validating an appropriate muscle set and the methodology for synergy extraction, the next step consisted in identifying if a representative kinematic and control strategy exists for overhead throwing. In other words, if similar strategies are employed across subjects in spite of differences in morphology and physical conditions. To identify such a strategy the muscle Set_6 and the methods in Sections 3.3, 3.4, and 3.5 will be used. The results corroborate this hypothesis and show the existence of a common control strategy across subjects, consisting of an agonist and an antagonist synergy whose triggering intensity increases with the throwing distance, similar to the strategy found for a single subject in Section 3.6.1.

3.6.2.1 Representative kinematic strategy

To identify if a representative kinematic strategy existed, first, a task feature vector ($\mathbf{f}_{T,s}$) was extracted containing the mean hand velocity ($\overline{v}$) and height at ball release ($\overline{h}$) for each subject s. Figure 3.13 shows all task feature vectors.

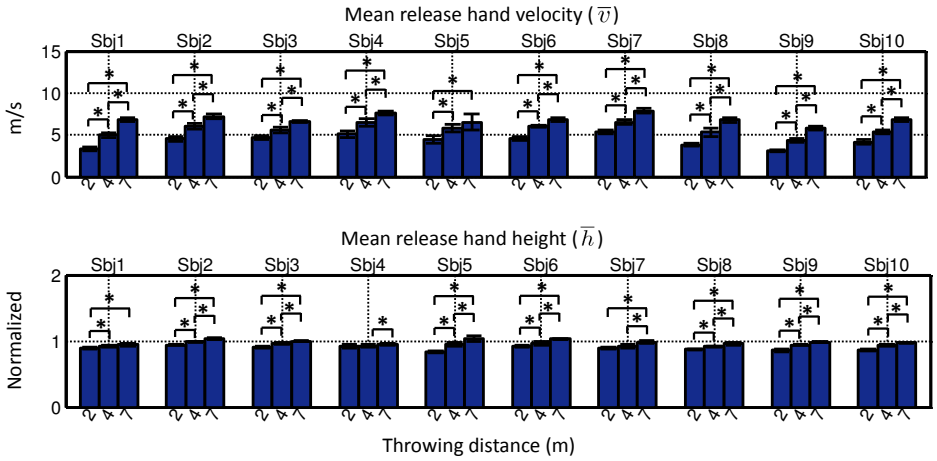

Figure 3.13 – **Task space features per subject and throwing distance.** Mean hand velocity $\overline{v}$ and height $\overline{h}$ at each throwing distance per subject. Statistically relevant increments are denoted by the symbol *.

A gradual increase in hand release velocity and height can be seen across subjects as the throwing distance increases. The statistical relevance, or the assertion that these increments are large enough and unlikely to have occurred solely by chance, was then quantified via the Wilcoxon rank sum test. These increment were statistically relevant in 9/10 subjects for the hand velocity, and in 7/10 subjects for the hand height.

Next, k-means and hierarchical clustering were applied on the ensemble of fea-

ture vectors ($\mathbf{f}_{T,s}$) in order to determine if one sole task space strategy existed. A single strategy is expected if $k = 1$, that is, if a group of well separated clusters cannot be found. K-means was applied first while varying the number of clusters k. Figure 3.14 shows each cluster's silhouette as k increases. The average silhouette value $\overline{Sil}$ remains below the 0.71 threshold (Table 3.1) until $k = 5$. However, although the threshold is surpassed, clusters containing 1-2 subject vectors begin to be formed. Therefore, from the k-means analysis we can conclude that the subjects do not employ significantly different task space strategies, and that only one task space strategy exists with the chosen set of features.

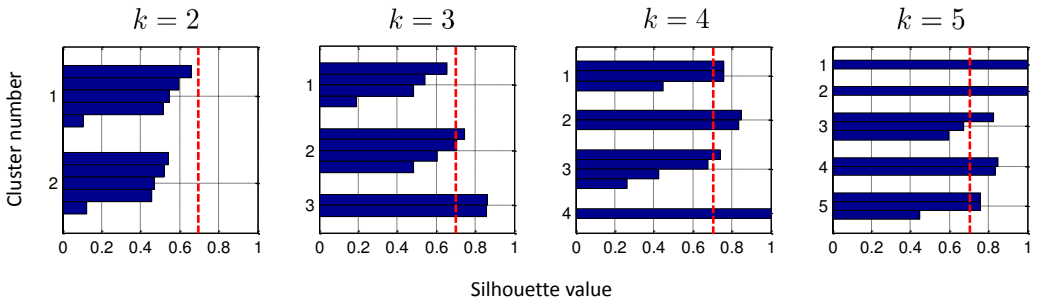

Figure 3.14 – **Task space cluster separation quality using k-means.** Strongly separated clusters ($\overline{Sil} \geq 0.71$) cannot be found. A single cluster or a common kinematic strategy in the task space exists across subjects.

Hierarchical clustering was then applied in order to verify if there was indeed only one strategy, and if there were any natural and significant divisions in the data. Figure 3.15 features the resulting cluster tree or dendrogram.

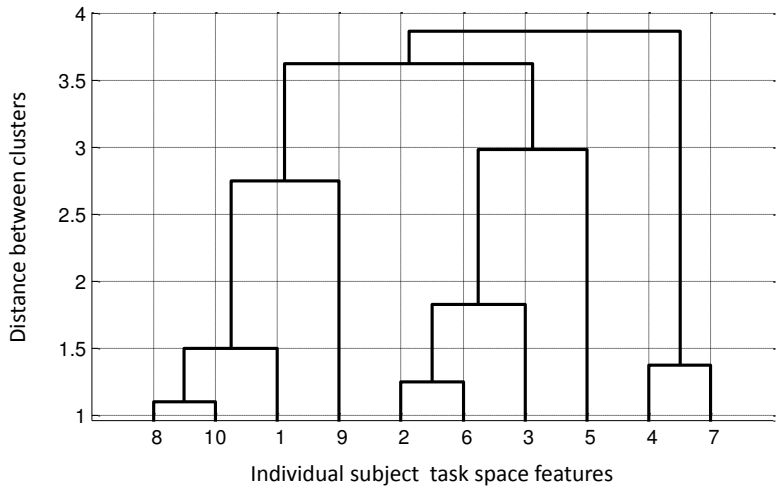

Figure 3.15 – **Task space cluster separation using hierarchical clustering.** Strongly separated clusters are not found. The heights of the links at the top of the hierarchy do not differ significantly from the heights of the links below them, indicating a shorter distance between clusters than between the features they contain.

In this tree no significant divisions are found. This is shown by the fact that heights of the links at the top of the hierarchy are not significantly different from the heights of the links below them, indicating similar and even shorter distances between clusters than between the features they contain. Furthermore, with this procedure we can also see that as the number of clusters increases, groups containing very few subject vectors begin to be formed.

Both clustering algorithms indicate that, given the analyzed set of features, there exists one kinematic strategy in the task space ($\mathbf{f}_{T,All}$) for all subjects. A strategy which consists in increasing the hand release velocity and height as the throwing distance increases (Figure 3.16).

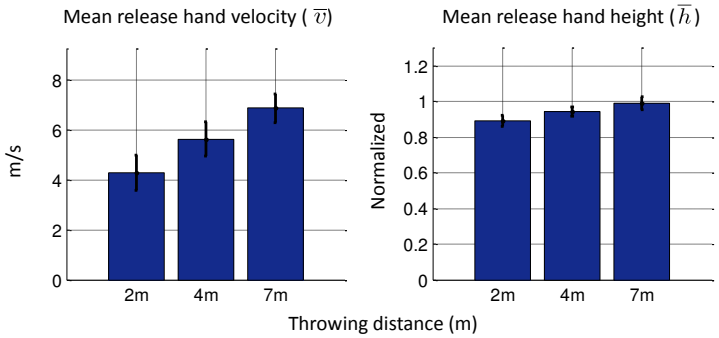

Figure 3.16 – **Representative task space strategy for all subjects ($\mathbf{f}_{T,All}$).** By averaging the task features across subjects, a representative hand velocity and height at release was obtained for all subjects.

In average, as this distance increased 2-3 m, the hand velocity (v) increased by 1.3 m/s , and the hand-height/subject-height (h) by a factor of 0.05. The distance or range, was also roughly proportional to the square of the release velocity, as can be evidenced through the equations of projectile motion. Both of these observations are consistent with other studies that indicate an increase in height and speed with throwing distance, and the existence of a proportionality relationship between speed and range [KXY+10].

3.6.2.2 Representative control strategy

The next step was to determine if a representative control strategy existed. First, the synergy identification strategy described in section 3.4 was applied on each of the subject's EMG dataset (using the muscles in Set_6) while varying the number of synergies. The objective of this was to identify for each subject, a model (W_s, C_s) with less synergies than muscles ($N < 6$) that would also guarantee a good reconstruction of the original EMG signals. Figure 3.17 shows the quality of reconstruction (r^2) for each subject and synergy model. The sharpest change in slope of

this curve occurred at $N = 2$ for 8 subjects, and at $N = 3$ for 2 subjects. Thus, as in the individual subject analysis, 2-synergy models were chosen.

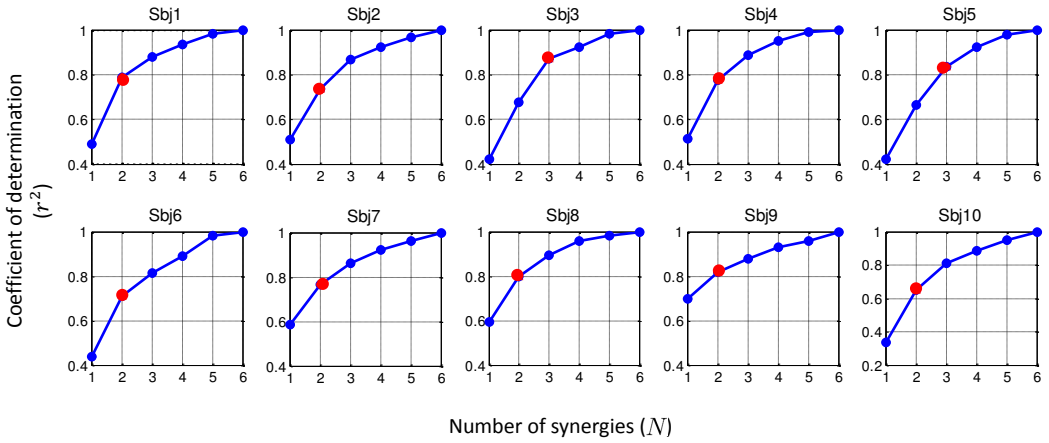

Figure 3.17 – **Activation reconstruction quality across synergy models per subject.** The NMF algorithm was applied on each subject's EMG data set while varying the number of synergies (N). The resulting curve depicts the r^2 values for each model. The sharpest changes in slope are denoted by the red dots.

The accuracy of activation reconstruction varied among subjects, possibly due to the different abilities to perform repeatable throwing motions at each distance. However, in average, these models allowed a reconstruction quality of 0.7382. An accuracy, which is again comparable to those found in studies on fast reaching motions ($r^2 = 0.7 - 0.8$) [dPFL06].

The consistent existence of a 2-synergy model across subjects, further motivated the identification of a common control strategy. To do this, the synergy identification procedure of [dSB03] (Section 3.5.2) was used. Therefore, a large EMG matrix (A_{All}) was constructed with 6 signals (one per muscle). Each of these signals was composed of 180 concatenated activations, corresponding to each of the subject's trials (10 subjects, 3 throwing distances, 6 trials per distance). Next, the NMF algorithm was applied on this matrix, and the synergy model corresponding to the sharpest change in the r^2 curve was selected. This change occurred again at $N = 2$ synergies, where the reconstruction quality was of 0.6526. This slight decrease in reconstruction quality with respect to the individual extractions was expected since this method attempts to reconstruct a higher number of trials simultaneously (180 trials instead of 18), which are performed by a variety of subjects. However, the reconstruction quality is comparable to other studies extracting synergies from the concatenated muscle signals of multiple trials and subjects, such as [dSB03], where the activation patterns of over 200 frog kicks were reconstructed with an r^2 of about 0.6.

The resulting representative synergy matrix W_{All} is depicted in Figure 3.18.

Each synergy contains the relative activation levels of a group of muscles throughout the motions. As in the single subject analysis (Figure 3.7, Set_6), the first synergy ($\mathbf{w}_1$) can be seen as the agonist synergy, and the second synergy ($\mathbf{w}_2$) can be seen as the antagonist synergy to the motion. Therefore, $\mathbf{w}_1$ contains a high activation of muscles corresponding to shoulder flexion and internal rotation (*deltoid anterior*), elbow extension (*triceps longs*), and wrist flexion (*forearm flexor bundle*). While $\mathbf{w}_2$ contains a high activation of muscles corresponding to elbow flexion (*biceps*), wrist extension (*forearm extensor bundle*), and a very lower activation of the deltoid muscles.

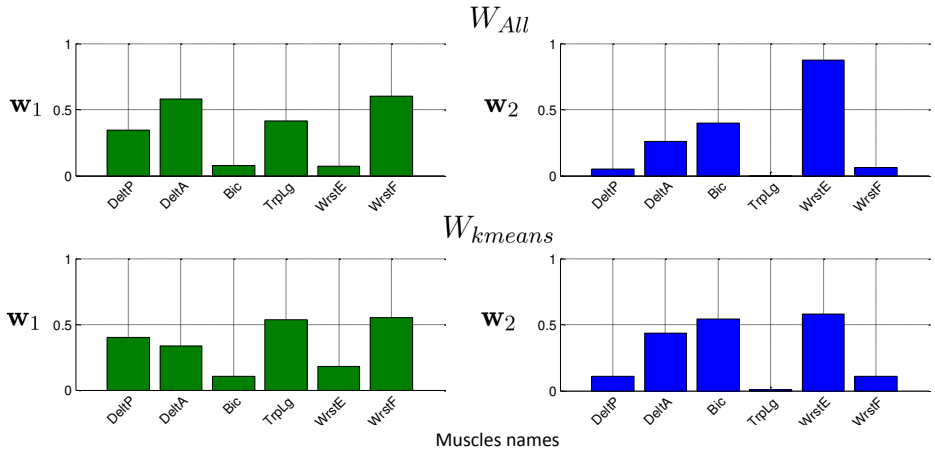

Figure 3.18 – **Representative control strategy (synergies) W_{All} and W_{kmeans} for all subjects.** A common control strategy was identified for the time-invariant part of the synergies through two different methods: the method described in [dL13] and k-means clustering.

An interesting difference between this model and the single subject model (Figure 3.7, Set_6), is that the muscle actions on the wrist are also separated into agonist and antagonist actions, with a high activation of the forearm flexor bundle in $\mathbf{w}_1$ and a high activation of the forearm extensor bundle in $\mathbf{w}_2$. This is due to fact that the majority of subjects did not consistently co-activated these two muscle groups with similar intensities, but allowed the extensor group to play a more important role before the acceleration phase, and the flexor group in the acceleration phase.

A second method based on clustering was then applied in order to validate the representative synergy W_{All} against the individual synergy models (W_s, C_s). Therefore, a pool containing the synergy vectors $\mathbf{w}_i$ of all subjects was constructed without specifying if the synergies belonged to the same subject. Thus, the pool contained 20 synergies (2 synergies per subject). First, k-means clustering was applied on the pool while varying the number of clusters k. A single control strategy is expected to exist when $k = N$, or when the number of clusters is equal to the number of synergies extracted per each subject, 2 in this case. Figure 3.19 shows

that indeed, the best cluster separation is achieved at $k = 2$, where the average silhouette value for both clusters is equal to 0.7181. If a higher number of clusters or separations are made, the average silhouette values decrease and clusters containing very few synergies are formed.

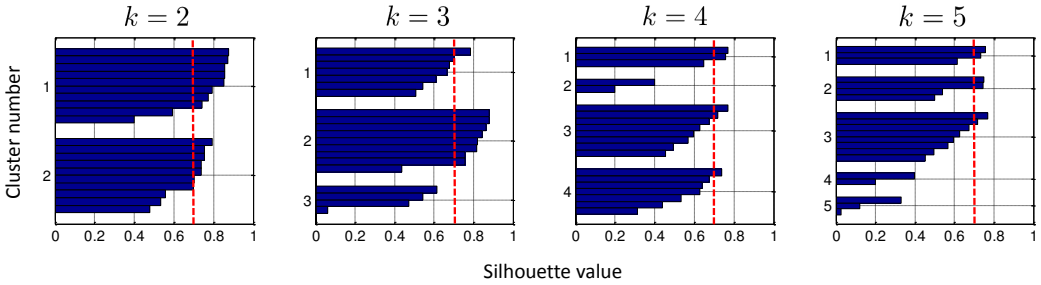

Figure 3.19 – **Synergy cluster separation quality using k-means.** Strongly separated clusters ($\overline{Sil} > 0.71$) are found at $k = 2$. Therefore, a common control strategy exists across subjects.

To further verify if the natural divisions of the data corresponded to 2 groups of distinctive synergies, hierarchical clustering was applied. This resulted in the cluster tree (dendrogram) in Figure 3.20. The tree shows how the 20 synergies in the pool are partitioned into 2 clusters as well.

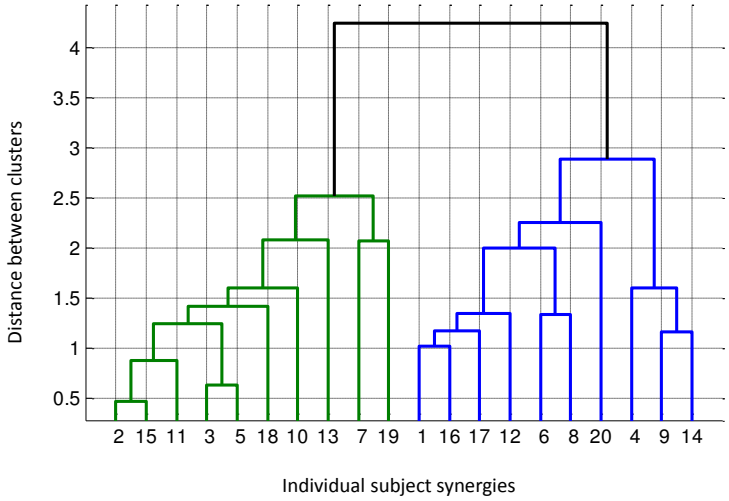

Figure 3.20 – **Synergy clusters using hierarchical clustering.** Two strongly separated clusters are found. The height of the link dividing the data into two branches differs significantly from the heights of the links below it, indicating a larger distance between clusters than between the features they contain.

This is evidenced by the fact that the link separating the synergy data into two branches is inconsistent with the links below it. In other words, its height is significantly different from that of the links below it, indicating a larger distance between clusters than between the synergies they contain. Interestingly, the individual syn-

ergies within each cluster in the tree matched those in the clusters computed via k-means. Thus, the clustering algorithms also support the existence of a 2-synergy model across subjects. Therefore, a mean activation strategy (W_{kmeans}) was extracted from the centroids of the 2-cluster model obtained via k-means (Figure 3.18).

Finally, the synergy matrices computed via both methods (W_{All} and W_{kmeans}) were compared by computing their normalized dot products. This resulted in a normalized dot product of 0.9248 for $\mathbf{w}_1$ and 0.9524 for $\mathbf{w}_2$, indicating a high similarity between the synergy matrices. These results partly evidence the existence of common control strategy for different subjects and throwing distances. However, in order to conclude on this, it is also necessary to analyze the time-varying part of the synergies (combination coefficients).

The first method [dSB03], also resulted in a set of time-varying coefficients (C_{All}) which encoded when and with how much intensity the representative synergy (W_{All}) was triggered per subject and trial. These coefficients were averaged per subject at each throwing distance and are featured in Figures 3.21 and 3.22.

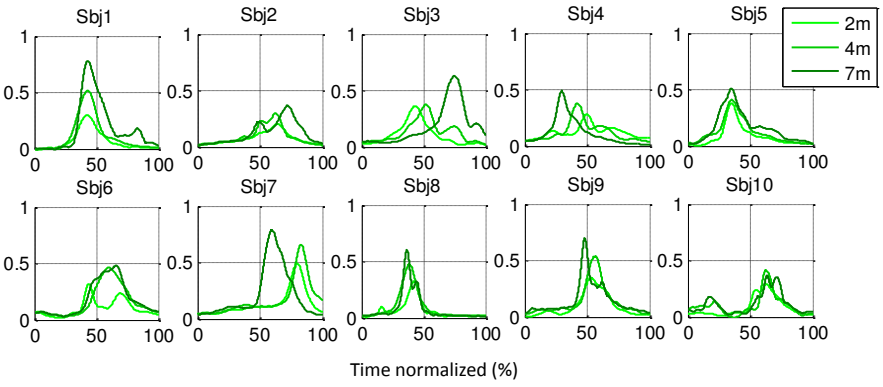

Figure 3.21 – **Average combination coefficient $c_1(t) \in C_{All}$ per subject at each throwing distance.**

Repeatable trends can be seen among and across subjects. In general, as in the single subject analysis (Figure 3.8), the first coefficient $c_1(t)$ is characterized by a bell shaped profile, while the second one $c_2(t)$ is characterized by a more irregular profile, with a lower amplitude that decreases as the throw is performed. The repeatability of these coefficients across subjects at each throwing distance is also demonstrated by high cross-correlation coefficients at lags (delay/signal length) between 0.0320 and 0.2232, as featured in Table 3.7.

The previous results outline the existence of a common strategy for triggering each synergy across subjects and throwing distances. Therefore, a common strategy $\overline{C}_{All}$ was computed by performing averages across subjects at each throwing

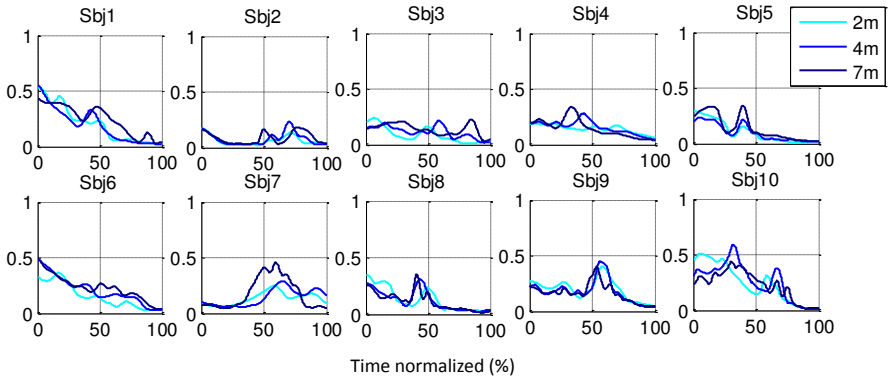

Figure 3.22 – **Average combination coefficient $c_2(t) \in C_{All}$ per subject at each throwing distance.**

Table 3.7 – $c_i(t)$ **inter-subject comparison at each throwing distance.**

Mean cross-correlation and lags (delay/signal length)						
$c_i(t)$	$corr_{2m}$	$corr_{4m}$	$corr_{7m}$	lag_{2m}	lag_{4m}	lag_{7m}
$c_1(t)$	0.9129 $\pm$0.0534	0.9390 $\pm$0.0320	0.9264 $\pm$0.0382	0 $\pm$0.1787	0 $\pm$0.1999	0 $\pm$0.2163
$c_2(t)$	0.8761 $\pm$0.0727	0.8615 $\pm$0.0769	0.8702 $\pm$0.0650	0 $\pm$0.1524	0 $\pm$0.2232	0 $\pm$0.1797

distance. The representative coefficients per distance are depicted in Figure 3.23. These coefficients not only preserve the main trends in each of the subjects' averages but also the similarities in terms of shape across throwing distances, as evidenced in Table 3.8.

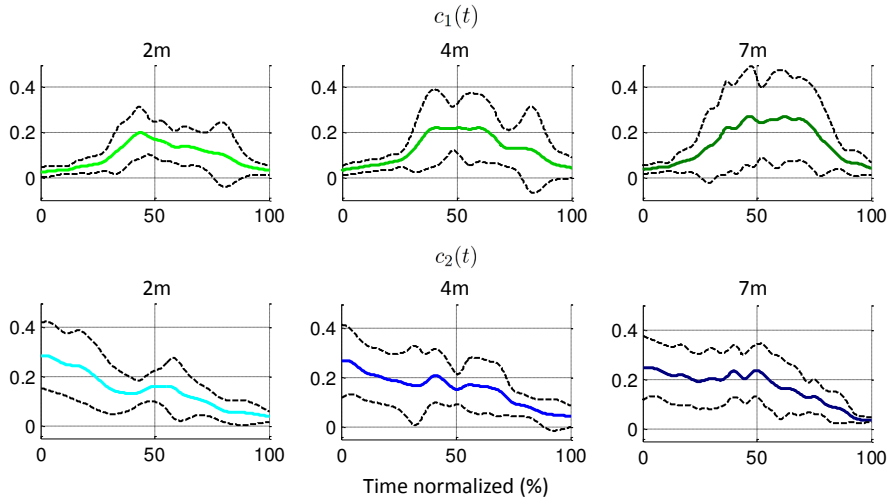

Figure 3.23 – **Representative control strategy (combination coefficients) $\overline{C}_{All}$ for all subjects.** A common control strategy was identified for the time-variant part of the synergies through the method described in [dL13], and by averaging the coefficients across subjects.

Table 3.8 – $c_i(t)$ **inter-subject and inter-distance comparison.**

Mean cross-correlation and lags (delay/signal length)		
$c_i(t)$	$corr_{2m,4m,7m}$	$lag_{2m,4m,7m}$
$c_1(t)$	0.9895 ± 0.0035	0 ± 0.0091
$c_2(t)$	0.9833 ± 0.0089	0 ± 0

After analyzing the shape of the coefficients, the second characteristic that was studied was their timing. To facilitate this, the coefficient $c_1(t)$ (agonist synergy) and $c_2(t)$ (antagonist synergy) from Figures 3.21 and 3.22 were plotted in one the same figure (Figure 3.24). This figure shows in which order the coefficients were triggered for each subject and throwing distance.

As in the single subject analysis (Figure 3.8), a "triad" burst sequence (from antagonist to agonist, and from agonist to antagonist) is observed. Also, the most significant co-activation among the synergies occurs as the agonist synergy $c_1(t)$ is triggered before ball release. These observations are consistent with the antagonist activity in the upper extremity while throwing [HKS+02] and performing ballistic movements [LMO+99]. The same behavior is seen in the common control strategy in Figure 3.23.

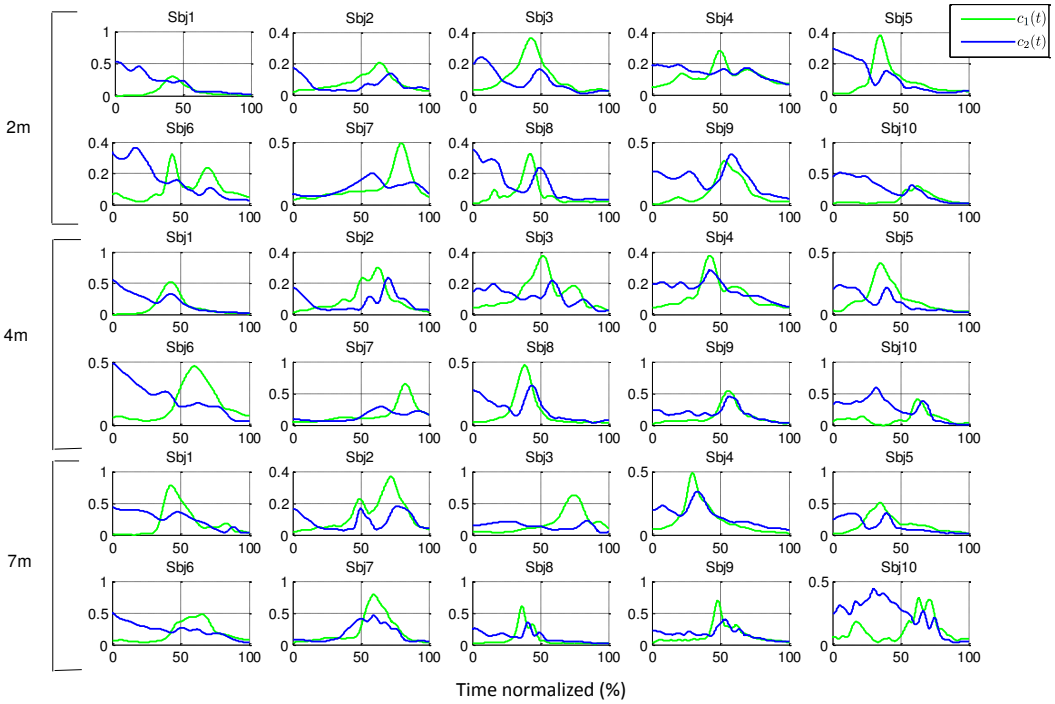

Figure 3.24 – $c_i(t)$ **triggering order and co-activation per subject and throwing distance.** A repeatable triggering tendency is seen across subjects and throwing distances: First $c_2(t)$ is triggered, followed by $c_1(t)$, and the $c_2(t)$ again. This sequence is consistent with the expected triggering in ballistic motions.

The last characteristic that was analyzed was the changes in energy of the coefficients across throwing distances. Figure 3.25 shows the average energy at each throwing distance per subject as described in Equation 3.8. Similarly to the single subject analysis, the changes in energy of the coefficients are linked to changes in the kinematic features (Figure 3.13). As the throwing distance increases the energy of the coefficients and the magnitude of the task space features increases. For $c_1(t)$ (agonist synergy), this increment is always gradually incrementing, and it is statistically relevant for 6/10 subjects. These results are consistent with other studies showing an increase in actuation signal amplitude as the throwing range increases [KXY+10].

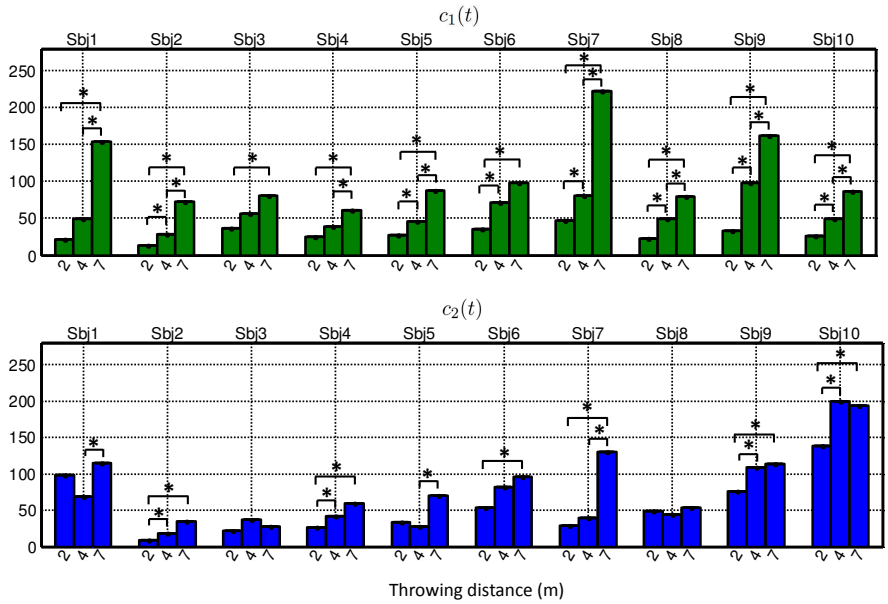

Figure 3.25 – $c_i(t)$ **energy per subject and throwing distance.** The energy in $c_1(t)$ (agonist synergy) gradually increases with throwing distance. Statistically relevant increments are denoted by the symbol *.

Finally, the representative synergy matrix W_{All}, and the subject-trial specific matrix $\overline{C}_{All}$ were used to reconstruct the original EMG signals. An overall reconstruction quality of $r^2 = 0.6526$ was obtained for the 180 concatenated muscle activations. Figure 3.26 and Figure 3.27 show examples of the activation reconstruction of a $7m$ trial for different subjects. In the first case, the triggering order and shape of the reconstructed activations follow closely the recorded ones. In the second example, the original activations contain many small oscillations, which are not well reconstructed. Considering the number of trials that are being reconstructed simultaneously, such differences in reconstruction accuracy were expected.

Furthermore, as of the r^2 criterion most of the information lost corresponds to noise-dependent variability, and the most important trends in the activation signals

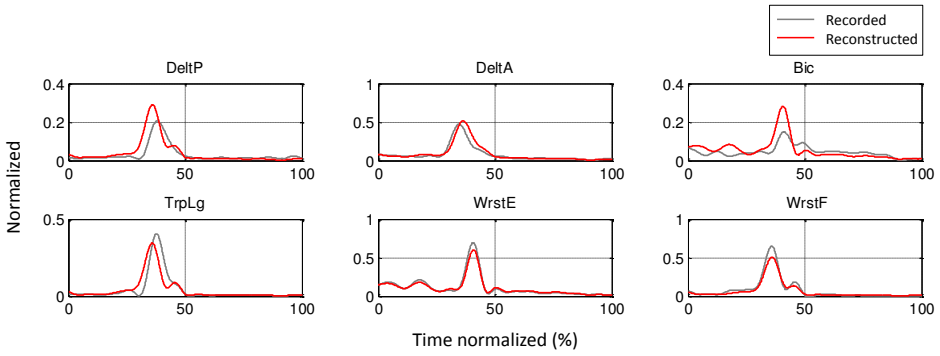

Figure 3.26 – **Example 1: Activation reconstruction using W_{All} and C_{All}.** The triggering order and shape of the activations are well reconstructed by the synergies.

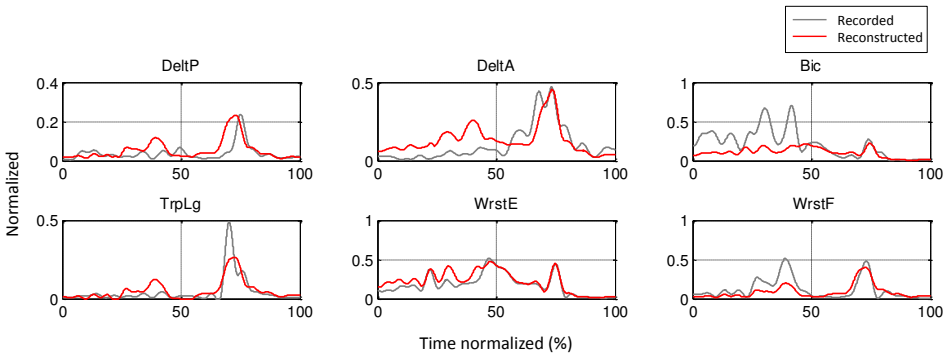

Figure 3.27 – **Example 2: Activation reconstruction using W_{All} and C_{All}.** The original activations contain many small oscillations, which are not well reconstructed by the synergies.

are preserved in the majority of muscles and trials. Thus, the previously presented synergies encode important temporal and spatial information regarding the muscle activations, for a variety of subjects and throwing distances.

3.7 Conclusion

In this analysis overhead throwing motions were performed to different throwing distances by untrained subjects with different physical conditions. The fact that such motions could be decomposed into a few spatial and temporal components, promotes the idea that synergies could be the redundancy reduction mechanism employed by the CNS.

Low-dimensional strategies were identified for a single and multiple subjects. In both cases 2 synergies explained more than 60% of the EMG-variability during throwing. In other words, given the chosen DoF and muscle set, only 2 control variables were necessary to encode important temporal and spatial muscle activation

trends during a variety of throwing motions. This reduced the number of control variables from 6 muscle activations to 2 synergies, a third of the original control representation. Each of these synergies was composed of a spatial (task-independent) and a temporal (task-dependent) component, which are featured in Figures 3.18 and 3.23. The spatial component or synergy ($\mathbf{w}_i$) encoded the relative activation of muscles throughout all the analyzed throws, while the temporal component or combination coefficient ($c_i(t)$) encoded when and with what intensity each synergy was triggered at each throwing distance

Such synergies contained groups of muscles with predominantly opposing actions, suggesting that muscles are controlled jointly according to their function. For instance, the function of initiating motion and moving the different segments of the arm forward corresponded to an agonist synergy $\mathbf{w}_1$, while the function of decelerating the limb corresponded to an antagonist synergy $\mathbf{w}_2$. Furthermore, these synergies were triggered in a manner which is consistent with the antagonistic activity observed in the upper extremity while throwing and performing ballistic motions [HKS+02, LMO+99]: a first activation is needed to accelerate the limb forward and a second decelerate it. It was also observed that the synergies were linked to changes in the kinematic features and throwing distance. As the throwing distance increased, so did the magnitudes of the release speed, height, and the amplitudes of the coefficients. This is an indication that to adapt to changes within the same task, the CNS might modulate the same low-dimensional control representation, as suggested in other studies on upper [dPFL06] and lower-body motions [TOT07, ST11].

From this analysis two important observations can be extracted for the motion generation application in the next chapter. The first is that synergies can provide a means to encode motions in significantly less control variables than actuators, and secondly, that they are modulated by kinematic features and task goals. Thus, by mimicking this control mechanism, a synergy-based control solution could be designed to generate motions with muscle-based characters, while reducing redundancy. However, it remains to be shown if synergies extracted from a complex human morphology can be used as a initial control representation for virtual characters whose morphology may differ to different levels with regard to that of a real human. Furthermore, the synergies presented in this chapter were shown to be able to reconstruct muscle activations, but their effect at a kinematic level has not been validated yet, as is the case with most synergy studies.

The next chapter will answer both of these questions by using synergies as input control functions in forward dynamics simulations, and evidencing that synergies can be used to control a character with a simple muscle topology while reconstructing the kinematics of an overhead throwing motion.

Chapter 4

Muscle synergies as control functions for virtual characters

MUSCLE synergies are low-dimensional control representations that are modulated according to task gols, and are present in a variety of human motions, including overhead throws (as shown in Chapter 3). The objective of this chapter is to evidence if such representations are good candidate solutions to simplify the control of muscle-based virtual characters by significantly reducing actuation redundancy, while successfully performing a task.

As seen in Chapter 2 (Equation 2.1), some of the usual command signals ($\mathbf{u}(t)$) to control muscle-based characters are muscle activations. However, for a character with D-muscles, this representation results in a high dimensional space containing D control signals, one for each muscle. The size of this space can be reduced by redefining the control input through a muscle synergy model (Section 2.2.1). Specifically, by defining ($\mathbf{u}(t)$) as the task-dependent part of the synergies.

This chapter focuses on redefining this control input through N-synchronous time-invariant synergies (Equation 2.10). Specifically, by defining $\mathbf{u}(t)$ as the task-dependent part of the synergies, the coefficients $c_i(t)$:

$$\mathbf{u}(t) = \begin{bmatrix} u_1(t) \\ u_i(t) \\ ... \\ u_N(t) \end{bmatrix} = \begin{bmatrix} c_1(t) \\ c_i(t) \\ ... \\ c_N(t) \end{bmatrix} \tag{4.1}$$

By replacing this new control input in Equation 2.10, D-muscle activation patterns can be expressed in terms of N-control variables, where $N < D$:

$$\mathbf{a}(t) = \sum_{i=1}^{N} \mathbf{w}_i u_i(t) \tag{4.2}$$

A synergy-driven forward dynamics simulation can be finally constructed, by replacing Equation 4.2 in in Equation 2.7 (Section 2.1.1.3), as shown in Figure 4.1.

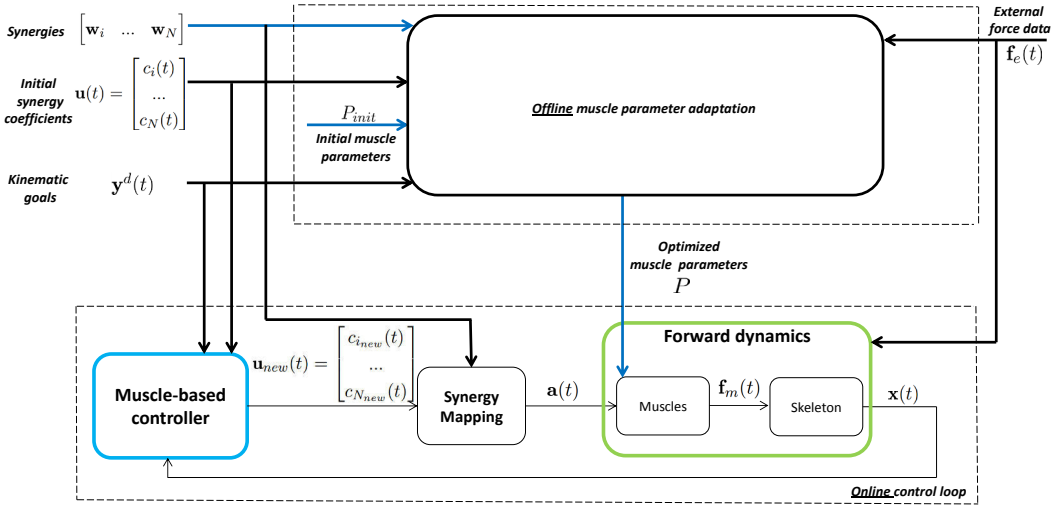

Figure 4.1 – **A general synergy-driven forward dynamics pipeline using *synchronous time-invariant synergies***. A pipeline for reproducing or synthesizing new motions with a muscle-based character. The pipeline is composed of two parts: 1) an offline adaptation to determine the character's muscle parameters, 2) an online control loop to adapt the task-dependent part of the synergy ($c_i(t)$) to reproduce or synthesize motions.

The pipeline is divided into two parts: an offline and online part. The offline part consists of an adaptation to scale the character's muscle parameters P to fit the experimental data (skeletal parameters should have been previously determined). This procedure is necessary in order to make the muscle models reflect the capacities of real muscles. On the other hand, the online part consists of a *muscle-based controller* that adapts the task-dependent part of the synergy ($\mathbf{u}(t)$), containing the coefficients $c_i(t)$, according to a set of kinematic goals ($\mathbf{y}^d(t)$) and the current state of the character ($\mathbf{x}(t)$). If the objective is motion reproduction, the controller adapts the synergies according to the same motion goals as in the experimental data, and to the distinct dynamics of the character with respect to the real subject. For motion synthesis, the same approach is followed except that the adaptation is made according to a new set of motion goals. Once this adaptation is made, a new control input ($\mathbf{u}_{new}(t)$) is obtained. This input and the original synergies ($\mathbf{w}_i$) are then given to the *synergy mapping* module, which converts the synergies into muscle activations ($\mathbf{a}(t)$) through the time-invariant synergy model. Finally, the activations are used to drive the character in the *forward dynamics* module, resulting in skeletal

motion. Such a scheme could be used, for instance, to synthesize new throwing motions from recorded ones by modulating the combination coefficients according to the desired angle, speed, and height of the ball at release.

It is worth noting that the *muscle-based controller* could be constructed using a variety of solutions, such as the control methods presented in Chapter 2. The adaptation of the $c_i(t)$ coefficients could be made through a control law, as in Section 2.1.2.3, or directly through a trajectory optimization (static or dynamic), as shown in Section 2.1.2.4. In the next sections, the previous synergy-driven pipeline will be implemented using a trajectory optimization method for reproducing overhead throwing motions with a muscle-based character. The results show that motion can be reproduced while preserving important characteristics in the original synergies or control signals.

4.1 A synergy-driven forward dynamics pipeline for overhead throwing

The previous section presented time-invariant synergies as potential low-dimensional representations for controlling virtual characters. This section shows an implementation of the general pipeline in Figure 4.1 for reproducing throwing motions with a muscle-based character [CRPLD15, CRPD16]. For simplicity, the pipeline was first used for controlling a subset of DoF (B) of the throwing arm which were actuated by muscles. The rest of the character was driven with recorded kinematics. Figure 4.2 shows this implementation.

The inputs to the pipeline are: 1) a set of time-invariant synergies ($\mathbf{w}_i$, $c_i(t)$) and desired joint trajectories ($\mathbf{y}^d(t) = [\, q_1^d(t)\ q_b^d(t)\ \ldots\ q_B^d(t)\,]$) extracted from the throwing experiments in Chapter 3, and 2) the external force of gravity ($\mathbf{f}_e(t)$). The desired joint trajectories are kinematic features describing the motion in the joint space, unlike the kinematic features in the previous chapter which describe motion in the task space. They were selected as kinematic goals for the pipeline, due to the fact that they allow the specification of motion goals for each DoF in the character, which facilitates the control task.

The offline muscle parameter adaptation consists of an optimization to determine the muscle parameters that fit with the desired joint trajectories and the initial synergies. Furthermore, the online control loop consists of a trajectory optimization and a filter, which adjusts the combination coefficients ($c_i(t)$) according to the desired joint trajectories, and the current joint positions of the character ($\mathbf{x}(t) = [\, q_1(t)\ q_b(t)\ \ldots\ q_B(t)\,]$).

The following sections detail the main components in this pipeline. First, the

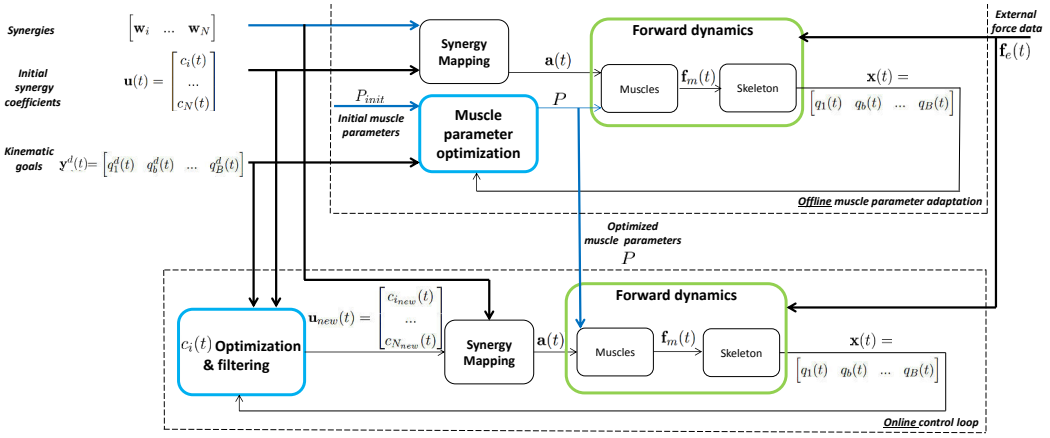

Figure 4.2 – **A synergy-driven forward dynamics pipeline for overhead throwing.** An implementation of the pipeline in Figure 4.1 for reproducing overhead throws.

character used in the forward dynamics simulation is introduced (Section 4.2). Next, the muscle parameter adaptation, and the optimization and filtering of the coefficients are detailed (Sections 4.3 and 4.4). Finally, the resulting synergy-driven motions and the limitations of the pipeline are presented in Sections 4.5 and 4.6. The results show that the framework is able to reproduce throwing motions with a simple muscle-based character, while reducing redundancy and preserving important temporal and spatial characteristics in the original synergies or control signals.

4.2 Character modeling

The character used in the previous pipeline was developed in MATLAB® SimMechanics. It consists of a full body skeletal model with a musculoskeletal arm (Figure 4.3). The skeletal model consists of 21 rigid bodies linked by 17 joints, and exhibits 32 degrees of freedom (Appendix C). Furthermore, to make a first proof of concept, only key DoF of the right arm with important contributions during throwing (Section 3.2.4) were actuated by muscles.

The arm exhibits 3 DoF at the shoulder, 2 at the elbow and 2 at the wrist. The muscle-actuated DoF are the shoulder, elbow, and wrist flexion (positive joint positions) and extension (negative joint positions). The remaining DoF of the arm and body are kinematically driven. For simplicity, pairs of antagonistic muscle models were used in order to reflect the action of real muscles on the segments [RAPC10]. Figure 4.3 features a view of the musculoskeletal arm from the sagittal plane. The first antagonistic pair (m_1 and m_2) produces flexion/extension at the shoulder. The contraction of muscle m_1 generates shoulder flexion, while the contraction of muscle m_2 generates shoulder extension. The second pair (m_3 and m_4) produces elbow flexion/extension. And finally the third pair (m_5 and m_6) produces

wrist flexion/extension. The muscles is each pair can be described geometrically, through their routing and changes in length, and functionally, through their force generation capabilities. Figure 4.4 features the geometry of a single musculotendon unit j, and an example of a changes in length during an elbow extension.

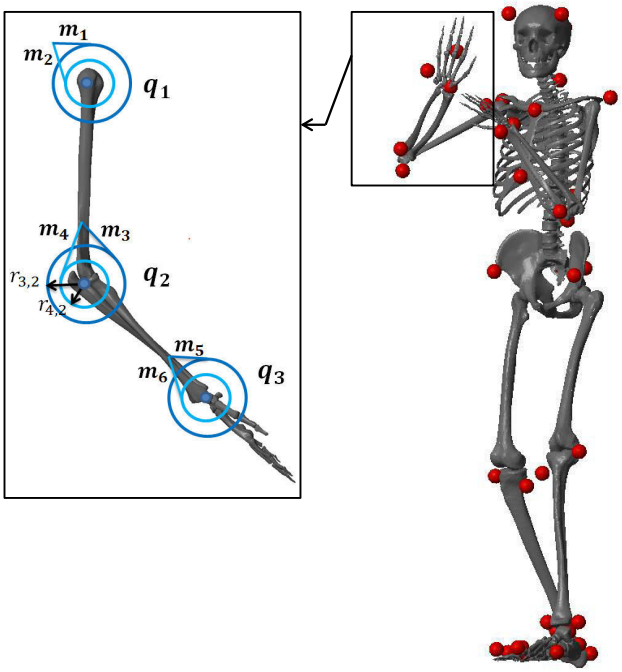

Figure 4.3 – **Full body skeletal model and musculoskeletal arm model [CRPLD15, CRPD16]** (bone graphics issued from [Any]).

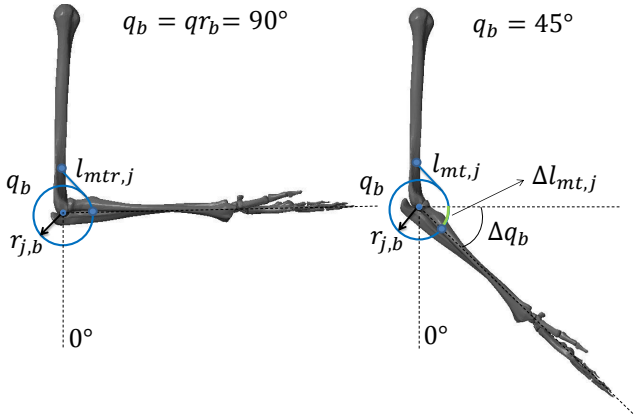

Figure 4.4 – **Musculotendon geometric model [CRPLD15, CRPD16]** (bone graphics issued from [Any]).

Each musculotendon unit is composed of a muscle and an infinitely rigid tendon of constant length. The muscle routing is pulley-like. In other words each unit is wrapped around a circumference of constant radius $r_{j,b}$, centered at the axis of

rotation of its corresponding degree of freedom q_b. The changes in length of these units are given with respect to a joint rest position qr_b and a musculotendon rest length $l_{mtr,j}$ (which is simply the sum of the muscle rest length $l_{mr,j}$ and constant tendon length $l_{t,j}$). The total length of the musculotendon unit can be expressed as:

$$l_{mt,j} = l_{mtr,j} - r_{j,b}(q_b - qr_b) \tag{4.3}$$

or as the sum of the muscle length $l_{m,j}$ and the constant tendon length $l_{t,j}$ (infinitely rigid tendon):

$$l_{mt,j} = l_{m,j} + l_{t,j} \tag{4.4}$$

Finally, by solving Equation 4.4 for $l_{m,j}$ and replacing $l_{mt,j}$ from Equation 4.3, the changes in muscle length $l_{m,j}$ and shortening velocity $\dot{l}_{m,j}$ can be described as follows:

$$l_{m,j} = l_{mtr,j} - r_{j,b}(q_b - qr_b) - l_{t,j} \tag{4.5}$$

$$\dot{l}_{m,j} = -r_{j,b}\dot{q}_b \tag{4.6}$$

Each musculotendon unit can apply a force $f_{m,j}$ on a specific DoF, generating a torque that moves the skeletal system. Therefore, the total torque of a set D_b of muscles on the degree of freedom k, can be expressed as:

$$\Gamma_b = f_{m,j}(a_j, f_{o,j}, l_{m,j}, \dot{l}_{m,j}) \cdot r_{j,b}, \quad j \in D_b \tag{4.7}$$

Where $f_{m,j}$ is generated via the Hill muscle model (Equation 2.3), and is a function of the muscle's activation signal a_j, maximum isometric force $f_{o,j}$, length $l_{m,j}$, and shortening velocity $\dot{l}_{m,j}$.

4.3 Muscle parameter adaptation (Offline)

The estimation of the character's muscle parameters is important since they affect the mapping from synergies to motion. Thus, the simplified muscular topology should reflect as much as possible the real muscular topology to better evaluate the effect of the synergies. Therefore, an optimization was designed in order to determine a set of parameters that enhanced this mapping. These parameters were: the maximal forces $f_{o,j}$, moment arms $r_{j,b}$, rest lengths $l_{mr,j}$, and joint rest positions qr_b. The following optimization was repeated for each muscle-actuated degree of

freedom q_b with the purpose of finding the parameters P_b of the muscles acting directly on it:

$$\begin{aligned} &\underset{P_b}{\text{minimize}} \quad \sum_{n=1}^{Nsamples} (q_b(t_n) - q_b^d(t_n))^2 \\ &P_b = [f_{o,j}, l_{mr,j}, r_{j,b}, qr_b], \quad j \in D_b, \quad P_b \in P \end{aligned} \tag{4.8}$$

$$\text{subject to} = \begin{cases} f_{o,j} > 0 \\ r_{j,b} > 0 \text{ or } r_{j,b} < 0 \text{ (action dependent)} \\ 0.8 \leq \frac{l_{mr,j}}{lo,j} \leq 1.2 \\ -180^\circ \leq qr_b \leq 180^\circ \end{cases}$$

Where, $Nsamples$ is the total number of samples, t_n is the current time sample, D_b is a set containing the muscles acting on joint q_b, and P is the set containing the parameters for all joints. The constraints on $f_{o,j}$ ensure that the muscle are only pulling (positive muscle forces). The constraints on $r_{j,b}$ are action dependent. In other words the moment arms are positive or negative depending on the sign of their expected actions on the joints. Average initial values for $f_{o,j}$ and $r_{j,b}$ were based on the biomechanical study in [HMD05], and each muscle was assigned values based on real muscles with similar actions. For instance m_1 and m_2 were assigned the parameters of the deltoid anterior and posterior, m_3 and m_4 were assigned the parameters of the biceps and triceps long, and finally m_5 and m_6 were assigned the parameters of the flexor carpi radialis and extensor carpi ulnaris.

The parameters qr_b and $l_{mr,j}$ are specific to the muscle routing used in this study. The joint rest angle corresponds to the position where passive torque is equal to zero, and $l_{mr,j}$ to the length at that angle. Thus, a rough initial guess was made on these parameters as follows. The initial $l_{mr,j}$ were equal to the optimal fiber lengths $l_{o,j}$ in [HMD05] (the length at which muscles have greatest ability to produce force) and they were constrained with regard to these values. While the initial qr_b were chosen by testing different angles, within a wide range of motion (-180° to 180°), and selecting those which improved motion reconstruction after optimization.

In each optimization, only the DoF of interest was populated with muscles, while the rest of the skeleton was driven kinematically. At each iteration, the entire throw was simulated by driving the arm with the extracted synergies. Then, the global error in joint position was computed, and new muscle parameters were proposed until the error was minimized. The algorithm to solve this and the following problems was MATLAB fmincon's default optimization algorithm: interior-point [WMNO06]. An algorithm for non-linear constrained optimization that consists in transforming the original problem and its inequality constraints, into a sequence of

equality constrained problems which are solved using newton and gradient conjugate steps.

4.4 $c_i(t)$ optimization and filtering (Online)

After determining the muscle parameters, the next stage was the optimization of the coefficients $c_i(t)$. In this stage, the original synergies are adapted to distinct dynamics of the character with respect to the real human (due to different muscle routing, muscle parameters etc.), in order to achieve the desired kinematic goals ($q_b^d(t)$). Thus, the synergy coefficients were adapted at each time step as follows:

$$\begin{aligned} &\underset{c_i(t_{n-1})}{\text{minimize}} \quad \sum_{b=1}^{B} |q_b(t_n) - q_b^d(t_n)| \\ &\text{subject to} \quad 0 < c_i(t_{n-1}) < 1, \\ &c_i(t_{n-1}) \in C, \quad i = 1...N \end{aligned} \tag{4.9}$$

Where B is the total number of muscle actuated DoF in the model (3 in this case), and N is the number of synergies.

Essentially, by adapting the coefficients, the optimization changes when and how much each synergy is triggered. However, these changes are made without taking into consideration the activation dynamics, or the delay between the neural stimulation and the actual activation of each muscle, as described in Equation 2.5 (Section 2.1.1). This results in apparently noisy signals that are more comparable to neural excitations than to a real muscle activations. Thus, to circumvent this issue, a second order numerical filter representing the activation dynamics was applied to the optimized signals.

Assuming that the activation and deactivation constant times in Equation 2.5 are equal, and that the relation between the coefficient $c_i(t)$ and the activations is straightforward, such a filter can be written in the Laplace domain as:

$$\frac{c_{i_{new}}(p)}{c_i(p)} = \frac{1}{(1 + \tau_{act}p)(1 + \tau_{ne}p)} \tag{4.10}$$

Where $c_i(p)$ represents the optimized coefficients before filtering and $c_{i_{new}}(p)$ represents the coefficients after filtering. The time delays, τ_{act} and τ_{ne}, were set to 50 ms and 1 ms respectively.

A discrete version of this filter can be obtained through the z-transform as follows:

$$\frac{c_{i_{new}}(z)}{c_i(z)} = \frac{\sigma_1 z + \sigma_0}{\kappa_2 z^2 + \kappa_1 z + \kappa_0} \tag{4.11}$$

With

$\sigma_1 = \frac{\tau_{ne}(1-e^{-T_e/\tau_{ne}})-\tau_{act}(1-e^{-T_e/\tau_{act}})}{\tau_{ne}-\tau_{act}}$

$\sigma_0 = e^{-T_e/\tau_{ne}}e^{-T_e/\tau_{act}} - \frac{e^{-T_e/\tau_{ne}}-e^{-T_e/\tau_{act}}}{\tau_{act}-\tau_{ne}}$

$\kappa_2 = 1$

$\kappa_1 = -(e^{-T_e/\tau_{ne}} + e^{-T_e/\tau_{act}})$

$\kappa_0 = e^{-T_e/\tau_{ne}}e^{-T_e/\tau_{act}}$

Next, by multiplying Equation 4.11 by z^{-2} to be only dependent of negative powers of z, and using the delay theorem, the following recursive equation is obtained:

$$\begin{aligned} c_{i_{new}}(nT_e) &= -\kappa_1 c_{i_{new}}((n-1)T_e) - \kappa_0 c_{i_{new}}((n-2)T_e) \\ &\quad +\sigma_1 c_i((n-1)T_e) + \sigma_0 c_i((n-2)T_e) \end{aligned} \tag{4.12}$$

Where T_e is the sampling time, $0.01s$ in this case, as the time sampling used for kinematic data acquisition during the experiments in Chapter 3. Finally, the sampling resulted in a static gain equal to $\Lambda = \frac{(\sigma_1+\sigma_0)}{(\kappa_2+\kappa_1+\kappa_0)}$, therefore by diving Equation 4.13 by this gain, normalized combination coefficients are obtained :

$$c_{i_{new}}(nT_e) = \frac{c_{i_{new}}(nT_e)}{\Lambda} \tag{4.13}$$

4.5 Results

The pipeline described in Section 4.1 was tested using different synergy models as control functions. This was done in order to: 1) show the impact of using different muscle sets for synergy extraction, and 2) demonstrate that redundancy can be reduced to different levels while accurately reconstructing a desired motion. The results show that the choice of muscle set impacts the number of adaptations on $c_i(t)$, and that redundancy can be reduced to different levels while conserving a similar motion reconstruction accuracy.

Choosing an appropriate synergy model involves considering three important criteria: 1) The model should contain significantly less synergies (N) than muscles on the character (D), 2) the synergies should be extracted from muscles with matching actions to the character's muscles, and 3) the synergies should be extracted from clean EMG signals. The two synergy models used for testing the pipeline respect these criteria at different levels, and they were extracted from different muscle sets, as featured in Table 4.1. The first model (Figure 4.5) consists of a 5-synergy model, extracted from a set of 10 muscles, and trials containing ECG-artifacts in the pectoralis muscle signals. The second model (Figure 4.6) was previously presented

Table 4.1 – **Synergy models used as input control functions for the pipeline in Figure 4.2.**

Synergy models	
Synergy model	**Muscle set used for extraction**
5-synergy model	Set_{10}: Posterior deltoid, anterior deltoid, middle deltoid, pectoralis major (clavicular head), pectoralis major (sternocostal head) biceps, triceps (long head), triceps (lateral head), forearm extensor bundle, forearm flexor bundle.
2-synergy model	Set_6: Posterior deltoid, anterior deltoid, biceps, triceps (long head), forearm extensor bundle, forearm flexor bundle.

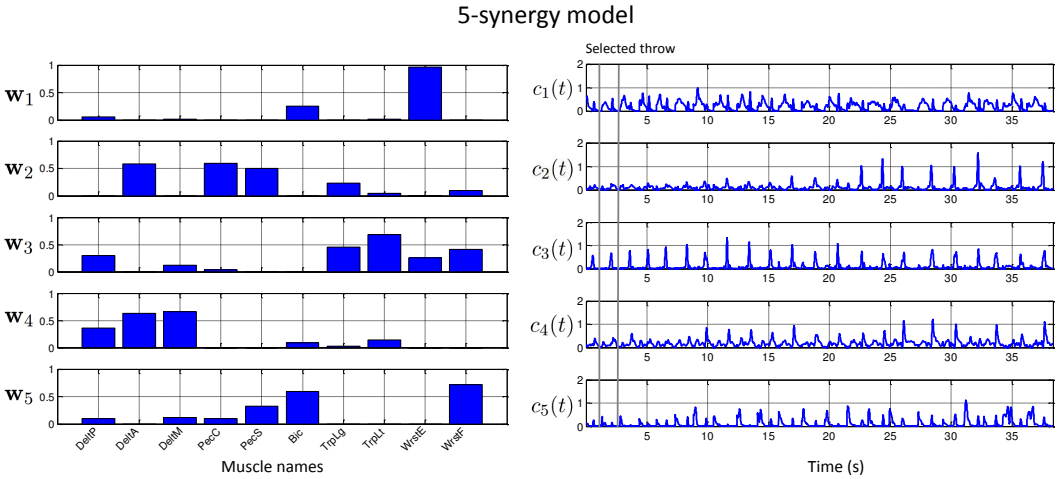

Figure 4.5 – **5-synergy model [CRPLD15].** A synergy model composed of 5-synergies, extracted from a set of 10 muscles.

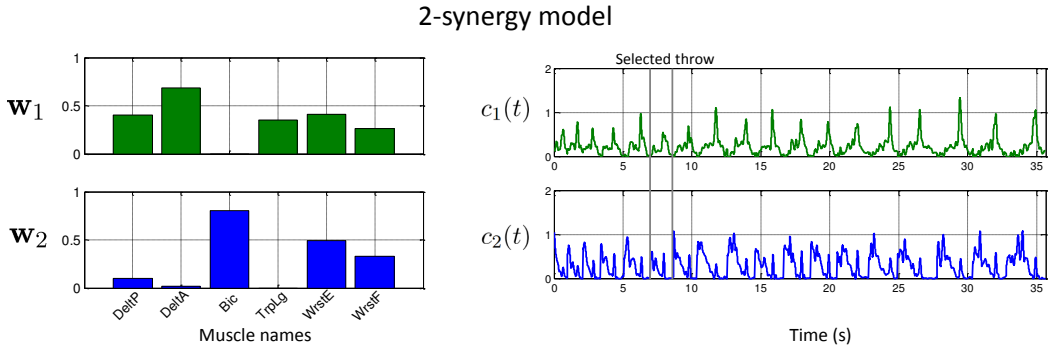

Figure 4.6 – **2-synergy model [CRPD16].** A synergy model composed of 2 synergies, extracted from a set of 6 muscles.

and analyzed in Chapter 3 (Figure 3.7 (Set_6)). It consists of a 2-synergy model, extracted from a set of 6 muscles, and clean EMG signals.

As shown in Figure 4.5 and 4.6, both models were extracted from a set of throws, and therefore, the coefficients ($c_i(t)$) encode the temporal evolution of the synergies

for all throws. However, in the next sections only the part of these coefficients corresponding to the same $2m$ throw will be used. This segment of the coefficients $(c_i(t))$ was linearly combined with the synergy vectors $(\mathbf{w}_i)$ to generate the muscle activations to drive the character model. Specifically, the muscles m_1 and m_2 were driven with the resulting muscle activation of the deltoid anterior and posterior, m_3 and m_4 were driven with the activation of the biceps and triceps long, and finally m_5 and m_6 were driven with the activation of the forearm flexor and extensor bundle.

4.5.1 5-synergy driven motion

To begin, the 5-synergy model in Figure 4.5 was used as an initial control representation for the pipeline. That is, the synergies $\mathbf{w}_i$ and $c_i(t)$ of this model were linearly combined to generate an activation signal for each muscle in the model. The following results feature the resulting joint trajectories as the different stages in the pipeline are executed. After each stage, motion reproduction accuracy increases. This is reflected by joint trajectories that follow closely the desired ones and by computing the coefficient of determination between them.

First, the synergies were used to drive the model without adapting the muscle parameters or the combination coefficients. Figure 4.7 shows the resulting angular trajectories versus the trajectories obtained from the motion capture data.

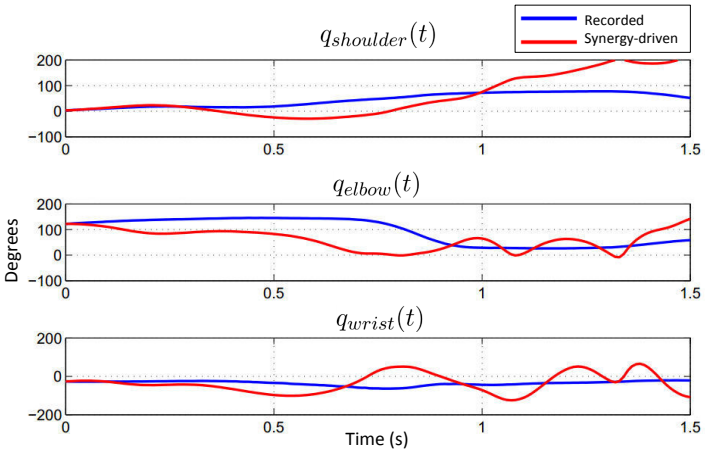

Figure 4.7 – 5-**synergy model: Synergy-driven motion without muscle parameter adaptation [CRPLD15].**

The resulting motion diverges from the desired joint trajectories. Without adapting the muscle parameters this behavior was expected since the mapping made from synergies to motion was especially hindered by the rough choice of resting angles (qr_b) and lengths $(l_{mr,j})$, which determine the equilibrium position of the joint. Furthermore, the synergies also encode unnecessary information, such as ECG-artifacts and additional muscle actions that are not actuated or controlled

by muscles in the pipeline. For instance, the synergies contain the actions of the pectoralis muscles, which include shoulder adduction and internal rotation. These actions were not actuated with muscles, but kinematically driven.

To improve these results, the offline parameter adaption stage (Section 4.3) was executed. This resulted in the motion featured in Figure 4.8. As seen in this figure, the resulting joint trajectories follow more closely the recorded ones, with coefficient of determinations of $r^2_{shoulder} = 0.8971$, $r^2_{elbow} = 0.8904$ and negative for the wrist. This improvement, evidences that the original synergies are able to capture and roughly reproduce general trends in the joint positions on a character with a simple muscle structure.

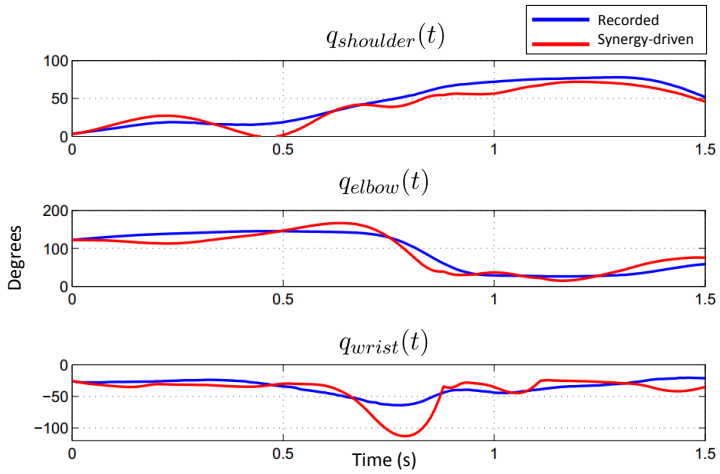

Figure 4.8 – 5-**synergy model: Synergy-driven motion with adapted muscle parameters [CRPLD15].**

For instance, shoulder flexion gradually increases and then decreases towards the end of the motion, and elbow extension is made halfway through the motion (during the acceleration phase) as the highest wrist extended position is reached. Nevertheless, small variations still remain, and a huge off-hook is visible for the wrist trajectory. This behavior can be a consequence of the fact that all muscle parameters were not optimized in one sole procedure.

To enhance these results further, the online adaptation of the coefficients ($c_i(t)$) (Section 4.4) was performed, which resulted in the motion in Figure 4.9. By modulating when and how much each synergy ($\mathbf{w}_i$) was triggered according to the character model and the desired motion, the resulting motion follows even more closely the desired joint positions. Thus, the coefficient of determination for all DoF increases, especially for the wrist ($r^2_{shoulder} = 0.9268$, $r^2_{elbow} = 0.9420$, and $r^2_{wrist} = 0.8136$). These results validate synergies as a relevant control strategy to reduce redundancy while accurately reconstructing a motion. Only 5 synergies were used as control functions for the 6 muscles in the character. These control functions allowed an

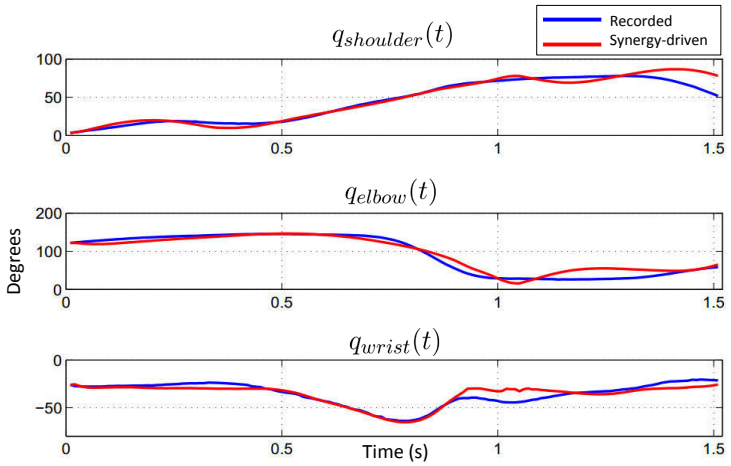

Figure 4.9 – 5-**synergy model: Synergy-driven motion after muscle parameter adaptation and $c_i(t)$ optimization and filtering [CRPLD15].**

accurate reconstruction of the desired joint trajectories. However, in spite of these results, attaining the desired kinematics resulted in high modifications on the combination coefficients. As shown in Figure 4.10, the original or initial coefficients ($c_i(t)$) are significantly different than the optimized and filtered ones ($c_{i_{new}}(t)$).

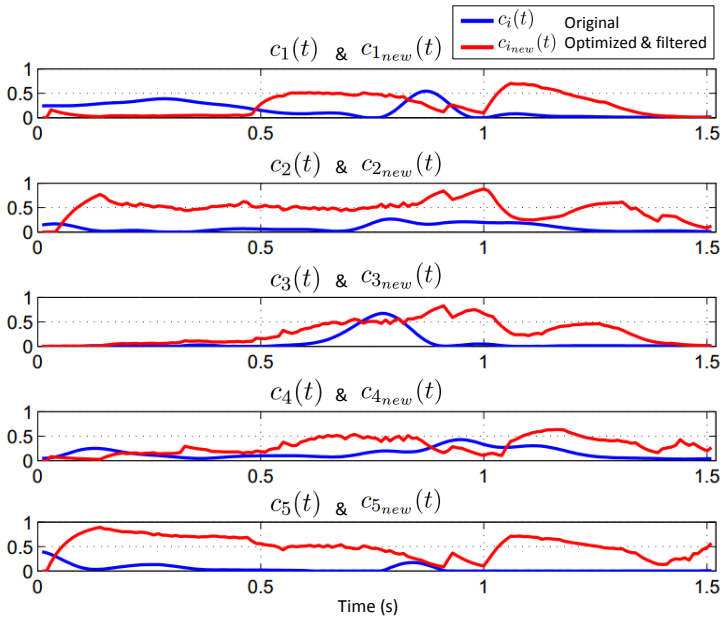

Figure 4.10 – 5-**synergy model: Initial coefficients ($c_i(t)$) and coefficients after optimization and filtering ($c_{i_{new}}(t)$) [CRPLD15].**

The next section shows that by using a synergy model that adheres better to the criteria presented in the beginning of Section 4.5, redundancy can be further reduced while better preserving the original combination coefficients.

4.5.2 2-synergy driven motion

The 2-synergy model in Figure 4.6 was then used as an initial control representation for the pipeline in Figure 4.2. As in the previous section, a simulation was done to demonstrate the effect of each stage in the pipeline on the reconstructed motion. Thus, three simulations were done: 1) synergy driven motion without adapted muscles parameters and synergies, 2) synergy driven motion with adapted muscle parameters, and 3) synergy driven motion with adapted muscle parameters and synergies. The results show that the quality of motion reconstruction at each stage of the pipeline is maintained with significantly less synergies, and that important characteristics in original or initial combination coefficients are preserved.

Similarly to Section 4.5.1, without adapting the muscle parameters or combination coefficients the motion does not follow the general trends of the desired trajectories (Figure 4.11). Again, this behavior was expected due to the rough choice of muscle parameters, and the fact that although less muscles were used in the extraction, the set still encodes supplementary actions, such as the deltoid's internal/external rotation.

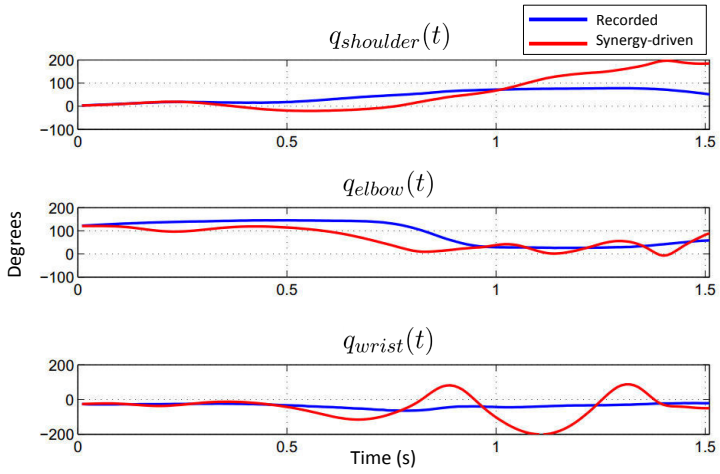

Figure 4.11 – **2-synergy model: Synergy-driven motion without muscle parameter adaptation [CRPD16].**

The previous results were subsequently enhanced by applying the offline muscle parameter adaptation followed by the online adaptation of the coefficients $c_i(t)$. As shown in Figures 4.12 and 4.13, as each adaptation is applied, the resulting joint trajectories follow more closely the desired ones.

However, unlike the 5-synergy model, after these adaptations the resulting coefficients were better preserved. As shown in Figure 4.14, although the antagonist synergy ($c_{2_{new}}(t)$) was significantly modified, the triggering times and intensity of the agonist synergy ($c_{1_{new}}(t)$) were better preserved.

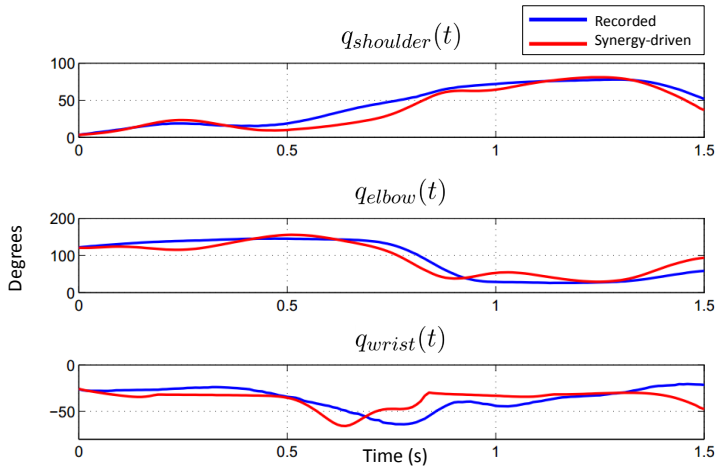

Figure 4.12 – 2-**synergy model: Synergy-driven motion with adapted muscle parameters [CRPD16].**

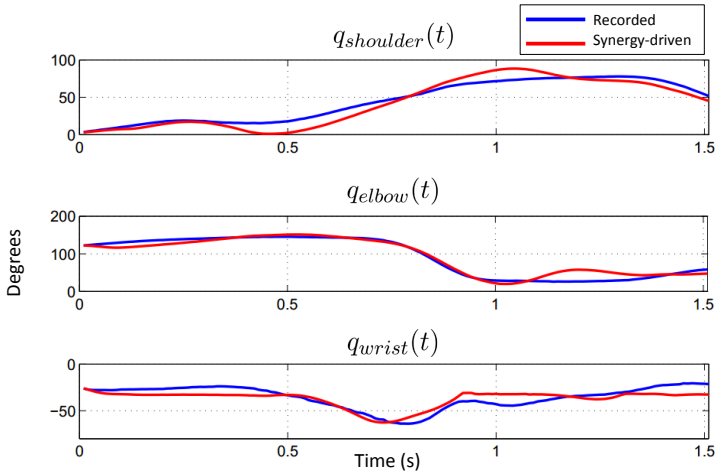

Figure 4.13 – 2-**synergy model: Synergy-driven motion after muscle parameter adaptation and $c_i(t)$ optimization and filtering [CRPLD15].**

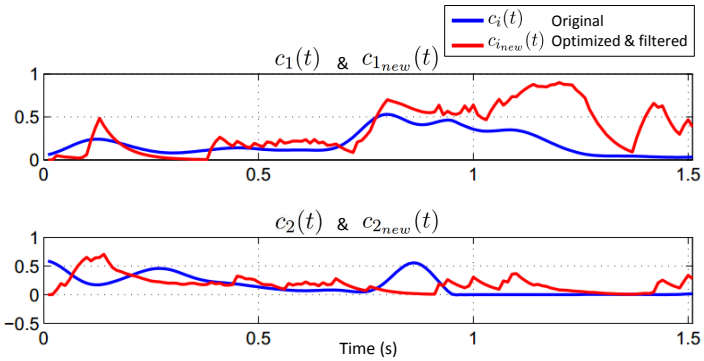

Figure 4.14 – 2-**synergy model: Initial coefficients ($c_i(t)$) and coefficients after optimization and filtering ($c_{i_{new}}(t)$) [CRPD16].**

In the next section, the 5 and 2-synergy models will be compared in terms of their ability to reconstruct the desired kinematics and how well they are preserved after the synergy adaptation procedure.

4.5.3 5-synergy versus 2-synergy driven motion

The previous results showed that the pipeline allows to reproduce an overhead throwing motion with different synergy models. This section focuses on comparing these models in terms of how well they reconstructed the motion, and how they are preserved after adapting the synergies. The results show that the 2-synergy model, which adheres better to criteria for choosing synergy models in Section 4.5, is a more feasible control representation.

Both models resulted in similar motion reconstruction qualities, as shown by the coefficients of determination of the resulting synergy-driven motions. Table 4.2 shows that, except for a slight decrease in the wrist motion quality, the coefficients were maintained in spite of changing the number of synergies. The fact that similar motions can be obtained with a 2-synergy model, evidences that this model encodes essential muscle activation information.

Table 4.2 – **Quality of motion reconstruction.**

Coefficient of determination (r^2)				
Stage	Synergy model	Shoulder	Elbow	Wrist
Muscle param. adaptation	2-synergies	0.8939	0.8843	0.2732
	5-synergies	0.8971	0.8904	negative
$c_i(t)$ optimization & filtering	2-synergies	0.8859	0.9489	0.6746
	5-synergies	0.9268	0.9420	0.8136

The preservation of the combination coefficients after the synergy adaptation can be quantified by computing the cross-correlation between their initial and final shapes, and plotting these values against the time delays (Figure 4.15). In the case of the 5-synergy model, all coefficient comparisons are characterized by high and low correlation peaks, sometimes at considerable lags. This indicates that the initial and final coefficients in this model are very different from each other. On the other hand, in the 2-synergy model, the agonist synergy ($c_1(t)$) comparison is characterized by a bell-shaped curve with a maximum correlation at almost zero lag, indicating a similarity between the initial and final coefficients. Nevertheless, in spite of the fact that the 2-synergy model adheres better to the criteria presented in the beginning of Section 4.5, clear differences remain between the initial and final coefficients. The causes of these differences stem from a set of limitations that will be discussed in Section 4.6.

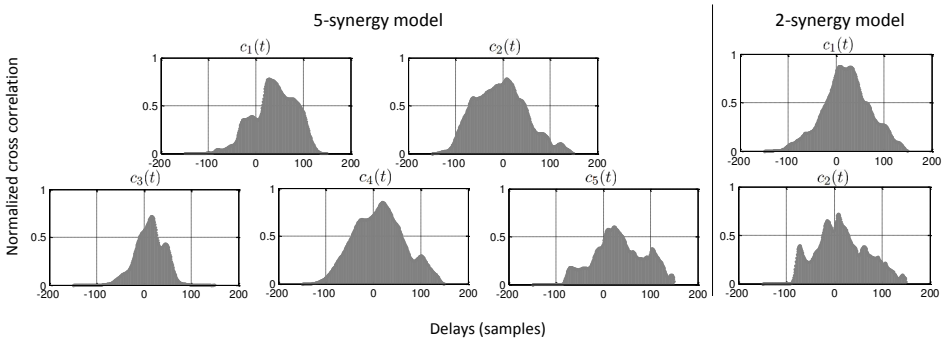

Figure 4.15 – **Cross-correlation between the initial coefficients $c_i(t)$, and the optimized and filtered coefficients $c_{i_{new}(t)}$ for both synergy models [CRPD16].**

The previous comparisons evidenced that the 2-synergy model, which adheres better to the criteria presented in Section 4.5, is a more feasible control representation. It allows to reconstruct the throwing motion with an average r^2 of 0.8365, using less synergies and less coefficient adaptations than the 5-synergy model. Furthermore, with this model, only 2 synergies were used to control 6 muscles and 3 DoF of the character's throwing arm. This validates the extracted synergies as a control representation and a means to store meaningful muscle information. Moreover, it also shows their feasibility for reducing redundancy in forward dynamics, while achieving a set of kinematic goals.

4.6 Limitations

The previous results demonstrated that the synergy-driven pipeline can be used to reproduce a throwing motion, while significantly reducing actuation redundancy and partially preserving the original synergies. However, there are two limitations regarding the optimizations which should be addressed to improve the quality of the final results and reduce computation times.

The first limitation is the implementation of the muscle parameter adaptation. This adaptation consisted in finding a set of parameters that minimized a nonlinear objective function through a local gradient-based search method. Thus, the adaptation was very sensitive to the initial conditions and multiple starting points had to be tested. A global search method, such as scatter search using a local solver [ULP+07], could be used instead to guarantee the discovery of the best set of muscle parameters in a shorter period of time.

The second limitation lies in the formulation and implementation of the $c_i(t)$ optimization. A static optimization was used, consisting of optimizing the coefficients at each time step. This resulted in high computations times which should be reduced. For the 5-synergy model, 12 hours were needed, while for the 2-synergy

model 8h were needed on an HP Intel(R) Core(TM) i7-3740QM CPU 2.70GHz [CRPLD15]. To overcome this, other nonlinear programming methods such as sequential quadratic programming (SQP) could be used. Ultimately, this problem could also be addressed by parameterizing the synergy coefficients through a more efficient representation (e.g., polynomial, B-splines representation) which would allow the adaptation of a few control points instead of an entire trajectory, for instance through a dynamic optimization. Such an adaptation is also expected to enhance the preservation the shapes of the initial coefficients.

Finally, the pipeline should be extended to more characters and throwing motions to evidence its usability. To do this, generic synergy models could be extracted and optimized with respect to task space goals (instead of joint trajectories) and energy-based criterions. Such open issues are further discussed in Section 5.2.

The last two limitations are due to the character modeling and not the pipeline. Firstly, the muscle models used did not have the ability to vary their capacity to exert torque against the joint positions, as real muscles do. Their simple muscle routing, which consisted in constant moment arms to each DoF, distorted the motion and provoked unnecessary adaptations on $c_i(t)$. This limitation could be assessed by using a more realistic muscle routing with position-varying moment arms. Secondly, the activation dynamics (Equation 2.5) was not included in the muscle model, but considered a posteriori after the synergy adaptation. This relationship between excitations and activations has a natural filtering effect, which would lead to smoother motions. Considering this relationship a priori would also lead to a time-dependent optimization which could be solved through an optimal control problem.

4.7 Conclusion

Muscle synergies were used to track a throwing motion, while simplifying the control of a muscle-based virtual character by significantly reducing redundancy. This was achieved through the proposal, formulation, and testing of a synergy-driven forward dynamics pipeline based on time-invariant synergies extracted from experimental data. This pipeline consisted of two main components: an offline adaptation to determine the character's muscle parameters, and an online control loop to adapt the task-dependent part of the synergies ($c_i(t)$ coefficients) according to a set of kinematic goals, and to the distinct dynamics of the character with respect to the real subject. This synergy-driven solution was then tested for the reproduction of a throwing motion using a character with a simple musculoskeletal arm. The results showed that: 1) Only 2 synergies (an agonist and an antagonist) are necessary to control 3-DoF and 6 muscles of a virtual arm, 2) the original synergies are able

to reproduce important kinematic trends after muscle parameter adaptation, in spite of the simplicity of the arm model, 3) by adapting the synergy coefficients motion reproduction is enhanced, and 4) important characteristics in the agonist synergy shape, such as triggering times and intensity are preserved after the synergy adaptation.

These results evidence the potential of synergies as a low-dimensional control representation in forward dynamics, and the relevance of the extracted synergy models. A reduced set of control signals, which are less than the number of actuators, and in this case, also less than the number of DoF, where used to track a throwing motion with an overactuated model. Moreover, the synergies encode essential information that can be used to control a character with a simple morphology, as demonstrated by the reproduction of important kinematic trends using the original synergies, and the partial preservation of the coefficients $c_i(t)$ after the synergy adaptation procedure. The pipeline has limitations linked to the optimizations (Section 4.6) that need to be addressed to enhance its usability, accuracy, and extend it to motion synthesis applications. Future developments would also be needed to generalize it to other morphologies and motions (as discussed in Section 5.2). Nevertheless, this first implementation has evidenced the potential of synergies as a solution to reduce the redundancy of overactuated characters in phyiscs-based simulations.

Chapter 5

Conclusions and perspectives

5.1 Summary and contributions

THIS thesis addressed one of the main challenges of controlling muscle-based characters in physics-based simulations: actuation redundancy. A challenge that has not been efficiently addressed by most state of the art solutions (Section 2.1), which continue to compute a large number of actuation signals for each muscle in the character. Humans are by far the best example of how actuation redundancy is managed fast and efficiently (Section 2.2). Humans possess a motor control system that is able to plan complex motions intuitively in spite of having to coordinate numerous muscles at the same time. Inspired by this, a popular motor control theory, called the *theory of muscle synergies*, was hypothesized as a potential solution to solve actuation redundancy in muscle-based virtual characters. This theory assumes the existence of a reduced number of elementary control variables, called synergies, that are modulated in a task-dependent fashion to generate a larger number of muscle activations.

Based on this idea, a control solution for muscle-based characters was proposed consisting of identifying and adapting low-dimensional control representations (or synergies) according to a set of kinematic goals. Such a solution was built in two stages: a motion analysis and a motion generation stage. The motion analysis stage (Chapter 3) consisted in extracting kinematic features and time-invariant synergies from overhead throwing motions. The results evidenced that for the analyzed subjects, only 2 synergies or control variables were necessary to encode the important activation trends of sets containing 6-14 muscles. These synergies consisted of an agonist and an antagonist synergy, each composed of a spatial (task-independent) and a temporal (task-dependent) component. The temporal aspect of these synergies was modulated according to the throwing distance. As throwing distance increased, so did the kinematic features' magnitude and the triggering intensity of the tem-

poral aspect of the synergies. These low-dimensional control representations were then used as input control functions to a synergy-driven forward dynamics pipeline (Chapter 4). The aim of this pipeline was to scale the character's muscle parameters and adapt the initial synergies according to a set of kinematic goals and the distinct dynamics of the character with respect to the real subject. The results show that motion can be reproduced by modulating the temporal components of the synergies, while preserving important characteristics in their shapes. Using only 2 synergies, 6 muscles were controlled to reproduce the motion of 3 DoF of the character's throwing arm. Furthermore, the results also revealed that the original or initial synergies (before adaption) were able to reproduce important kinematic trends, in spite of the simplicity of the arm model.

Thus, the initial hypothesis was confirmed by evidencing the potential of synergies as a solution to solve actuation redundancy in muscle-based virtual characters. Solving this challenge and simplifying control tasks, is essential to ease the adoption of muscle-based characters and exploit the benefits of using muscles as actuators (Section 2.1). This concerns a variety of domains performing physical simulations with muscle-based characters, which range from rehabilitation to animation. Moreover, the use of muscle synergies within a motion generation context challenges and contributes to the validation of the muscle synergy theory as the modular mechanism behind human motion generation.

5.2 Open issues and perspectives

This thesis showed that a synergy-based solution is feasible for simplifying the control of a muscle-based character during overhead throwing. However some open questions remain, such as: *Can this solution be used to synthesize new throwing motions?*, and *would a synergy-based solution be feasible for controlling other morphologies and motions?*

To answer to the first question, a formal mathematical formulation would have to be defined for the observed relationship between the synergies and the task space features during throwing (Chapter 3). That is, the increase in the energy of the synergies, and the increase in release speed and height magnitude with throwing distance. For instance, the synergies' temporal components could be parametrized as polynomials whose coefficients would be expressed in terms of the release speed and height, and if necessary, also in terms of hand positions and velocities at key instants during each throwing motion phase. The synergy adaptation would then consist, for example, in a dynamic optimization to modulate these coefficients such that the desired kinematic goals are achieved in a given time. Such an optimization could consist in minimizing: a neuromuscular objective encoding muscle effort or

fatigue (Table A.2), and a task objective encoding the desired release speed and height, or the velocity and position of the hand at specific points in time.

To make a first assessment of the ability of a synergy-based solution to control different morphologies, the generic synergy model presented in Chapter 3 could be used to drive different characters, scaled to the different subjects that participated in the experiments. Afterwards, an evaluation could take place comparing desired versus real joint trajectories, release heights, and speeds, to assess how well this generic model is able to reproduce or synthesize motions with different characters. At the same time, it would also be interesting to quantify the modifications in the initial synergies before and after the adaptation, to determine their robustness across characters.

Ultimately, it remains to be shown if a synergy-based solution can be used to synthesize a rich variety of motions. This idea is encouraged by the multiple studies in neuroscience that have also described a variety of motions through a few set of synergies and well defined kinematic goals and features. It would be interesting to test these results in forward dynamics simulations and at the same time validate synergies as a feasible solution for generating motions with virtual characters. To do this, a database could be constructed containing time-invariant synergies and their relationship with kinematic goals and features. To start, other arm motions such as reaching, writing on a board, and other arm gestures could be analyzed. Eventually, motions involving whole body control, such as walking, could also be analyzed. However, the adaptation of the synergies would involve a more complex synergy adaptation than the one proposed in this work, for instance, to ensure balance.

The term "synergy" literally means "working together". The fact that our muscles work together when performing all sorts of motor tasks is well known. However, how they are controlled is still an enigma that needs to be thoroughly deciphered. Nevertheless, the assumption that this cooperation has a neural origin is interesting because it would explain why humans are able to control highly redundant musculoskeletal systems fast and efficiently. If the objective of performing physics-based simulations with virtual characters is to mimic the way humans move, it is only natural to do this by mimicking or replicating the control mechanisms that originate motion and manage a complex system of actuators. This thesis aimed at accomplishing this by identifying synergies as control mechanisms in humans and using them to construct simple, modular, and low-dimensional solutions to control a muscle-based virtual character.

Appendix A

Synopsis of muscle-based control in animation

A.1 Muscle-based controllers

A synopsis of the controller classification and key characteristics of each control approach are featured in Table A.1. The controllers were classified according to *control type*, following the classification made in Chapter 2.1: controller optimization (Section 2.1.2.3), or trajectory optimization (Section 2.1.2.4) methods. An additional "hybrid method" category was added, since the approach by [Si13] used both a controller optimization and a trajectory optimization.

The control methods are also classified by their *control space*, or the space in which their output signal is generated. This category is an indicator of the degree of detail with which the muscles are modeled. Motor space control methods generate excitations or activations to control characters with detailed muscle representations. Force space control methods generate forces to control characters with less detailed muscle representations (such as spring muscle models). Hybrid space control methods generate both motor signals and servo signals (torques) for characters that are actuated by muscles and servos.

The table also features the main *tasks* for which the controllers were employed. These can be: locomotion (L), kicking (K), jumping (J), balancing (B), gestures (G), posture adjustment (P), torso motion (T), neck motion (N), arm motion (A), hand motion (H), target tracking (Tr), and character interaction (CI).

The *models* commanded by these controllers are described by their degrees of freedom (DoF), number of muscles (Ms), and muscle groups (MGs). The muscle *actuators* are classified by the force generation model employed as either spring elements, Hill-type models, or other. The references from which the muscle models

were extracted or based are specified in parenthesis.

The most important characteristic is the *control strategy*, which indicates the muscle control method as seen in Section 2.1.2.3 and 2.1.2.4. Next, we find the *Main User Input*. The objective of this characteristic is to denote what are the main user input commands to the control frameworks. For instance, the required user input can be a compact goal (such as a desired walking speed or direction), it can also consist of more detailed motion data (recorded or specified by the animator), or sometimes less intuitive variables such as controller parameters directly. Finally, the *cost function* column contains the objective functions used, if the strategy involved an optimization procedure. In the case that no cost function was used the field reads NA (not applicable).

Table A.1 – Main muscle-based controllers for animation

Control Type	Control Space	Controller Reference	Task	Character	Model	Actuation Type	Control Strategy	Main User Input	Cost Function
Controller Optimization Methods	**Force Space**	[NF02]	B,G,P	Human, Human Torso	Human 47 DoF 94 Ms	Springs	Antagonistic control	Joint positions	NA
	Motor Space	[GvdPvdS13]	B,L	Humanoids, Imaginary creatures	40 DoF 27 Ms	Hill-type ([Zaj89])	PD controllers Muscle reflexes Constant excitations	Locomotion speed Locomotion direction	Pose tracking Velocity tracking Stability Muscle effort
	Hybrid Space	[WHDK12]	B,L	Humanoid	30 DoF 16 Ms (legs)	Hill-type ([Zaj89]) (Lower-body) Servos (Upper-body)	PD controllers Muscle reflexes Constant excitations	Locomotion speed	Pose tracking Velocity tracking Stability Muscle effort
Trajectory Optimization Methods	**Force Space**	[Mil88]	L	Snakes, Worms	–	Springs	Function primitives Muscle groups	Function primitive parameters	NA
		[TT94]	CI,L	Fishes	91 Ms	Springs	Function primitives Muscle groups	Pre-defined habits	NA
		[TTL12]	B,L	Alphabet Letters	Ex. Letter I 104 DoF 4 Ms	Springs	No function primitives No muscle groups	Task positions Task velocities	Pose tracking Velocity tracking Momentum tracking Base contact tracking
		[GT95]	L,Tr	Snakes, Marine animals	Snake 126 DoF 40 Ms	Springs	No function primitives No muscle groups	Locomotion speed Distance to goal	Velocity tracking Distance to goal tracking Muscle effort

Continued on next page

Table A.1 – *Continued from previous page*

Control Type	Control Space	Controller Reference	Task	Character	Model	Actuation Type	Control Strategy	Main User Input	Cost Function
	Motor Space	[GTH98]	L	Dolphin	12 Ms	Springs	No function primitives No muscle groups	Locomotion speed Distance to goal	Velocity tracking Distance to goal tracking Muscle effort
		[KSK00]	B,K,L	Human	86 Ms (legs)	Hill-type ([DLH+90] [Del90])	No function primitives No muscle groups	Joint positions	Stability Muscle fatigue Motion feasibility Joint limit accordance
		[AHS03]	H	Human hand & Forearm	–	Other ([BH93])	Function primitives Muscle groups	Contraction values at keyframes	NA
		[HMOA03]	B,L	Human	19 DoF 60 Ms	Other ([Hat77])	No function primitives No muscle groups	Locomotion speed Ratio of period of foot-ground contact	*Offline:* Criterion based locomotion speed and ratio of period of foot-ground contact Energy efficiency and motion smoothness *Online:* Muscle fatigue
		[TSF05]	H	Human hand & forearm	41 Ms 16 DoF	Hill-type ([Zaj89])	No function primitives No muscle groups	Joint positions Joint velocities Muscle activations	Pose tracking Muscle effort
		[ZCCD06]	T	Human Torso	5 MGs	Hill-type ([Zaj89])	Function primitives Muscle groups	Function primitive parameters	NA

Continued on next page

Table A.1 – *Continued from previous page*

Control Type	Control Space	Controller Reference	Task	Character	Model	Actuation Type	Control Strategy	Main User Input	Cost Function
		[LT06]	CI,N	Human neck & head	72 Ms	Linearized Hill-Type ([NTH01] [WC00])	No function primitives No muscle groups	Initial and final head positions	*Offline:* Muscle effort *Online:* Minimal joint displacement
		[SKP08]	A,H	Human hand & forearm	54 Ms	Hill-Type No FV-relationship ([SKP08])	No function primitives No muscle groups	Task velocities	Velocity tracking Muscle effort
		[LST09]	A,T	Human upper body	147 DoF 814 Ms	Linearized Hill-type ([LT06])	No function primitives No muscle groups	Joint positions target coactivation	Muscle effort
		[LPKL14]	B,L	Human	25-39 DoF 62-120 Ms	Hill-type ([Zaj89])	No function primitives No muscle groups	Joint positions Joint velocities Task positions	Pose tracking Velocity tracking Acceleration tracking Stability Muscle effort Energy efficiency Pain avoidance
		[CRPLD15, CRPD16]	A,H	Human arm & hand	3 DoF 6 Ms	Hill-Type ([Hil38] [RAPC10])	Function primitives Muscle groups	Joint positions	Pose tracking

Continued on next page

Table A.1 – *Continued from previous page*

Control Type	Control Space	Controller Reference	Task	Character	Model	Actuation Type	Control Strategy	Main User Input	Cost Function
		[SSB+15]	H	Human hand	–	Piece-wise linear muscle model ([SSB+15])	No function primitives No muscle groups	Task positions	Velocity tracking Muscle effort
	Hybrid Space	[DZS08]	T	Human Torso	3 MGs	Hill-type ([Zaj89] [NTH01] [BLMB04]) Servos (Spine)	Function primitives Muscle groups	Audio track	Pressure tracking
		[MWTK13]	B,J,K,L	Humanoid	36 DoF 28 Ms (legs)	Hill-type ([MD12] [GH10]) (Lower-body) Servos (Upperbody)	Function primitives Muscle groups	Locomotion speed Jumping height Kicking foot speed	Pose tracking Velocity tracking Virtual force reduction Dynamical consistency Muscle effort Muscle force physiological consistency Self-collision avoidance Joint limit accordance

Continued on next page

Table A.1 – *Continued from previous page*

Control Type	Control Space	Controller Reference	Task	Character	Model	Actuation Type	Control Strategy	Main User Input	Cost Function
Hybrid Method *(Using: Controller and Trajectory optimization)*	**Motor Space**	[Si13]	L	Human	163 DoF 823 Ms	Linearized Hill-Type ([LST09])	*Locomotion tasks:* Controller optimization: Neural networks PD controllers *Non-locomotion tasks:* Trajectory optimization: No function primitives	*Locomotion tasks:* Joint positions High level CPG parameters *Non-locomotion tasks:* Trunk orientation Motion capture data	*Locomotion tasks:* Time-varying muscle length tracking *Non-locomotion tasks:* Pose tracking Motion naturalness Self collision avoidance

A.2 Cost functions

Table A.2 features a list of neuromuscular objective terms which correspond to the categorization introduced in section 2.1.2.1, inspired by [ZW90]. This categorization is based on a generalized performance criterion which includes three components: task specific (tracking a giving trajectory, minimizing jerk), neuromuscular (minimizing muscle stress, neural effort) and bone joint (minimizing contact forces, avoiding certain ranges of motion) objectives. Task specific kinematics and bone joint objectives are already popular in animation. Therefore, a focus is given to the neuromuscular objectives, the novelty of muscle-based controllers. These neuromuscular objectives were divided into those that describe muscle fatigue and those that describe muscle effort (following the distinction made by [AvdB10]). Thus, cost functions presenting muscle volume weighting and lower exponents were classified as effort-like, while cost functions without muscle volume weighting and higher exponents were classified as fatigue-like. An additional category was added for the functions that did not fit these two categories (*Alternative muscle-based terms*). The final classification and details of these functions are featured in Table A.2.

Fatigue-like functions Muscle fatigue occurs when there is a failure to maintain a required or expected force [Edw08], and it is related to the amount of synergy between the muscles. A high synergy implies that all muscles contribute during the motion in a way that the maximum relative load of any muscle remains as small as possible. In other words they work well together by helping each other and ensuring that no muscle works more than the rest.

Effort-like functions Muscle effort is a substitute for muscle energy expenditure. It is related to the volume of activated muscle tissue [AvdB10]. These functions have been more popular than fatigue-like functions, among animators.

Table A.2 – Neuromuscular objectives used in animation

Type	Controller	Cost Function	Formula	Terms
Effort-like	[WHDK12]	Muscle-effort	$w_M J_M + w_R J_R + w_L J_L$ $J_M = \dot{A} + \dot{M} + \dot{S} + \dot{W}$	J_M, J_R, J_L = Average rate of metabolic energy expenditure, sum of torques squared, sum of squared soft joint limit torques $\dot{A}, \dot{M}, \dot{S}, \dot{W}$ = Muscle activation, muscle maintenance, muscle shortening heat rates, positive mechanical work rate w = Scalar weights
	[GvdPvdS13]	Muscle effort	$J_M = \dot{A} + \dot{M} + \dot{S} + \dot{W}$	Same terminology as above
	[GT95] [GTH98]	Muscle effort	$\frac{1}{2}\left(w_a \left\lvert \frac{du}{dt} \right\rvert^2 + w_b \left\lvert \frac{d^2u}{dt^2} \right\rvert^2\right)$	u = Control signal
	[TSF05]	Muscle effort	$\frac{1}{2}\lVert a \rVert^2$	a = Muscle activation
	[LT06]	Muscle effort	$\lVert W^{-1} f_c \rVert^2$	W = Weights matrix f_c = Muscle forces
	[SKP08] [SSB+15]	Muscle effort	$w_a \lVert a \rVert^2 + w_d \lVert a - a^o \rVert^2$	a = Muscle activation a^o = Activation previous timestep w_a, w_d = Regularization and damping scalar weights
	[LST09]	Muscle effort	$\frac{1}{2}\sum (w_i a_i)^2$	w_i = Variable weight (regularizes muscle activation levels)
	[MWTK13]	Muscle effort	$J_M + J_{upper}$ $J_M = \dot{A} + \dot{M} + \dot{S} + \dot{W}$ $J_{upper} = w_m \sum \left(f^i_{motor}\right)^2 + \ddot{q}^T W_a \ddot{q}$	J_{upper} = Upper-body effort, f^i_{motor} = Active motor torques W_a = Diagonal weight matrix, q =Articular positions
	[LPKL14]	Muscle effort	$\lVert a \rVert^2$	a = Muscle activation
		Energy efficiency	$-\frac{1}{D}\sum_{1}^{Nfall}(J_M)$	J_M = Average rate of metabolic energy expenditure D = Total moving distance before falling $Nfall$ = Number simulation time slots before falling
Fatigue-like	[KSK00] [HMOA03]	Muscle fatigue	$\int_{t_0}^{t_f} \sum \left(\frac{f_i}{f^i_{max}}\right)^2 dt$	i = ith-muscle , f_i = Muscle force f^i_{max} = Maximum muscle force, t_0, t_f = Initial and final time

Continued on next page

Table A.2 – *Continued from previous page*

Type	Controller	Cost Function	Formula	Terms
Alternative muscle-based objectives	[HMOA03]	Energy efficiency and motion smoothness	$\frac{1}{S+w_o D}$	S = Specific power D = Rate of change of muscular tensions
	[MWTK13]	Muscle force physiological consistency	$\sum_i \left(F^i_{SE} - F^i_{CE} - F^i_{PE} - m_{CE}\,\ddot{l}^i_{CE}\right)$	$F^i_{SE}, F^i_{CE}, F^i_{PE}$ = Serial-elastic, contractile, passive forces m_{CE} = Pointmass between contractile element and tendon l^i_{CE} = Length contractile element
	[LPKL14]	Pain avoidance	$\sum_{1}^{Nfall} \left(f^i_c\right)$	$(f)^i_c$ = ith-muscle force

Appendix B

Data acquisition details

During the experiments whole body kinematics and the muscle activity of 16 muscles of the back and right arm were recorded. The electrodes were placed according to the surface electrode placement protocols in [HFM+99, Cri10]. Table B.1 lists and details the function of each of these muscles. The reflective markers were placed according to the M2S laboratory protocol and are featured in Table B.2 and Figure B.1.

Table B.1 – **Recorded muscles and their function**

Recorded muscles and their function	
Muscle name	**Function**
1. Erector spinae longissimus (Thoracic)	Assists in the motion of backward and sidewards bending, keeping the spine erect and pulling the ribs downward to help with breathing.
2. Erector spinae iliocostalis	Assisting extension and laterally flex of the vertebral column, maintaining erect posture as well as bending the vertebral column to the same side.
3. Lastissimus dorsi	Adducts, medially rotates and extends the arm at the shoulder (glenohumeral) joint.
4. Upper trapezius	Elevates and upwardly rotates the scalpula; extends the neck
5. Middle trapezius	Adducts (retracts) scalpula.
6. Lower trapezius	Depresses and helps upper trapezius upwardly rotate the scalpula.
7. Posterior deltoid	Laterally rotates and extends the arm at the shoulder (glenohumeral) joint.

8. Anterior deltoid	Flexes and medially rotates the arm at the shoulder.
9. Middle deltoid	Abducts the arm at the shoulder.
10. Pectoralis major (Clavicular head)	Flexes the arm at the shoulder (glenohumeral) joint.
11. Pectoralis major (Sternocostal head)	Extends the arm at the shoulder (glenohumeral) joint from a flexed position. (*Note: as a whole, both pectoralis adduct, medially rotate the humerus, and draw the scalpula anteriorly and inferiorly.*)
12. Biceps	Flexes and supinates forearm at elbow (also weakly flexes the arm at shoulder).
13. Triceps (long head)	Extends the forearm at the elbow (also extends the arm at the shoulder (glenohumeral) joint).
14. Triceps (lateral head)	Extends the forearm at the elbow.
15. Forearm extensor bundle	Extends the wrist. The bundle encompasses the extensor digitorium, brachioradialis, extensor carpi radialis, and pronator teres.
16. Forearm flexor bundle	Flexes the wrist. The bundle encompasses the flexor digitorium, flexor carpi radialis and ulnaris, and flexor pollicis longus.

Table B.2 – **Recorded markers and their placement**

Recorded markers and their placement	
Marker name	**Body landmark**
1. RFHD	Frontal bone right side
2. LFHD	Frontal bone left side
3. RBHD	Occipital bone right side
4. LBHD	Occipital bone left side
5. CLAV	Jugular incision of the sternum (junction of the clavicles)
6. STRN	Xiphoid process
7. C7	Spinous process of the 7th cervical vertebrae
8. T10	Spinous process of the 10th dorsal vertebrae
9. RSHO	Right acromion
10. LSHO	Left acromion
11. RBAC	Asymmetrical marker over right scalpula
12. RUPA	Asymmetrical marker over right arm

13. LUPA	Asymmetrical marker over left arm
14. RHUM	Medial epicondyle of right humerus
15. LHUM	Medial epicondyle of left humerus
16. RRAD	Head or right radius
17. LRAD	Head or left radius
18. RWRA	Styloid process of right radius
19. LWRA	Styloid process of left radius
20. RWRB	Styloid process of right ulna
21. LWRB	Styloid process of left ulna
22. RCAR	Third metacarpal process of the right hand
23. LCAR	Third metacarpal process of the left hand
24. RFWT	Right anterior superior iliac spine
25. LFWT	Left anterior superior iliac spine
26. RBWT	(Right) posterior superior iliac spine
27. LBWT	(Left) posterior superior iliac spine
28. RTHI	Asymmetrical marker on right thigh
29. LTHI	Asymmetrical marker on left thigh
30. RKNE	Lateral condyle of right femur
31. LKNE	Lateral condyle of left femur
32. RKNI	Medial condyle of right tibia
33. LKNI	Medial condyle of left tibia
34. RANE	(Right) external malleolus
35. LANE	(Left) external malleolus
36. RANI	(Right) medial malleolus
37. LANI	(Left) medial malleolus
38. RHEE	(Right) posterior tuberosity of calcaneus
39. LHEE	(Left) posterior tuberosity of calcaneus
40. RTOE	(Right) head of big/innermost toe
41. LTOE	(Left) head of big/innermost toe
42. RTAR	Outer edge of right foot, tip of 5th metatarsal
43. LTAR	Outer edge of left foot, tip of 5th metatarsal
Not featured in Figure	
44. RTARI	Inner edge of right foot, tip of 1st metatarsal
45. LTARI	Inner edge of left foot, tip of 1st metatarsal
46. RFIN	Right index finger
47. LFIN	Left index finger
48. RFRI	Right ring finger

49. LFRI	Left ring finger

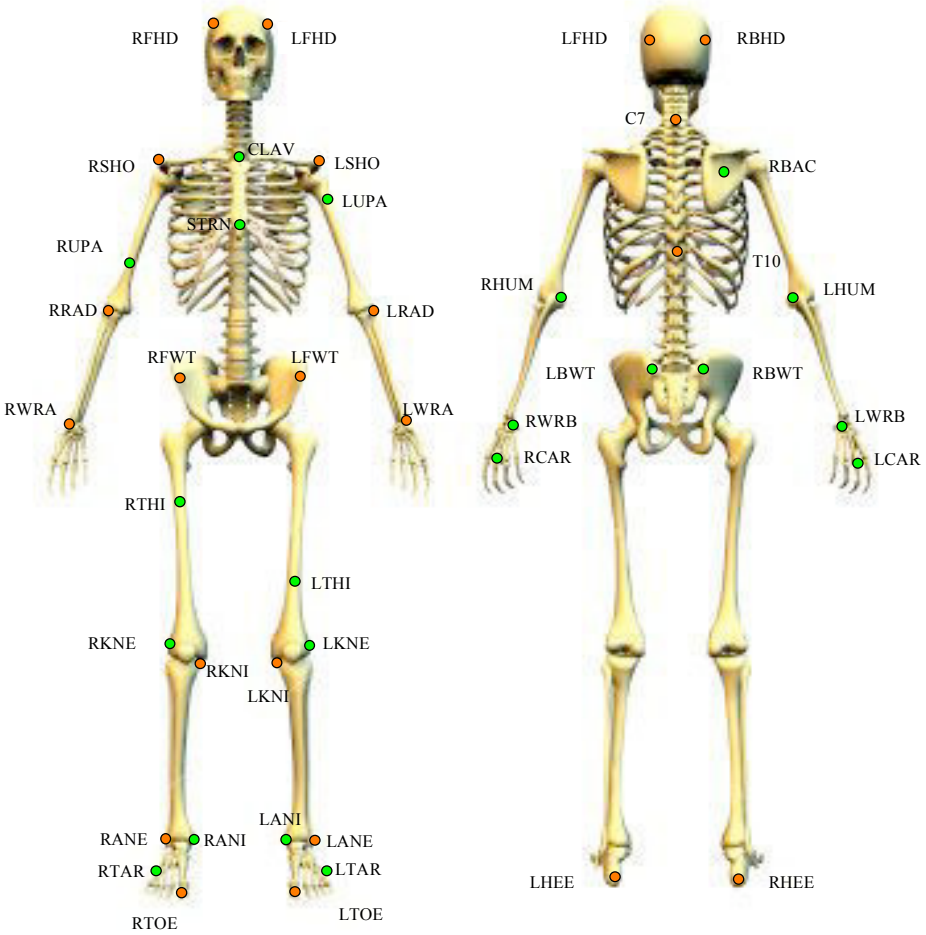

Figure B.1 – **Reflective marker placement.** (A) Frontal view (B) Back view. (Green markers: asymmetrical markers. Orange markers: necessary markers for the computation of anthropometric data.)

Appendix C

Character modeling details

THE full body skeletal model consists of 21 rigid bodies linked by 17 joints, and exhibits 32 degrees of freedom. The method used to describe the skeletal model is based on a systematic structural representation. Except for the root (pelvis), each segment integrates a joint and its adjoined body. Thus, the segment representation does not depend on the other segments connected to it. This structural representation is described according to a hierarchical tree. From the root, each solid owns one child and one sister.

A library containing several body part models issued from the literature, which can correspond to a segment or a set of segments, was used to build the model [MPGD15]. The model used in the current study consists of well known and validated biomechanical models of the spine [DZHW+07], the lower limbs [HKVdH+07] and the upper limbs [HMD05]. The complete skeletal model has been kinematically validated [MGPD15]. Furthermore, the bone graphics were adapted from the AnyBody Managed Repository [DRC+06, Any].

Standard Body Segment Inertial Parameters (BSIP) were estimated using an anthropometric scaling rule to adapt the model to the subject's morphology [DCV07].

References

Thesis related publications

[CRPD14] A. Cruz Ruiz, C. Pontonnier, and G. Dumont, "A bio-inspired limb controller for avatar animation," *Computer Methods in Biomechanics and Biomedical Engineering*, vol. 17, no. sup1, pp. 174–175, 2014.

[CRPD16] A. Cruz Ruiz, C. Pontonnier, and G. Dumont, "A synergy-based control solution for overactuated characters: Application to throwing," *To be published in Computer Animation and Virtual Worlds*, 2016.

[CRPLD15] A. Cruz Ruiz, C. Pontonnier, J. Levy, and G. Dumont, "Motion control via muscle synergies: Application to throwing," in *Proceedings of the 8th ACM SIGGRAPH Conference on Motion in Games*, ser. MIG '15. Paris, France: ACM, 2015, pp. 65–72.

[CRPPD16] A. Cruz Ruiz, C. Pontonnier, N. Pronost, and G. Dumont, "Muscle-based control for character animation," *Computer Graphics Forum (Online)*, 2016.

[CRPSD15] A. Cruz Ruiz, C. Pontonnier, A. Sorel, and G. Dumont, "Identifying representative muscle synergies in overhead football throws," *Computer Methods in Biomechanics and Biomedical Engineering*, vol. 18, no. sup1, pp. 1918–1919, 2015.

Bibliography

[ADN+13] C. Alessandro, I. Delis, F. Nori, S. Panzeri, and B. Berret, "Muscle synergies in neuroscience and robotics: from input-space to task-

space perspectives," *Frontiers in Computational Neuroscience*, vol. 7, no. 43, 2013.

[AHS03] I. Albrecht, J. Haber, and H.-P. Seidel, "Construction and animation of anatomically based human hand models," in *Proceedings of the 2003 ACM SIGGRAPH/Eurographics Symposium on Computer Animation*, ser. SCA '03. San Diego, California: Eurographics Association, 2003, pp. 98–109.

[And99] F. C. Anderson, "A dynamic optimization solution for a complete cycle of normal gait," Ph.D. dissertation, University of Texas at Austin, 1999.

[Any] "Anybody managed repository," http://anyscript.org/.

[AT05] S. Aoi and K. Tsuchiya, "Locomotion control of a biped robot using nonlinear oscillators," *Autonomous Robots*, vol. 19, no. 3, pp. 219–232, 2005.

[AT06] S. Aoi and K. Tsuchiya, "Stability analysis of a simple walking model driven by an oscillator with a phase reset using sensory feedback," *Robotics, IEEE Transactions on*, vol. 22, no. 2, pp. 391–397, 2006.

[AV07] D. Arthur and S. Vassilvitskii, "K-means++: The advantages of careful seeding," in *Proceedings of the Eighteenth Annual ACM-SIAM Symposium on Discrete Algorithms*, ser. SODA '07. Philadelphia, PA, USA: Society for Industrial and Applied Mathematics, 2007, pp. 1027–1035.

[AvdB10] M. Ackermann and A. J. van den Bogert, "Optimality principles for model-based prediction of human gait," *Journal of biomechanics*, vol. 43, no. 6, pp. 1055–1060, 2010.

[BAGD07] S. S. Blemker, D. S. Asakawa, G. E. Gold, and S. L. Delp, "Image-based musculoskeletal modeling: Applications, advances, and future opportunities," *Journal of magnetic resonance imaging*, vol. 25, no. 2, pp. 441–451, 2007.

[Bar08] R. Bartlett, *Biomechanics in Sport*. Blackwell Science Ltd, 2008, ch. Principles of Throwing, pp. 365–380.

[Ber67] N. A. Bernstein, "The co-ordination and regulation of movements," 1967.

[BH93] P. W. Brand and A. Hollister, *Clinical mechanics of the hand.* Mosby Year Book, 1993.

[BLMB04] T. S. Buchanan, D. G. Loyd, K. Manal, and T. F. Besier, "Neuromusculoskeletal modeling : Estimation of muscle forces and joints moments and movements from measurements of neural command," *Journal of Applied Biomechanics*, vol. 20, pp. 367–395, 2004.

[BS95] A. J. Bell and T. J. Sejnowski, "An information-maximization approach to blind separation and blind deconvolution," *Neural Comput.*, vol. 7, no. 6, pp. 1129–1159, Nov. 1995.

[BSF07] M. D. K. Breteler, K. J. Simura, and M. Flanders, "Timing of muscle activation in a hand movement sequence," *Cerebral Cortex*, vol. 17, no. 4, pp. 803–815, 2007.

[CB81] R. D. Crowninshield and R. A. Brand, "A physiologically based criterion of muscle force prediction in locomotion," *Journal of biomechanics*, vol. 14, no. 11, pp. 793–801, 1981.

[CIPL06] G. Cappellini, Y. P. Ivanenko, R. E. Poppele, and F. Lacquaniti, "Motor patterns in human walking and running," *Journal of Neurophysiology*, vol. 95, no. 6, pp. 3426–3437, 2006.

[CMD16] L. Chèze, F. Moissenet, and R. Dumas, "State of the art and current limits of musculo-skeletal models for clinical applications," *Movement & Sport Sciences*, no. 4, pp. 7–17, 2016.

[Cri10] E. Criswell, *Cram's introduction to surface electromyography.* Jones & Bartlett Publishers, 2010.

[Dar68] R. B. Darlington, "Multiple regression in psychological research and practice." *Psychological bulletin*, vol. 69, no. 3, p. 161, 1968.

[dB05] A. d'Avella and E. Bizzi, "Shared and specific muscle synergies in natural motor behaviors," *Proceedings of the National Academy of Sciences of the United States of America*, vol. 102, no. 8, pp. 3076–3081, 2005.

[DBN06] K. Davids, S. Bennett, and K. M. Newell, *Movement System Variability.* Human Kinetics, 2006, ch. Variability in Motor Output and Olympic Performers, pp. 89–92.

[DCD10] S. Duprey, L. Chèze, and R. Dumas, "Influence of joint constraints on lower limb kinematics estimation from skin markers using global optimization," *Journal of Biomechanics*, vol. 43, no. 14, pp. 2858 – 2862, 2010.

[DCV07] R. Dumas, L. Chèze, and J.-P. Verriest, "Adjustments to McConville et al. and Young et al. body segment inertial parameters," *Journal of biomechanics*, vol. 40, no. 3, pp. 543–553, 2007.

[Del90] S. L. Delp, "Surgery simulation: a computer graphics system to analyze and design musculoskeletal reconstructions of the lower limb," Ph.D. dissertation, Stanford University, 1990.

[Dem55] W. T. Dempster, "Space requirements of the seated operator," Wright-Patterson Air Force Base, Ohio, WADC Technical Report, 1955.

[dFPL08] A. d'Avella, L. Fernandez, A. Portone, and F. Lacquaniti, "Modulation of phasic and tonic muscle synergies with reaching direction and speed," *Journal of neurophysiology*, vol. 100, no. 3, pp. 1433–1454, 2008.

[DIC+11] N. Dominici, Y. P. Ivanenko, G. Cappellini, A. d'Avella, V. Mondì, M. Cicchese, A. Fabiano, T. Silei, A. Di Paolo, C. Giannini, R. E. Poppele, and F. Lacquaniti, "Locomotor primitives in newborn babies and their development," *Science*, vol. 334, no. 6058, pp. 997–999, 2011.

[DJPP92] N. M. DiGiovine, F. W. Jobe, M. Pink, and J. Perry, "An electromyographic analysis of the upper extremity in pitching," *Journal of Shoulder and Elbow Surgery*, vol. 1, no. 1, pp. 15–25, 1992.

[dL96] P. de Leva, "Adjustements to Zatsiorsky-Seluyanov's segment inertia parameters," *Journal of Biomechanics*, vol. 29, pp. 1223–1230, 1996.

[dL13] A. d'Avella and F. Lacquaniti, "Control of reaching movements by muscle synergy combinations," *Frontiers in computational neuroscience*, vol. 7, 2013.

[DLH+90] S. L. Delp, J. P. Loan, M. G. Hoy, F. E. Zajac, E. L. Topp, and J. M. Rosen, "An interactive graphics-based model of the lower extremity to study orthopaedic surgical procedures," *Biomedical Engineering, IEEE Transactions on*, vol. 37, no. 8, pp. 757–767, 1990.

[DLvdPY15] K. Ding, L. Liu, M. van de Panne, and K. Yin, "Learning reduced-order feedback policies for motion skills," in *Proceedings of the 14th ACM SIGGRAPH / Eurographics Symposium on Computer Animation*, ser. SCA '15. New York, NY, USA: ACM, 2015, pp. 83–92.

[dPFL06] A. d'Avella, A. Portone, L. Fernandez, and F. Lacquaniti, "Control of fast-reaching movements by muscle synergy combinations," *The Journal of Neuroscience*, vol. 26, no. 30, pp. 7791–7810, 2006.

[dPL11] A. d'Avella, A. Portone, and F. Lacquaniti, "Superposition and modulation of muscle synergies for reaching in response to a change in target location," *Journal of neurophysiology*, vol. 106, no. 6, pp. 2796–2812, 2011.

[DRC+06] M. Damsgaard, J. Rasmussen, S. T. Christensen, E. Surma, and M. de Zee, "Analysis of musculoskeletal systems in the anybody modeling system," *Simulation Modelling Practice and Theory*, vol. 14, no. 8, pp. 1100–1111, 2006.

[dSB03] A. d'Avella, P. Saltiel, and E. Bizzi, "Combinations of muscle synergies in the construction of a natural motor behavior," *Nature neuroscience*, vol. 6, no. 3, pp. 300–308, 2003.

[dT02] A. d'Avella and M. C. Tresch, "Modularity in the motor system: decomposition of muscle patterns as combinations of time-varying synergies," *Advances in neural information processing systems*, vol. 14, pp. 141–148, 2002.

[DZHW+07] M. De Zee, L. Hansen, C. Wong, J. Rasmussen, and E. B. Simonsen, "A generic detailed rigid-body lumbar spine model," *Journal of biomechanics*, vol. 40, no. 6, pp. 1219–1227, 2007.

[DZS08] P. C. DiLorenzo, V. B. Zordan, and B. L. Sanders, "Laughing out loud: Control for modeling anatomically inspired laughter using audio," *ACM Trans. Graph.*, vol. 27, no. 5, pp. 125:1–125:8, Dec. 2008.

[Edw08] R. H. T. Edwards, *Human Muscle Function and Fatigue*. John Wiley & Sons, Ltd., 2008, pp. 1–18.

[EMHvdB07] A. Erdemir, S. McLean, W. Herzog, and A. J. van den Bogert, "Model-based estimation of muscle forces exerted during movements," *Clinical Biomechanics*, vol. 22, no. 2, pp. 131–154, 2007.

[ENMC05] G. Endo, J. Nakanishi, J. Morimoto, and G. Cheng, "Experimental studies of a neural oscillator for biped locomotion with QRIO," in *Robotics and Automation, 2005. ICRA 2005. Proceedings of the 2005 IEEE International Conference on.* IEEE, 2005, pp. 596–602.

[FEA+96] C. S. Fleisig, R. F. Escamilla, J. R. Andrews, T. Matsuo, and S. W. Barrentine, "Kinematic and kinetic comparison between baseball pitching and football passing." *Journal of Applied Biomechanics*, vol. 12, no. 2, pp. 207–224, 1996.

[Fea14] R. Featherstone, *Rigid body dynamics algorithms.* Springer, 2014.

[Fel66] A. G. Feldman, "Functional tuning of nervous system with control of movement or maintenance of a steady posture. 2. controllable parameters of muscles," *BIOPHYSICS-USSR*, vol. 11, no. 3, p. 565, 1966.

[GEPD13] R. Gentner, T. Edmunds, D. Pai, and A. D'avella, "Robustness of muscle synergies during visuomotor adaptation," *Frontiers in Computational Neuroscience*, vol. 7, p. 120, 2013.

[GH10] H. Geyer and H. Herr, "A muscle-reflex model that encodes principles of legged mechanics produces human walking dynamics and muscle activities," *Neural Systems and Rehabilitation Engineering, IEEE Transactions on*, vol. 18, no. 3, pp. 263–273, 2010.

[GML93] Y. Giat, J. Mizrahi, and M. Levy, "A musculotendon model of the fatigue profiles of paralyzed quadriceps muscle under FES," *Biomedical Engineering, IEEE Transactions on*, vol. 40, no. 7, pp. 664–674, 1993.

[GML96] Y. Giat, J. Mizrahi, and M. Levy, "A model of fatigue and recovery in paraplegic's quadriceps muscle subjected to intermittent FES," *Journal of biomechanical engineering*, vol. 118, no. 3, pp. 357–366, 1996.

[GSB03] H. Geyer, A. Seyfarth, and R. Blickhan, "Positive force feedback in bouncing gaits?" *Proceedings of the Royal Society of London B: Biological Sciences*, vol. 270, no. 1529, pp. 2173–2183, 2003.

[GT95] R. Grzeszczuk and D. Terzopoulos, "Automated learning of muscle-actuated locomotion through control abstraction," in *Proceedings of the 22nd Annual Conference on Computer Graphics and Interactive Techniques*, ser. SIGGRAPH '95. ACM, 1995, pp. 63–70.

[GTH98] R. Grzeszczuk, D. Terzopoulos, and G. Hinton, "Neuroanimator: Fast neural network emulation and control of physics-based models," in *Proceedings of the 25th Annual Conference on Computer Graphics and Interactive Techniques*, ser. SIGGRAPH '98. ACM, 1998, pp. 9–20.

[GvdBHZ98] K. Gerritsen, A. van den Bogert, M. Hulliger, and R. Zernicke, "Intrinsic muscle properties facilitate locomotor control-a computer simulation study." *Motor control*, vol. 2, no. 3, pp. 206–220, 1998.

[GvdPvdS13] T. Geijtenbeek, M. van de Panne, and A. F. van der Stappen, "Flexible muscle-based locomotion for bipedal creatures," *ACM Trans. Graph.*, vol. 32, no. 6, pp. 206:1–206:11, Nov. 2013.

[Han06] N. Hansen, "The CMA evolution strategy: a comparing review," in *Towards a new evolutionary computation.* Springer, 2006, pp. 75–102.

[Hat77] H. Hatze, "A myocybernetic control model of skeletal muscle," *Biological cybernetics*, vol. 25, no. 2, pp. 103–119, 1977.

[HFH98] S. M. Henry, J. Fung, and F. B. Horak, "EMG responses to maintain stance during multidirectional surface translations," *Journal of Neurophysiology*, vol. 80, no. 4, pp. 1939–1950, 1998.

[HFM+99] H. J. Hermens, B. Freriks, R. Merletti, D. Stegeman, J. Blok, G. Rau, C. Disselhorst-Klug, and G. Hägg, "European recommendations for surface electromyography," *Roessingh Research and Development*, vol. 8, no. 2, pp. 13–54, 1999.

[Hil38] A. V. Hill, "The heat of shortening and the dynamic constants of muscle," *Proceedings of the Royal Society of London B: Biological Sciences*, vol. 126, no. 843, pp. 136–195, 1938.

[HKS+02] M. Hirashima, H. Kadota, S. Sakurai, K. Kudo, and T. Ohtsuki, "Sequential muscle activity and its functional role in the upper extremity and trunk during overarm throwing," *Journal of Sports Sciences*, vol. 20, no. 4, pp. 301–310, 2002.

[HKVdH+07] M. K. Horsman, H. Koopman, F. Van der Helm, L. P. Prosé, and H. Veeger, "Morphological muscle and joint parameters for musculoskeletal modelling of the lower extremity," *Clinical Biomechanics*, vol. 22, no. 2, pp. 239–247, 2007.

[HMD05] K. R. S. Holzbaur, W. M. Murray, and S. L. Delp, "A model of the upper extremity for simulating musculoskeletal surgery and analyzing neuromuscular control," *Annals of Biomedical Engineering*, vol. 33, no. 6, pp. 829–840, 2005.

[HMOA03] K. Hase, K. Miyashita, S. Ok, and Y. Arakawa, "Human gait simulation with a neuromusculoskeletal model and evolutionary computation," *The Journal of Visualization and Computer Animation*, vol. 14, no. 2, pp. 73–92, 2003.

[Hoo01] S. L. Hooper, *Central Pattern Generators.* John Wiley & Sons, Ltd, 2001.

[HR11] J. C. Houk and W. Z. Rymer, *Neural Control of Muscle Length and Tension.* John Wiley & Sons, Inc., 2011.

[HSWH02] P. A. Højen-Sørensen, O. Winther, and L. K. Hansen, "Mean-field approaches to independent component analysis," *Neural Computation*, vol. 14, no. 4, pp. 889–918, 2002.

[HTCD11] F. Hug, N. A. Turpin, A. Couturier, and S. Dorel, "Consistency of muscle synergies during pedaling across different mechanical constraints," *Journal of Neurophysiology*, vol. 106, no. 1, pp. 91–103, 2011.

[Hui98] P. Huijbregts, "Biomechanics and pathology of the overhead throwing motion: a literature review," *Journal of Manual & Manipulative Therapy*, vol. 6, no. 1, pp. 17–23, 1998.

[HZN+06] J. Higginson, F. Zajac, R. Neptune, S. Kautz, and S. Delp, "Muscle contributions to support during gait in an individual with post-stroke hemiparesis," *Journal of Biomechanics*, vol. 39, no. 10, pp. 1769 – 1777, 2006.

[IGZ+03] Y. P. Ivanenko, R. Grasso, M. Zago, M. Molinari, G. Scivoletto, V. Castellano, V. Macellari, and F. Lacquaniti, "Temporal components of the motor patterns expressed by the human spinal cord reflect foot kinematics," *Journal of Neurophysiology*, vol. 90, no. 5, pp. 3555–3565, 2003.

[Ijs08] A. J. Ijspeert, "Central pattern generators for locomotion control in animals and robots: a review," *Neural Networks*, vol. 21, no. 4, pp. 642–653, 2008.

[IPL04] Y. P. Ivanenko, R. E. Poppele, and F. Lacquaniti, "Five basic muscle activation patterns account for muscle activity during human locomotion," *The Journal of Physiology*, vol. 556, no. 1, pp. 267–282, 2004.

[JL11] S. Jain and C. K. Liu, "Modal-space control for articulated characters," *ACM Trans. Graph.*, vol. 30, no. 5, pp. 118:1–118:12, Oct. 2011.

[KBWW02] B. T. Kelly, S. I. Backus, R. F. Warren, and R. J. Williams, "Electromyographic analysis and phase definition of the overhead football throw," *The American journal of sports medicine*, vol. 30, no. 6, pp. 837–844, 2002.

[KGZL03] V. Krishnamoorthy, S. Goodman, V. Zatsiorsky, and L. M. Latash, "Muscle synergies during shifts of the center of pressure by standing persons: identification of muscle modes," *Biological Cybernetics*, vol. 89, no. 2, pp. 152–161, 2003.

[KH10] T. Kwon and J. Hodgins, "Control systems for human running using an inverted pendulum model and a reference motion capture sequence," in *Proceedings of the 2010 ACM SIGGRAPH/Eurographics Symposium on Computer Animation*, ser. SCA '10. Madrid, Spain: Eurographics Association, 2010, pp. 129–138.

[KLSZ03] V. Krishnamoorthy, M. L. Latash, J. P. Scholz, and V. M. Zatsiorsky, "Muscle synergies during shifts of the center of pressure by standing persons," *Experimental Brain Research*, vol. 152, no. 3, pp. 281–292, 2003.

[Knu07] D. Knudson, *Fundamentals of biomechanics*. Springer Science & Business Media, 2007.

[Kon05] P. Konrad, "The ABC of EMG: A practical introduction to kinesiological electromyography. version 1.0, Noraxon Inc," pp. 1–43, 2005.

[KP08] H. Kim and H. Park, "Nonnegative matrix factorization based on alternating nonnegativity constrained least squares and active set method," *SIAM Journal on Matrix Analysis and Applications*, vol. 30, no. 2, pp. 713–730, 2008.

[KR08] L. Kaufman and P. J. Rousseeuw, *Partitioning Around Medoids (Program PAM)*. John Wiley & Sons, Inc., 2008, pp. 68–125.

[KSK97] T. Komura, Y. Shinagawa, and T. L. Kunii, "A muscle-based feed-forward controller of the human body," *Computer Graphics Forum*, vol. 16, no. 3, pp. C165–C176, 1997.

[KSK00] T. Komura, Y. Shinagawa, and T. L. Kunii, "Creating and retargetting motion by the musculoskeletal human body model," *The Visual Computer*, vol. 16, no. 5, pp. 254–270, 2000.

[Kuo98] A. D. Kuo, "A least-squares estimation approach to improving the precision of inverse dynamics computations," *Journal of biomechanical engineering*, vol. 120, no. 1, pp. 148–159, 1998.

[KXY+10] J. H. Kim, Y. Xiang, J. Yang, J. S. Arora, and K. Abdel-Malek, "Dynamic motion planning of overarm throw for a biped human multibody system," *Multibody System Dynamics*, vol. 24, no. 1, pp. 1–24, 2010.

[LAdZR11] M. E. Lund, M. S. Andersen, M. de Zee, and J. Rasmussen, "Functional scaling of musculoskeletal models," in *Congress of the International Society of Biomechanics, ISB*, 2011.

[Lee08] S. H. Lee, "Biomechanical modeling and control of the human body for computer animation," Ph.D. dissertation, University of California at Los Angeles, 2008.

[LGK+10] D. Lee, M. Glueck, A. Khan, E. Fiume, and K. Jackson, "A survey of modeling and simulation of skeletal muscle," *ACM Trans. Graph.*, vol. 28, no. 4, pp. 1–13, 2010.

[Lin01] N. P. Linthorne, "Optimum release angle in the shot put," *Journal of Sports Sciences*, vol. 19, no. 5, pp. 359–372, 2001.

[LMO+99] J. Lee, T. Matsumoto, T. Othman, M. Yamauchi, A. Taimura, E. Kaneda, N. Ohwatari, and M. Kosaka, "Coactivation of the flexor muscles as a synergist with the extensors during ballistic finger extension movement in trained kendo and karate athletes," *International journal of sports medicine*, vol. 20, no. 1, pp. 7–11, January 1999.

[LPKL14] Y. Lee, M. S. Park, T. Kwon, and J. Lee, "Locomotion control for many-muscle humanoids," *ACM Trans. Graph.*, vol. 33, no. 6, pp. 218:1–218:11, Nov. 2014.

[LS99] D. D. Lee and H. S. Seung, "Learning the parts of objects by non-negative matrix factorization," *Nature*, vol. 401, no. 6755, pp. 788–791, 1999.

[LST09] S.-H. Lee, E. Sifakis, and D. Terzopoulos, "Comprehensive biomechanical modeling and simulation of the upper body," *ACM Trans. Graph.*, vol. 28, no. 4, pp. 99:1–99:17, Sep. 2009.

[LT06] S.-H. Lee and D. Terzopoulos, "Heads up!: Biomechanical modeling and neuromuscular control of the neck," *ACM Trans. Graph.*, vol. 25, no. 3, pp. 1188–1198, Jul. 2006.

[Mac67] J. MacQueen, "Some methods for classification and analysis of multivariate observations," in *Proceedings of the Fifth Berkeley Symposium on Mathematical Statistics and Probability, Volume 1: Statistics*. Berkeley, Calif.: University of California Press, 1967, pp. 281–297.

[MBdF10] S. Muceli, A. T. Boye, A. d'Avella, and D. Farina, "Identifying representative synergy matrices for describing muscular activation patterns during multidirectional reaching in the horizontal plane," *Journal of Neurophysiology*, vol. 103, no. 3, pp. 1532–1542, 2010.

[MD12] M. Millard and S. Delp, "A computationally efficient muscle model," in *ASME 2012 Summer Bioengineering Conference*. American Society of Mechanical Engineers, 2012, pp. 1055–1056.

[MGPD15] A. Muller, C. Germain, C. Pontonnier, and G. Dumont, "A simple method to calibrate kinematical invariants: Application to overhead throwing," in *33rd International Conference on Biomechanics in Sports (ISBS 2015)*, 2015.

[Mil88] G. S. P. Miller, "The motion dynamics of snakes and worms," *SIGGRAPH Comput. Graph.*, vol. 22, no. 4, pp. 169–173, Jun. 1988.

[MKB80] K. Mardia, J. Kent, and J. Bibby, *Multivariate Analysis*. CA: Academic Press, 1980.

[MPGD15] A. Muller, C. Pontonnier, C. Germain, and G. Dumont, "Dealing with modularity of multibody models," *Computer methods in biomechanics and biomedical engineering*, p. 2, 2015.

[MR05] O. Maimon and L. Rokach, *Data Mining and Knowledge Discovery Handbook*. Secaucus, NJ, USA: Springer-Verlag New York, Inc., 2005.

[MS14] M. Moltedo and S. Sakka, "Improving skin artifacts compensation for knee flexion/extension and knee internal/external rotation," in

2014 IEEE International Conference on Robotics and Automation (ICRA), May 2014, pp. 4825–4830.

[MTP12] I. Mordatch, E. Todorov, and Z. Popović, "Discovery of complex behaviors through contact-invariant optimization," *ACM Trans. Graph.*, vol. 31, no. 4, pp. 43:1–43:8, Jul. 2012.

[MWTK13] I. Mordatch, J. M. Wang, E. Todorov, and V. Koltun, "Animating human lower limbs using contact-invariant optimization," *ACM Trans. Graph.*, vol. 32, no. 6, pp. 203:1–203:8, Nov. 2013.

[MZS09] A. Macchietto, V. Zordan, and C. R. Shelton, "Momentum control for balance," *ACM Trans. Graph.*, vol. 28, no. 3, pp. 80:1–80:8, Jul. 2009.

[NF02] M. Neff and E. Fiume, "Modeling tension and relaxation for computer animation," in *Proceedings of the 2002 ACM SIGGRAPH/Eurographics Symposium on Computer Animation*, ser. SCA '02. San Antonio, Texas: ACM, 2002, pp. 81–88.

[NTH01] V. Ng-Thow-Hing, "Anatomically-based models for physical and geometric reconstruction of humans and other animals," Ph.D. dissertation, University of Toronto, 2001.

[Pan01] M. G. Pandy, "Computer modeling and simulation of human movement," *Annual review of biomedical engineering*, vol. 3, no. 1, pp. 245–273, 2001.

[PD09] C. Pontonnier and G. Dumont, "Inverse dynamics method using optimization techniques for the estimation of muscles forces involved in the elbow motion," *International Journal on Interactive Design and Manufacturing (IJIDeM)*, vol. 3, no. 4, pp. 227–236, 2009.

[PGB97] A. Prochazka, D. Gillard, and D. J. Bennett, "Positive force feedback control of muscles," *Journal of Neurophysiology*, vol. 77, no. 6, pp. 3226–3236, 1997.

[PSVV07] E. Pennestrì, R. Stefanelli, P. P. Valentini, and L. Vita, "Virtual musculo-skeletal model for the biomechanical analysis of the upper limb," *Journal of Biomechanics*, vol. 40, no. 6, pp. 1350–1361, 2007.

[Rao09] S. S. Rao, *Nonlinear Programming III: Constrained Optimization Techniques*. John Wiley & Sons, Inc., 2009, pp. 380–491.

[RAPC10] C. Rengifo, Y. Aoustin, F. Plestan, and C. Chevallereau, "Distribution of forces between synergistics and antagonistics muscles using an optimization criterion depending on muscle contraction behavior," *Journal of biomechanical engineering*, vol. 132, no. 4, 2010.

[RHWZ08] R. Riemer, E. T. Hsiao-Wecksler, and X. Zhang, "Uncertainties in inverse dynamics solutions: a comprehensive analysis and an application to gait," *Gait & posture*, vol. 27, no. 4, pp. 578–588, 2008.

[Rou87] P. Rousseeuw, "Silhouettes: A graphical aid to the interpretation and validation of cluster analysis," *J. Comput. Appl. Math.*, vol. 20, no. 1, pp. 53–65, Nov. 1987.

[RRB12] J. Roh, W. Z. Rymer, and R. F. Beer, "Robustness of muscle synergies underlying three-dimensional force generation at the hand in healthy humans," *Journal of Neurophysiology*, vol. 107, no. 8, pp. 2123–2142, 2012.

[SADM94] C. Sunada, D. Argaez, S. Dubowsky, and C. Mavroidis, "A coordinated jacobian transpose control for mobile multi-limbed robotic systems," in *Robotics and Automation, 1994. Proceedings., 1994 IEEE International Conference on*, May 1994, pp. 1910–1915 vol.3.

[Sak02] S. Sakurai, "Biomechanics of overhand throwing motion: past, present, and future research trend," *International Research in Sports Biomechanics*, pp. 17–26, 2002.

[SALC03] A. Soares, A. Andrade, E. Lamounier, and R. Carrijo, "The development of a virtual myoelectric prosthesis controlled by an emg pattern recognition system based on neural networks," *Journal of Intelligent Information Systems*, vol. 21, no. 2, pp. 127–141, 2003.

[SCMB15] S. Sakka, D. Chablat, R. Ma, and F. Bennis, "Predictive model of the human muscle fatigue: application to repetitive push-pull tasks with light external load," *International Journal of Human Factors Modelling and Simulation*, vol. 5, no. 1, pp. 81–97, 2015.

[SCSB16] D. Seth, D. Chablat, S. Sakka, and F. Bennis, "Experimental validation of a new dynamic muscle fatigue model," in *18th International Conference on Human-Computer Interaction*, Toronto, Canada, Jul. 2016.

[SHP04] A. Safonova, J. K. Hodgins, and N. S. Pollard, "Synthesizing physically realistic human motion in low-dimensional, behavior-specific spaces," *ACM Trans. Graph.*, vol. 23, no. 3, pp. 514–521, Aug. 2004.

[Si13] W. Si, "Realistic simulation and control of human swimming and underwater movement," Ph.D. dissertation, University of California, 2013.

[Sif07] E. Sifakis, "Algorithmic aspects of the simulation and control of computer generated human anatomy models," Ph.D. dissertation, Stanford University, 2007.

[SKP08] S. Sueda, A. Kaufman, and D. K. Pai, "Musculotendon simulation for hand animation," *ACM Trans. Graph.*, vol. 27, no. 3, pp. 83:1–83:8, Aug. 2008.

[SLST14] W. Si, S.-H. Lee, E. Sifakis, and D. Terzopoulos, "Realistic biomechanical simulation and control of human swimming," *ACM Trans. Graph.*, vol. 34, no. 1, pp. 10:1–10:15, Dec. 2014.

[SO00] S. Sakurai and T. Ohtsuki, "Muscle activity and accuracy of performance of the smash stroke in badminton with reference to skill and practice," *Journal of Sports Sciences*, vol. 18, no. 11, pp. 901–914, 2000.

[SSB+15] P. Sachdeva, S. Sueda, S. Bradley, M. Fain, and D. K. Pai, "Biomechanical simulation and control of hands and tendinous systems," *ACM Trans. Graph.*, vol. 34, no. 4, pp. 42:1–42:10, Jul. 2015.

[ST11] S. A. Safavynia and L. H. Ting, "Task-level feedback can explain temporal recruitment of spatially fixed muscle synergies throughout postural perturbations," *Journal of Neurophysiology*, vol. 107, no. 1, pp. 159–177, 2011.

[STP13] K. M. Steele, M. C. Tresch, and E. J. Perreault, "The number and choice of muscles impact the results of muscle synergy analyses," *Frontiers in Computational Neuroscience*, vol. 7, no. 105, 2013.

[Str96] S. Stroeve, "Learning combined feedback and feedforward control of a musculoskeletal system," *Biological Cybernetics*, vol. 75, no. 1, pp. 73–83, 1996.

[SWDd+01] P. Saltiel, K. Wyler-Duda, A. d'Avella, M. C. Tresch, and E. Bizzi, "Muscle synergies encoded within the spinal cord: Evidence from

focal intraspinal NMDA iontophoresis in the frog," *Journal of Neurophysiology*, vol. 85, no. 2, pp. 605–619, 2001.

[Tag98] G. Taga, "A model of the neuro-musculo-skeletal system for anticipatory adjustment of human locomotion during obstacle avoidance," *Biological Cybernetics*, vol. 78, no. 1, pp. 9–17, 1998.

[TC10] L. H. Ting and S. A. Chvatal, "Decomposing muscle activity in motor tasks," *Motor Control Theories, Experiments and Applications. Oxf. Univ. Press, New York*, pp. 102–138, 2010.

[TCd06] M. C. Tresch, V. C. K. Cheung, and A. d'Avella, "Matrix factorization algorithms for the identification of muscle synergies: Evaluation on simulated and experimental data sets," *Journal of Neurophysiology*, vol. 95, no. 4, pp. 2199–2212, 2006.

[Tin07] L. H. Ting, "Dimensional reduction in sensorimotor systems: a framework for understanding muscle coordination of posture," *Progress in brain research*, vol. 165, pp. 299–321, 2007.

[TOMT06] G. Torres-Oviedo, J. M. Macpherson, and L. H. Ting, "Muscle synergy organization is robust across a variety of postural perturbations," *Journal of Neurophysiology*, vol. 96, no. 3, pp. 1530–1546, 2006.

[TOT07] G. Torres-Oviedo and L. H. Ting, "Muscle synergies characterizing human postural responses," *Journal of Neurophysiology*, vol. 98, no. 4, pp. 2144–2156, 2007.

[TSF05] W. Tsang, K. Singh, and E. Fiume, "Helping hand: An anatomically accurate inverse dynamics solution for unconstrained hand motion," in *Proceedings of the 2005 ACM SIGGRAPH/Eurographics Symposium on Computer Animation*, ser. SCA '05. Los Angeles, California: ACM, 2005, pp. 319–328.

[TST+10] M. T. Tran, P. Souères, M. Taïx, M. N. Sreenivasa, and C. Halgand, "Humanoid human-like reaching control based on movement primitives," in *19th International Symposium in Robot and Human Interactive Communication*, Sept 2010, pp. 546–551.

[TT94] X. Tu and D. Terzopoulos, "Artificial fishes: Physics, locomotion, perception, behavior," in *Proceedings of the 21st Annual Conference on Computer Graphics and Interactive Techniques*, ser. SIGGRAPH '94. ACM, 1994, pp. 43–50.

[TTL12] J. Tan, G. Turk, and C. K. Liu, "Soft body locomotion," *ACM Trans. Graph.*, vol. 31, no. 4, pp. 26:1–26:11, Jul. 2012.

[TTSG13] M. Taïx, M. T. Tran, P. Souères, and E. Guigon, "Generating human-like reaching movements with a humanoid robot: A computational approach," *Journal of Computational Science*, vol. 4, no. 4, pp. 269 – 284, 2013.

[TYS91] G. Taga, Y. Yamaguchi, and H. Shimizu, "Self-organized control of bipedal locomotion by neural oscillators in unpredictable environment," *Biological Cybernetics*, vol. 65, no. 3, pp. 147–159, 1991.

[ULP+07] Z. Ugray, L. Lasdon, J. Plummer, F. Glover, J. Kelly, and R. Martí, "Scatter search and local nlp solvers: A multistart framework for global optimization," *INFORMS Journal on Computing*, vol. 19, no. 3, pp. 328–340, 2007.

[vdBS08] A. J. van den Bogert and A. Su, "A weighted least squares method for inverse dynamic analysis," *Computer methods in biomechanics and biomedical engineering*, vol. 11, no. 1, pp. 3–9, 2008.

[VDH94] F. C. T. Van Der Helm, "A finite element musculoskeletal model of the shoulder mechanism," *Journal of biomechanics*, vol. 27, pp. 593–633, 1994.

[vdKdGF+09] M. M. van der Krogt, W. W. de Graaf, C. T. Farley, C. T. Moritz, L. R. Casius, and M. F. Bobbert, "Robust passive dynamics of the musculoskeletal system compensate for unexpected surface changes during human hopping," *Journal of Applied Physiology*, vol. 107, no. 3, pp. 801–808, 2009.

[vSB93] A. J. van Soest and M. F. Bobbert, "The contribution of muscle properties in the control of explosive movements," *Biological cybernetics*, vol. 69, no. 3, pp. 195–204, 1993.

[Vuk90] M. Vukobratovic, *Biped locomotion.* Springer-Verlag New York, Inc., 1990.

[VYN05] G. Venture, K. Yamane, and Y. Nakamura, "Identifying musculotendon parameters of human body based on the musculo-skeletal dynamics computation and hill-stroeve muscle model," *2005 5th IEEE-RAS International Conference on Humanoid Robots*, pp. 351–356, 2005.

[VYN06] G. Venture, K. Yamane, and Y. Nakamura, "Application of nonlinear least square method to estimate the muscle dynamics of the elbow joint," in *IFAC - Int. Conf. on System Identification*, Newcastle, Australia, 2006, pp. 1168–1173.

[WC00] J. M. Winters and P. E. Crago, Eds., *Biomechanics and Neural Control of Posture and Movement*. New York, NY: Springer New York, 2000.

[WDKvD12] N. W. Willigenburg, A. Daffertshofer, I. Kingma, and J. H. van Dieën, "Removing ECG contamination from EMG recordings: A comparison of ICA-based and other filtering procedures," *Journal of electromyography and kinesiology*, vol. 22, no. 3, pp. 485–493, 2012.

[WF04] E. J. Weiss and M. Flanders, "Muscular and postural synergies of the human hand," *Journal of Neurophysiology*, vol. 92, no. 1, pp. 523–535, 2004.

[WHDK12] J. M. Wang, S. R. Hamner, S. L. Delp, and V. Koltun, "Optimizing locomotion controllers using biologically-based actuators and objectives," *ACM Trans. Graph.*, vol. 31, no. 4, pp. 25:1–25:11, Jul. 2012.

[Win05] D. A. Winter, *Biomechanics and motor control of human movement*. John wiley & sons, INC., New Jersey, USA, 2005.

[WK88] A. Witkin and M. Kass, "Spacetime constraints," *SIGGRAPH Comput. Graph.*, vol. 22, no. 4, pp. 159–168, Jun. 1988.

[WMNO06] R. Waltz, J. Morales, J. Nocedal, and D. Orban, "An interior algorithm for nonlinear optimization that combines line search and trust region steps," *Mathematical Programming*, vol. 107, no. 3, pp. 391–408, 2006.

[Woo98] W. L. Wooten, "Simulation of leaping, tumbling, landing, and balancing humans," Ph.D. dissertation, Georgia Institute of Technology, 1998.

[WSA+02] G. Wu, S. Siegler, P. Allard, C. Kirtley, A. Leardini, D. Rosenbaum, M. Whittle, D. D. D'Lima, L. Cristofolini, H. Witte *et al.*, "ISB recommendation on definitions of joint coordinate system of various joints for the reporting of human joint motion part I: ankle, hip, and spine," *Journal of biomechanics*, vol. 35, no. 4, pp. 543–548, 2002.

[WvdHV+05] G. Wu, F. C. T. van der Helm, H. E. J. D. Veeger, M. Makhsous, P. V. Roy, C. Anglin, J. Nagels, A. R. Karduna, K. McQuade, X. Wang, F. W. Werner, and B. Buchholz, "ISB recommendation on definitions of joint coordinate systems of various joints for the reporting of human joint motion–Part II: shoulder, elbow, wrist and hand," *Journal of Biomechanics*, vol. 38, no. 5, pp. 981–992, 2005.

[YL08] Y. Ye and C. K. Liu, "Animating responsive characters with dynamic constraints in near-unactuated coordinates," *ACM Trans. Graph.*, vol. 27, no. 5, pp. 112:1–112:5, Dec. 2008.

[YLvdP07] K. Yin, K. Loken, and M. van de Panne, "SIMBICON: Simple biped locomotion control," *ACM Trans. Graph.*, vol. 26, no. 3, Jul. 2007.

[Zaj89] F. E. Zajac, "Muscle and tendon: properties, models, scaling, and application to biomechanics and motor control." *Crit Rev Biomed Eng*, vol. 17, no. 4, pp. 359–411, 1989.

[ZCCD06] V. B. Zordan, B. Celly, B. Chiu, and P. C. DiLorenzo, "Breathe easy: model and control of human respiration for computer animation," *Graphical Models*, vol. 68, no. 2, pp. 113–132, 2006.

[ZDG+96] K. Zhou, J. C. Doyle, K. Glover *et al.*, *Robust and optimal control*. Prentice hall New Jersey, 1996, vol. 40.

[ZHK15] L. Zhu, X. Hu, and L. Kavan, "Adaptable anatomical models for realistic bone motion reconstruction," *Computer Graphics Forum*, vol. 34, no. 2, pp. 459–471, 2015.

[ZW90] F. Zajac and J. Winters, "Modeling musculoskeletal movement systems: Joint and body segmental dynamics, musculoskeletal actuation, and neuromuscular control," in *Multiple Muscle Systems*. Springer New York, 1990, pp. 121–148.

Abstract

The use of virtual characters in physics-based simulations has applications that range from biomechanics to animation. An essential component behind such applications is the character's motion controller, which transforms desired tasks into synthesized motions. The way these controllers are designed is being profoundly transformed through the integration of knowledge from biomechanics, which motivates the idea of using more detailed character models, inspired by the human musculoskeletal system (or muscle-based characters). Controlling these characters implies solving an important challenge: control redundancy, or the fact that numerous muscles or actuators need to be coordinated simultaneously to achieve the desired motion task.

The goal of this thesis is to address this challenge by taking inspiration from how the human motor control system manages this redundancy. A control solution for virtual characters is proposed based on the theory of muscle synergies, and applied on the control of throwing motions. Muscle synergies are low-dimensional control representations that allow muscles to be controlled in groups, thus reducing significantly the number of control variables.
Through this solution this thesis has the following contributions: 1) A contribution to the validation of the muscle synergy theory by using it to study a new motion, and challenging it with the control of a virtual character, and 2) a contribution to the variety of domains involving physical simulation with muscle-based characters (e.g, biomechanics, animation) by proposing a control solution that reduces redundancy.

Keywords
Control, redundancy, muscle synergies, physics-based simulation, virtual characters

Résumé

L'utilisation de personnages virtuels dans le cadre de simulations basées sur les lois de la physique trouve maintenant des applications allant de la biomécanique à l'animation. L'un des éléments incontournables de cette performance est le contrôleur de mouvement, capable de transformer les actions souhaitées en mouvements synthétisés. La conceptualisation de ces contrôleurs a profondément évolué grâce à l'apport des connaissances en biomécanique qui a conduit à l'utilisation de modèles de personnages encore plus détaillés car s'inspirant de l'appareil squelettique et surtout musculaire de l'être humain (ou personnages à modèle musculaire). Contrôler les personnages virtuels implique un défi de taille : contrôler la redondance, ou le fait même qu'un nombre important de muscles ou d'actionneurs aient besoin d'être contrôlés simultanément pour exécuter la tâche de motricité demandée.

L'objectif de cette thèse est d'y répondre en s'inspirant du système de contrôle moteur humain permettant de gérer cette redondance. Une solution de contrôle, pour les personnages virtuels, est proposée d'après la théorie des synergies musculaires et appliquée à des mouvements de contrôle du lancer. Les synergies musculaires sont des représentations de contrôle à faible dimension et qui permettent aux muscles d'être contrôlés en groupe, réduisant ainsi de manière significative le nombre de variables.
Grâce à cette stratégie, cette thèse permet les contributions suivantes : en premier lieu, la validation de la théorie des synergies musculaires, utilisée ici pour étudier un nouveau mouvement et pour tenter de contrôler un personnage virtuel. Et elle contribue également à l'ensemble des domaines impliquant des simulations corporelles, ayant recours aux personnages à modèle musculaire (comme par exemple, la biomécanique ou l'animation) en leur proposant une solution de contrôle permettant de réduire la redondance.

Mots-clés
Redondance, synergies musculaires, simulations basées sur les lois de la physique, personnages virtuels

École normale supérieure de Rennes
Campus de Ker Lann - Avenue Robert Schuman - 35170 BRUZ
Tél : +33(0)2 99 05 93 00 - Fax : +33(0)2 99 05 93 29 - **www.ens-rennes.fr**